SPECTRUM AMPLITUDE--
Definition, Generation and Measurement

James R. Andrews
M. Gerald Arthur

Electromagnetics Division
Institute for Basic Standards
National Bureau of Standards
Boulder, Colorado 80302

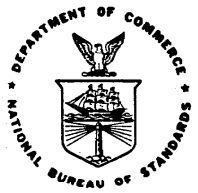

U.S. DEPARTMENT OF COMMERCE, Juanita M. Kreps, Secretary
Sidney Harman, Under Secretary
Jordan J. Baruch, Assistant Secretary for Science and Technology

NATIONAL BUREAU OF STANDARDS, Ernest Ambler, Acting Director

Issued October 1977

NATIONAL BUREAU OF STANDARDS TECHNICAL NOTE 699
Nat. Bur. Stand. (U.S.), Tech. Note 699, 100 pages(October 1977)
CODEN: NBTNAE

U.S. GOVERNMENT PRINTING OFFICE
WASHINGTON: 1977

For sale by the Superintendent of Documents, U.S. Government Printing Office, Washington, D.C. 20402

Stock No. 003-003-01865-1 Price $2.75 (Add 25 percent additional for other than U.S. mailing)

CONTENTS

CONTENTS (Cont)

SPECTRUM AMPLITUDE -- DEFINITION, GENERATION AND MEASUREMENT

James R. Andrews and M. Gerald Arthur

This technical note is a detailed discussion of the electromagnetic quantity, spectrum amplitude, which is used to characterize broadband signals and noise. The definition of spectrum amplitude is presented in detail. Several practical means of generating electrical signals with broadband spectrum amplitudes are included. Various techniques for the measurement of spectrum amplitude are described along with experimental comparisons. The NBS measurement service for the calibration of impulse generator spectrum amplitude is described along with an error analysis.

Key words: Electromagnetic interference; Fourier transformation; impulse; impulse generator; spectrum amplitude.

1. INTRODUCTION

In EMC work, and in the EMC literature, one often encounters an electromagnetic quantity that has the dimensional units of volts per hertz, or more commonly, microvolts per megahertz. However in reading the literature, one is sometimes puzzled or confused by the variety of names that this quantity is given, or may become suspicious that the way in which this quantity is being used is somehow different from the way that someone else has used it. This technical note addresses this quantity with the purpose of clarifying what some of its important characteristics are, and to attempt to reduce some of the large amount of confusion, half truths, and whole untruths about it. The most official name given to this quantity is found in the IEEE Dictionary [1] and IEEE Std. 376-1975 [2]. That name is Spectrum Amplitude. Spectrum amplitude, S(f), is defined in terms of the magnitude of the Fourier transform, V(f), of a time-domain signal function, v(t).

$$S(f) = 2|V(f)| \tag{1-1}$$

where

$$V(f) = \int_{-\infty}^{\infty} v(t)e^{-j2\pi ft}\,dt. \tag{1-2}$$

Other names that can be found in the EMC literature are Impulse Spectral Intensity, Spectral Intensity, Spectral Density, Voltage Spectrum, Impulse Strength and Interference Intensity. All of these names have been applied to quantities that have dimensional units of volts per hertz or its mathematical equivalent, volt-seconds. The unit in common usage is microvolts per megahertz (μV/MHz). Also in common usage is a decibel expression, decibel microvolts per megahertz (dBμV/MHz), above 1 μV/MHz.

$$S(db) = 20\ \log_{10}\left[\frac{S(\mu V/MHz)}{1\ \mu V/MHz}\right] \tag{1-3}$$

Background

Impulse generators are widely used as transportable field calibration instruments for the calibration of field intensity meters (FIM), spectrum analyzers, and receivers. FIM's are the basic instruments for measuring electromagnetic (EM) fields and the spectrum amplitude, S(f), of broadband impulsive noise.

The area of electromagnetic field (EM) measurement is of considerable importance. It is relevant to the broad area of interference described variously as RFI (radio frequency interference), TVI (television interference), and EMI (electromagnetic interference). It is the measurement base for frequency allocations based on EMC (electromagnetic compatibility). In national security electronic espionage and electronic warfare countermeasures, radiated impulse measurements (RIM) are very critical.

Present FIM calibration techniques utilize CW signal generators for narrowband measurements and impulse generators for broadband measurements. The CW signal generator presents no problem as its calibration is directly traceable to NBS. Impulse generators have been an entirely different matter in that their calibration has not been traceable to NBS. Users of impulse generators have had to rely upon the manufacturer's calibrations. There are discrepancies between various commercial impulse generators, as many users have discovered.

As a result of several years of effort dating back to 1966, NBS has developed a measurement service for the calibration of the spectrum amplitude output of impulse generators. This service was publicly announced in the Fall 1976 Appendix to NBS SP-250, "Calibration and Test Services of the National Bureau of Standards." This Technical Note summarizes the research and development effort at NBS necessary to establish this measurement service.

Funding for establishing NBS standards and traceability for impulse generator spectrum amplitude has come from both internal NBS funds and various contracts from the U.S. Department of Defense. The various DoD contracts were as follows:

1. U.S. Army Electronics Command, Ft. Monmouth, N.J., contract No. 67-95896, Dec. 1966 to Sept. 1971.
2. Army/Navy/Air Force Calibration Coordination Group (CCG), project CCG 69-26, FY 1969.
3. Army/Navy/Air Force Calibration Coordination Group, project CCG 72-70, FY 72.
4. Army/Navy/Air Force Calibration Coordination Group, project CCG 72-71A, FY 72.
5. Army/Navy/Air Force Calibration Coordination Group, project CCG 75-97, FY 75-76.

In addition to the above contracts, funding was received from the CCG for work in the related area of picosecond pulse measurements. As it turned out, a

great deal of this work was directly applicable to the impulse generator problem. In particular, the calibration console currently used for impulse generator calibrations was originally developed as a Time Domain Automatic Network Analyzer under CCG 72-68. Other related CCG projects were: 71-50, 71-52, 72-65, and 72-66. This Technical Note serves as part of the final report on the most recent contract CCG 75-97.

This Technical Note is organized in seven chapters and one appendix. The first chapter is this introduction. Chapter 2 discusses the definition of spectrum amplitude along with its mathematical and physical concepts. Chapter 3 discusses practical means of generating electrical signals with broadband spectrum amplitudes. Chapter 4 describes various techiques for the measurement of spectrum amplitude. Chapter 5 presents a summary of results obtained from experiments to compare the various measurement techniques of Chapter 4. Chapter 6 is an error analysis of the time domain measurement/Fourier transform computation technique of determining spectrum amplitude. Chapter 7 describes the NBS measurement service for impulse generator spectrum amplitude. An appendix describes in detail an impulse generator developed at NBS which produces an 8 V, 100 ps impulse with a spectrum useful to beyond 5 GHz. Chapter 2 was contributed by M.G. Arthur and the subsequent chapters were written by James R. Andrews.

2. FOUNDATIONS FOR THE DEFINITION OF SPECTRUM AMPLITUDE

This chapter deals with certain characteristics of the Fourier transform [3], upon which is based the spectrum amplitude S(f). Because many workers who deal with impulsive signals appear to have misunderstandings about this quantity, a review of certain of its more important characteristics may be helpful.

Every physical signal has an amplitude spectrum [4]; that is, every physical signal can be described in both the time domain and the frequency domain. One mathematical way of expressing this physical duality is by means of the Fourier transform pair of algebraic equations. It is certainly possible to postulate mathematical waveforms for which the Fourier transform, and hence the amplitude spectrum, does not exist [5]. However, because every signal which we might generate and every signal sample which we might extract from some arbitrary generating system is finite in both duration and amplitude, and hence has finite energy, the conditions for the existence of their Fourier transforms are always met.

Three major points will be emphasized concerning the Fourier transform as follows: (1) In the general case, it is mathematically a complex quantity having both magnitude and phase. (2) Its dimensional units are different from those of the waveform function being transformed. (3) It is a continuously defined function of frequency, and not a discontinuous, discrete function of frequency. After these points are discussed, we will point out that the magnitude of the Fourier transform appears explicitly in many signal equations, thus leading naturally to the definition of spectrum amplitude, S(f).

2.1 Fourier Transform Fundamentals

This section very briefly presents the basic information that will be needed in the following sections. More thorough treatments of the Fourier transform are available in the open literature.

The Fourier transform pair of equations are the following:

$$V(f) = \int_{-\infty}^{\infty} v(t) e^{-j2\pi ft}\, dt \quad \text{(Fourier transform)} \tag{2-1}$$

$$v(t) = \int_{-\infty}^{\infty} V(f) e^{j2\pi ft}\, df \quad \text{(inverse Fourier transform)} \tag{2-2}$$

This pair of equations can be used to mathematically represent a physical signal which is labeled v(t) in the time domain and V(f) in the frequency domain. Equation (2-1) transforms the time domain quantity, v(t), into the frequency domain quantity, V(f); and conversely for eq. (2-2). The physical signal itself is not transformed by the Fourier transform; it is a physical entity that exists in both the time and frequency domains. Transformation is a mathematical operation on the equations that algebraically represent the

signal. However, a graphic plot of the signal's time domain waveform, v(t), will in general have a different shape than a plot of its frequency domain waveform, V(f), because the two algebraic equations are usually different. (The single Gaussian pulse is an exception to this statement.)

To be transformable as indicated above, the algebraic time domain function, v(t), must satisfy the three Dirichlet conditions; viz.:

1. v(t) must be absolutely integrable; that is,

$$\int_{-\infty}^{\infty} |v(t)|\, dt < \infty. \tag{2-3}$$

2. v(t) must have a finite number of maxima and minima in any finite interval of time.
3. v(t) must have a finite number of discontinuities in any finite interval of time.

We will use the single rectangular baseband pulse shown in figure 2-1 as an example to illustrate the characteristics of the Fourier transform that we are emphasizing. This waveform has an amplitude of A from t = 0 to t = τ, and is zero elsewhere. Although this idealized waveform cannot be generated as a physical signal, it satisfies the Dirichlet conditions, and its mathematical representations are easy to work with and comprehend. All of the observations and conclusions we will make from this example generally apply to any physical signal, regardless of whether it is a single pulse of arbitrary shape, a series of pulses repeated at perfectly regular intervals, a series of pulses repeated at irregular intervals, or continuous-type signal functions of regular, irregular, or random shape.

Figure 2-1. Single rectangular baseband pulse.

2.2 Fourier Transform, a Complex Quantity

The time domain representation, $v_p(t)$, of the waveform of figure 2-1 is

$$v_p(t) = A, \quad 0 < t < \tau$$
$$= 0 \text{ elsewhere.} \tag{2-4}$$

The Fourier transform, $V_p(f)$, of $v_p(t)$ is obtained by substituting eq. (2-4) into eq. (2-1).

$$V_p(f) = A \int_0^{\tau} e^{-j2\pi ft}\, dt \tag{2-5}$$

$$= \frac{A}{2\pi f} [\sin(2\pi f\tau) - j2 \sin^2(\pi f\tau)]. \tag{2-6}$$

Equation (2-6) shows that $V_p(f)$ is a complex quantity having both a real and an imaginary part. This is true in general of any v(t), although some signal representations, depending upon their waveform and the choice of time origin, may have only a real or an imaginary part.

The purpose of emphasizing the complex nature of V(t) is the following: Spectrum amplitude, which is twice the magnitude of V(f), may not, in general, be sufficient to adequately describe the signal. Phase information may be needed, depending upon the application (for example, when predicting the effect of changing the measurement bandwidth of an EMI receiver). However, for many purposes found in EMC work, the magnitude, $|V(f)|$, is a very useful quantity, as is discussed later.

$V_p(f)$ may also be written in polar form in which the magnitude and phase are explicit.

$$V_p(f) = |V_p(f)| e^{j\phi_p(f)} \tag{2-7}$$

where

$$|V_p(f)| = \left| \frac{A}{2\pi f} \{|\sin(2\pi f\tau)]^2 + [-2 \sin^2(\pi f\tau)]^2\}^{1/2} \right| \tag{2-8}$$

$$= A\tau \left| \frac{\sin(\pi f\tau)}{\pi f\tau} \right| \tag{2-9}$$

and

$$\phi_p(f) = \tan^{-1}\left[\frac{-2 \sin^2(\pi f\tau)}{\sin(2\pi f\tau)}\right] \tag{2-10}$$

$$= \tan^{-1}[-\tan(\pi f\tau)]. \tag{2-11}$$

The interpretation of the multivalued arctangent function can be obtained by plotting $V_p(f)$ from eq. (2-6) in the complex plane as a function of frequency. Figure 2-2 shows such a plot from f = 0 to f = $2/\tau$. For positive frequencies, $V_p(f)$ occupies only the third and fourth quadrants. Thus the phase, $\phi_p(f)$, is written as

$$\phi_p(f) = -\pi f\tau + n\pi \tag{2-12}$$

where n = 0, ± 1, ± 2, ...

Substituting eqs. (2-9) and (2-12) into eq. (2-7) gives

$$V_p(f) = A\tau \left| \frac{\sin(\pi f\tau)}{\pi f\tau} \right| e^{j(-\pi f\tau + n\pi)} \tag{2-13}$$

A quasi-polar form for $V_p(f)$ is

$$V_p(f) = A\tau \frac{\sin(\pi f\tau)}{\pi f\tau} e^{-j\pi f\tau} \tag{2-14}$$

since, for the baseband pulse of figure 2-1,

$$A\tau \left| \frac{\sin(\pi f\tau)}{\pi f\tau} \right| e^{jn\pi} = A\tau \frac{\sin(\pi f\tau)}{\pi f\tau} . \tag{2-15}$$

Equation (2-15) can also be gotten directly from eq. (2-6).

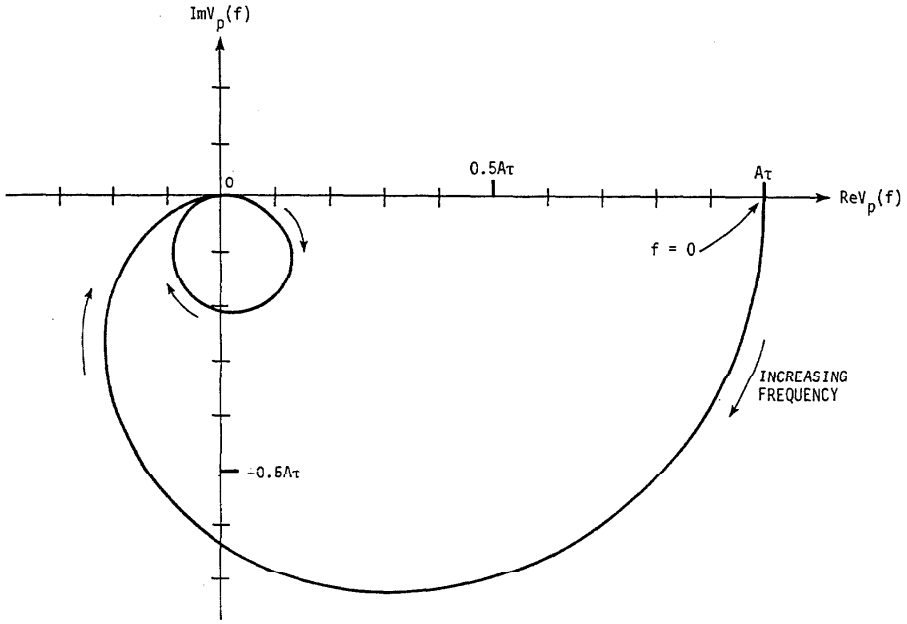

Figure 2-2. The locus of $V_p(f)$ for positive frequency.

2.3 Fourier Transform Dimensional Units

The dimensional units of the Fourier transform are different from those of the signal waveform which is being transformed; specifically, they are the units of the signal waveform multiplied by time (dimensional unit of seconds). The purpose of emphasizing this characteristic is to distinguish the Fourier transform representation of the signal from the Fourier series representation [3]. In the latter case, the spectrum is a discrete spectrum, the components of which are eternal sinusoids whose amplitudes have the same dimensional units as those of the physical signal. In the former case, the time domain function is transformed into an entirely different function with a different set of dimensional units. These different units warn us that we are dealing with a "transformed" function that may have different properties from the Fourier series components.

To illustrate how the Fourier transform differs from the Fourier series representation, we will make use of geometrical interpretations of the algebraic equations. Consider again the waveform given in figure 2-1. As before,

$$V_p(f) = \int_0^\tau Ae^{-j2\pi ft}\, dt. \tag{2-5}$$

The integrand, y, of eq. (2-5) is

$$\begin{aligned} y &= Ae^{-j2\pi ft} \\ &= A\cos(2\pi ft) - jA\sin(2\pi ft), \quad 0 < t < \tau \\ &= 0 \text{ elsewhere.} \end{aligned} \tag{2-16}$$

The function y is a function of both frequency and time; it is also complex. The real part of y in this example is

$$\mathrm{Re}[y] = A\cos(2\pi ft), \quad 0 < t < \tau \tag{2-17}$$

and the imaginary part is

$$\mathrm{Im}[y] = -A\sin(2\pi ft), \quad 0 < t < \tau. \tag{2-18}$$

Figure 2-3 shows a portion of a three-dimensional plot of the real part of y. It is three dimensional because y is a function of both frequency and time. The result is a wavy surface with a cosinusoidal variation in both directions.

Because V(f), in general, is an integral [see eq. (2-1)], it is geometrically an "area." The real part of the Fourier transform, $\mathrm{Re}[V_p(f)]$ at a specified frequency, f, is the area under the cosine curve of figure 2-3 at frequency f in the time direction. For example, figure 2-4 shows four "slices" through this wavy surface parallel to the time-axis and perpendicular to the frequency-axis. The value of $\mathrm{Re}[V_p(f)]$ at frequency f_c is the area marked "c." The imaginary part of $V_p(f)$ can be found in a similar way. $V_p(f)$ is the vector sum of the real and the imaginary parts (see the vector diagram at frequency f_b).

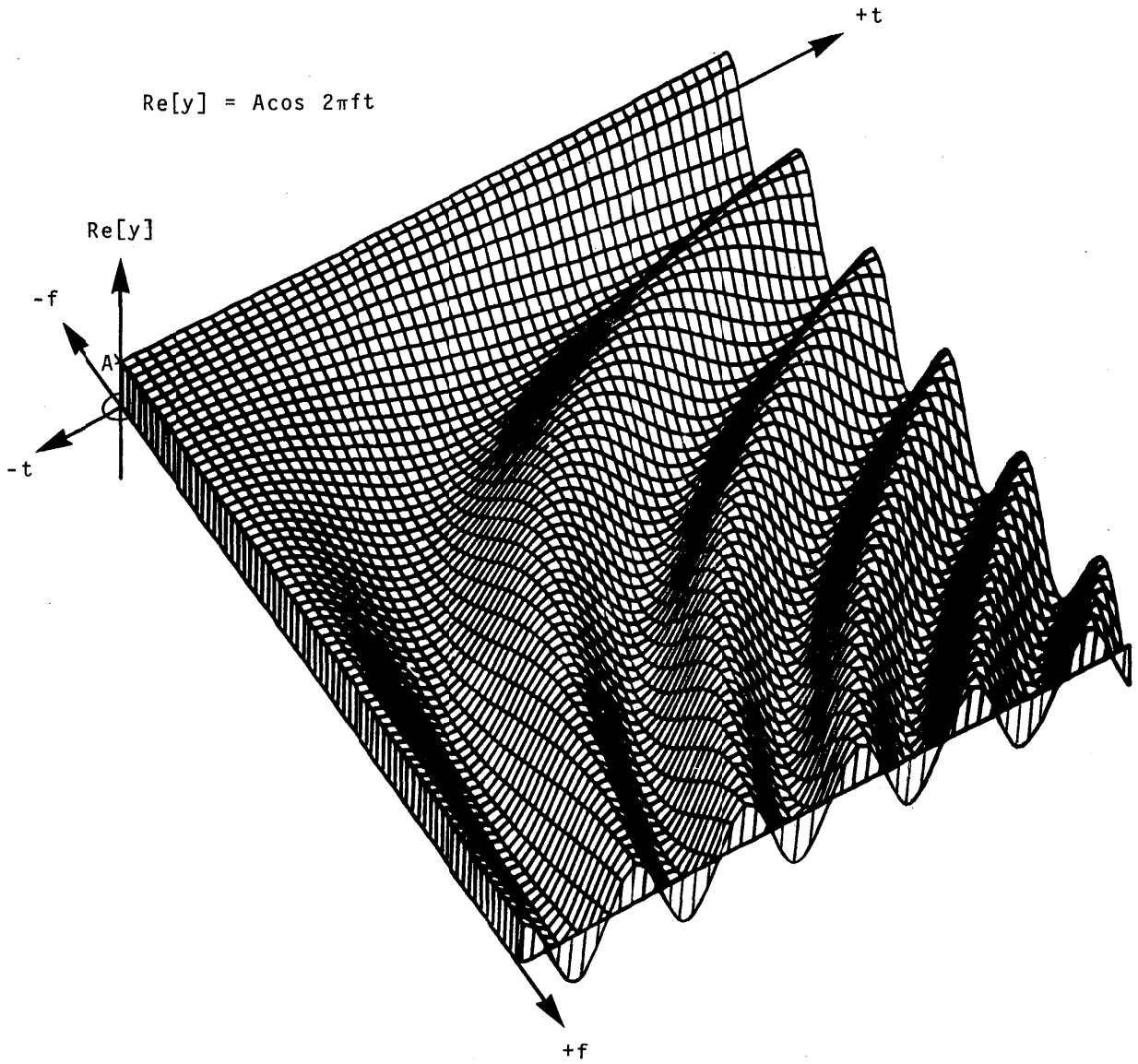

Figure 2-3. Three-dimensional plot of Re[y] = A cos 2πft.

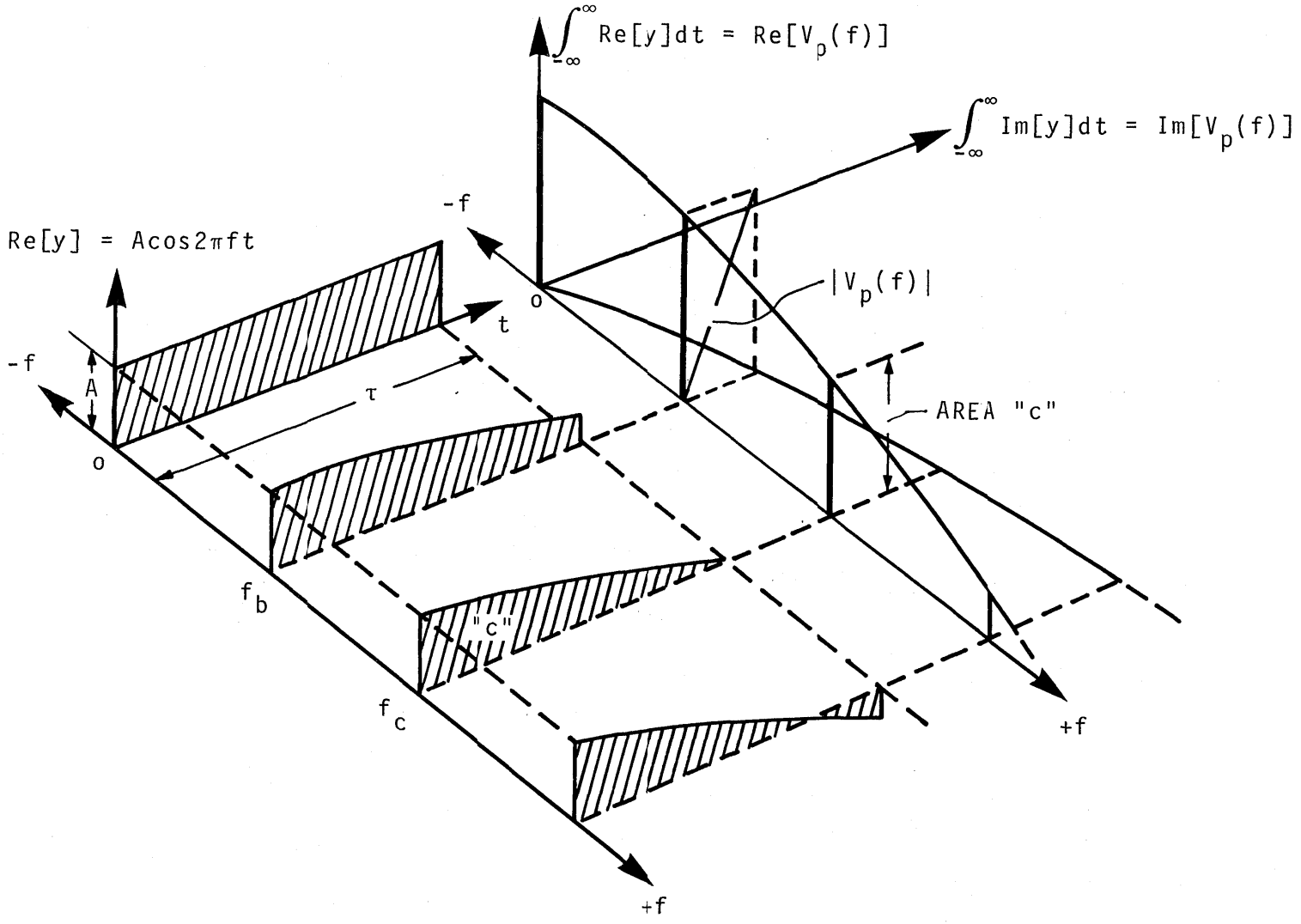

Figure 2-4. Illustrating the relationship between Re[y] and $Re[V_p(f)]$.

Being an area, V(f) has dimensional units which are the product of the units of its constituent parts, height (ordinate) and base (abscissa). If v(t) is a voltage, then V(f) has the units of volt-second. From this we can see that V(f) is not the amplitude per se of sinusoidal voltages that are components of the physical signal in the frequency domain. It is neither a voltage, a power, or an energy. Rather, because its dimensional units, volt-seconds, are mathematically equivalent to the units "volts per hertz," we see that spectrum amplitude, S(f), is a voltage density quantity, or, mathematically, a type of weighting function. It is a measure of the "strength," in volt-seconds or volts per hertz, of the physical signal.

There is a strong possibility for confusion and misapplication if the units of volts per hertz are used for V(f) rather than volt-seconds. It is true that mathematically they are equivalent. From a physical standpoint, volts per hertz suggests a density function whereas volt-seconds does not. No engineering justification can be found for using one set of units in preference to the other. However, the units, volts per hertz, can mislead one into thinking that he can simply integrate V(f) over a finite interval of frequency and obtain a voltage that has some useful physical meaning. Such may not be the case. What does have useful meaning, as was seen in eq. (2-2), is the integral of the product of V(f) with an (eternal) exponential function, which, for the infinite integral, yields the complete time-domain signal representation v(t). Incidentally, the infinite integral of just V(f) over the entire frequency interval is the value of the time-domain signal function at time t = 0. This is a basic theorem of Fourier transforms. Thus the integral of V(f) over a finite frequency interval yields the part of v(t) at t = 0 contributed by the frequency-domain signal in that band of frequencies. But these quantities are normally of limited interest, and most EMC instruments do not measure them.

2.4 Fourier Transform, a Continuous Function

Another important characteristic of V(f) is that it is a continuously defined function of frequency. Again, the purpose of emphasizing this characteristic is to distinguish it from the discrete spectrum of the Fourier series representation. Although there may be specific frequencies where the Fourier transform, V(f), is zero, it is generally true that there are no frequencies where V(f) is undefined. This is not the case with the Fourier series representation. There the spectrum is defined only at discrete frequencies.

A plot of $|V_p(f)|$ and $\phi_p(f)$ for the waveform of figure 2-1 is given in figure 2-5. $|V_p(f)|$ has the familiar "absolute sine x over x" shape and $\phi_p(f)$ is a linear sawtooth, as given by eqs. (2-9) and (2-12), respectively. Note that these plots are for the single rectangular pulse, figure 2-1.

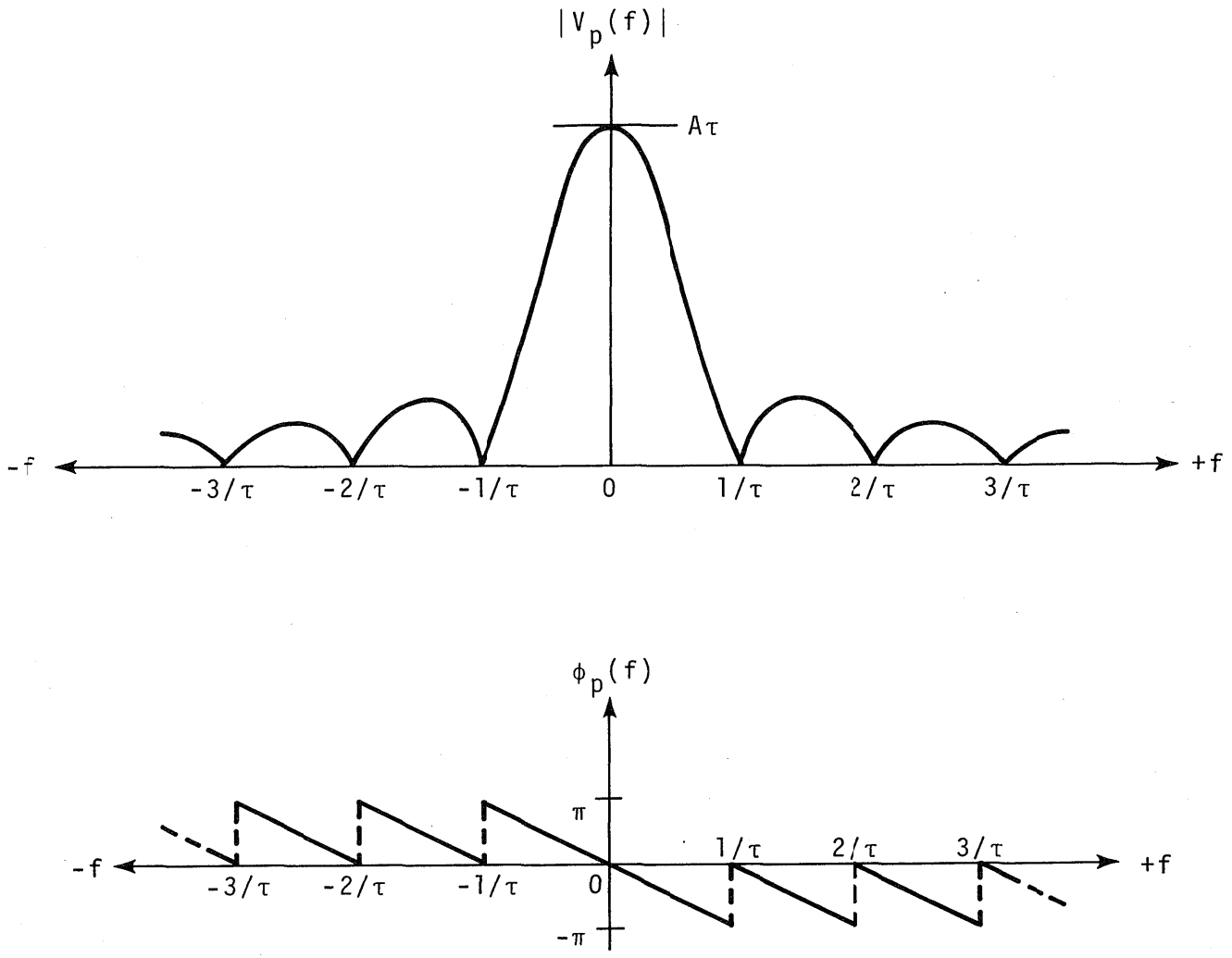

Figure 2-5. Plots of $|V_p(f)|$ and $\phi_p(f)$ versus frequency.

The Fourier transform, V(f), of a finite train of repeating pulses can appear experimentally to be a discrete line spectrum such as would be given by the Fourier series representation. Actually, the spectrum is not a true line spectrum, but only appears to be so because of the sensitivity and resolution characteristics of our test equipment. This can be shown as follows.

The Fourier transform of a regularly repeating rectangular function, such as the one illustrated in figure 2-6(a), which is of finite duration T (as all physical signals are), is a sum of terms given by the equation

$$V_r(f) = A\tau f_o T\left[\sum_{n=-\infty}^{n=\infty} \frac{\sin(\pi n f_o \tau)}{\pi n f_o \tau} \cdot \frac{\sin[\pi(f-nf_o)T]}{\pi(f-nf_o)T}\right] \qquad (2\text{-}19)$$

where f_o is the repetition rate of the physical signal (see section 2.7). Each term of this sum can be plotted as an individual spectral amplitude distribution centered at frequency $f = nf_o$. Three such terms are shown in figure 2-6(b) for $n = 0$ and $n = \pm 1$. As the time interval T becomes longer and longer, the amplitude distributions become more and more compact in the frequency dimension, and, as T approaches infinity, the total amplitude distribution approaches a line spectrum. However, in the regions between the frequencies where the amplitude distribution is bunched up in narrow clumps, $V_r(f)$ is not zero but only extremely small. Because of this limiting form, which is what is observed in practice, many investigators have the erroneous impression that the spectrum amplitude for a finite periodic signal is a line spectrum. More importantly, through confusion with the Fourier series line spectrum, this can mislead one into thinking that these "lines" represent the amplitudes of sinusoid voltages at specific frequencies. Such is not the case, as was shown in section 2.3.

Note from figure 2-4 that $V_p(f)$ is not constant with frequency. This is true for any physical signal. Thus, spectrum amplitude, S(f), is not constant with frequency, but varies in a manner that is determined by the signal waveform. Often an impulse generator will be specified by its spectrum amplitude at very low frequency, and it is then tacitly assumed that this value is applicable up to a frequency where S(f) is 3 dB below this value. It must be emphasized, however, that no physical signal is truly "flat" over all frequencies since this, of course, would require that it contain an infinite amount of energy.

2.5 Use of the Fourier Transform

The discussion thus far has focussed on three characteristics of the Fourier transform, V(f), that are often not understood. This section will give some examples of how V(f) occurs in equations relating to electromagnetic measurements.

First, consider the inverse Fourier transform, eq. (2-2), by which a physical signal can be described in the time domain when the frequency domain quantity V(f) is known. For the signal given by eq. (2-5), which originated from eq. (2-4), the inverse Fourier transform yields the expression (see

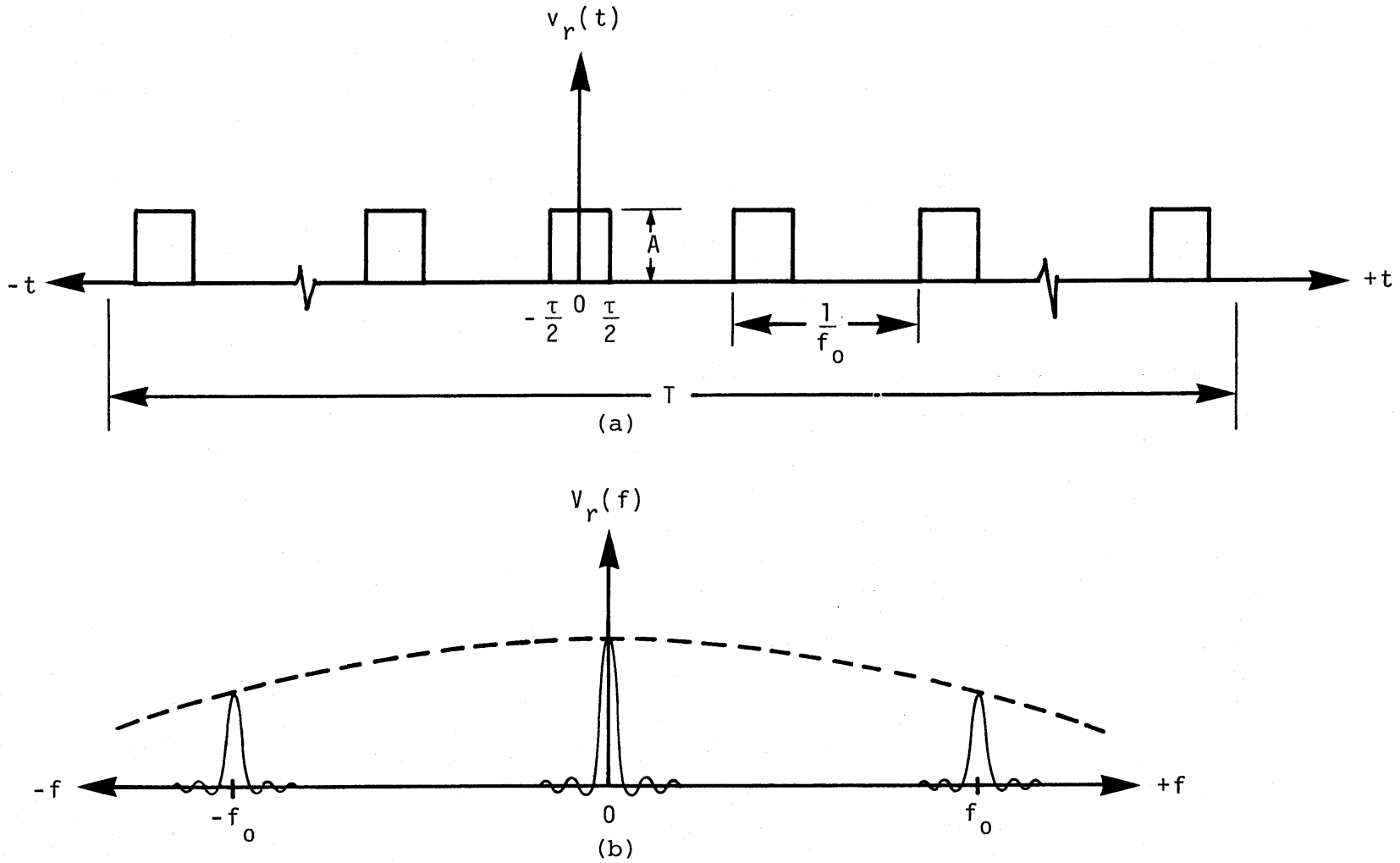

Figure 2-6. (a) Finite, regularly repeating rectangular baseband pulse train. (b) Fourier transform of above pulse train.

section 2.8)

$$v_p(t) = A\tau \int_{-\infty}^{\infty} \frac{\sin(\pi f\tau)}{\pi f\tau} \cos[2\pi f(t-\tau/2)]df. \qquad (2\text{-}20)$$

Note that, in general, the value of v(t) at any time t is an integral over frequency of a function of frequency. Thus, $v_f(t)$ is also an area which, in this example, has the dimensional unit of volts.

Figure 2-7 shows a portion of a three-dimensional plot of the integrand, z(f,t), of eq. (2-20), where

$$z(f,t) = A\tau \frac{\sin(\pi f\tau)}{\pi f\tau} \cos[2\pi f(t-\tau/2)]. \qquad (2\text{-}21)$$

This wavy surface has a "sine x over x" shape in the frequency direction at time $t = \tau/2$ and a cosine shape in the time direction. The surface extends to plus and minus infinity in both the time and frequency domains. The area under the function z(f,t), at a specified time t, is the value of $v_p(t)$ at that time (see figure 2-8).

Because v(t) for every physical signal is a purely real function of time, v(f) is Hermitian, and therefore its real part is alway an even function, its imaginary part is always odd, and

$$V(f) = V^*(-f). \qquad (2\text{-}22)$$

Using this mathematical property, eq. (2-2) can be written

$$v(t) = 2 \int_0^{\infty} |V(f)| \cos[2\pi ft + \phi(f)]df, \qquad (2\text{-}23)$$

where $\phi(f)$ is the phase of V(f). Equation (2-23) applies to all physical signals. This form of mathematical representation has the engineering merit that the integral is over the positive frequency domain only.

The spectrum amplitude

$$S(f) = 2|V(f)| \qquad (2\text{-}24)$$

thus appears explicitly in eq. (2-23) as the amplitude of a cosine function. The quantity $2|V(f)|$ also appears in other working equations where a spectrum amplitude is involved.

Three examples where S(f) is used are as follows:

1. If v(t) is applied to a two-port network which has an impulse response h(t), the network response, r(t), is given by the equation

$$r(t) = \int_0^{\infty} S(f) \cdot |H(f)| \cdot \cos[2\pi ft + \phi(f) + \theta(f)]df \qquad (2\text{-}25)$$

where $|H(f)|$ and $\theta(f)$ are the magnitude and phase of the transfer function of the network. It is this application for which the knowledge of spectrum amplitude has its greatest practical use, namely, for the calibration of Field Intensity Meters and Noise Meters.

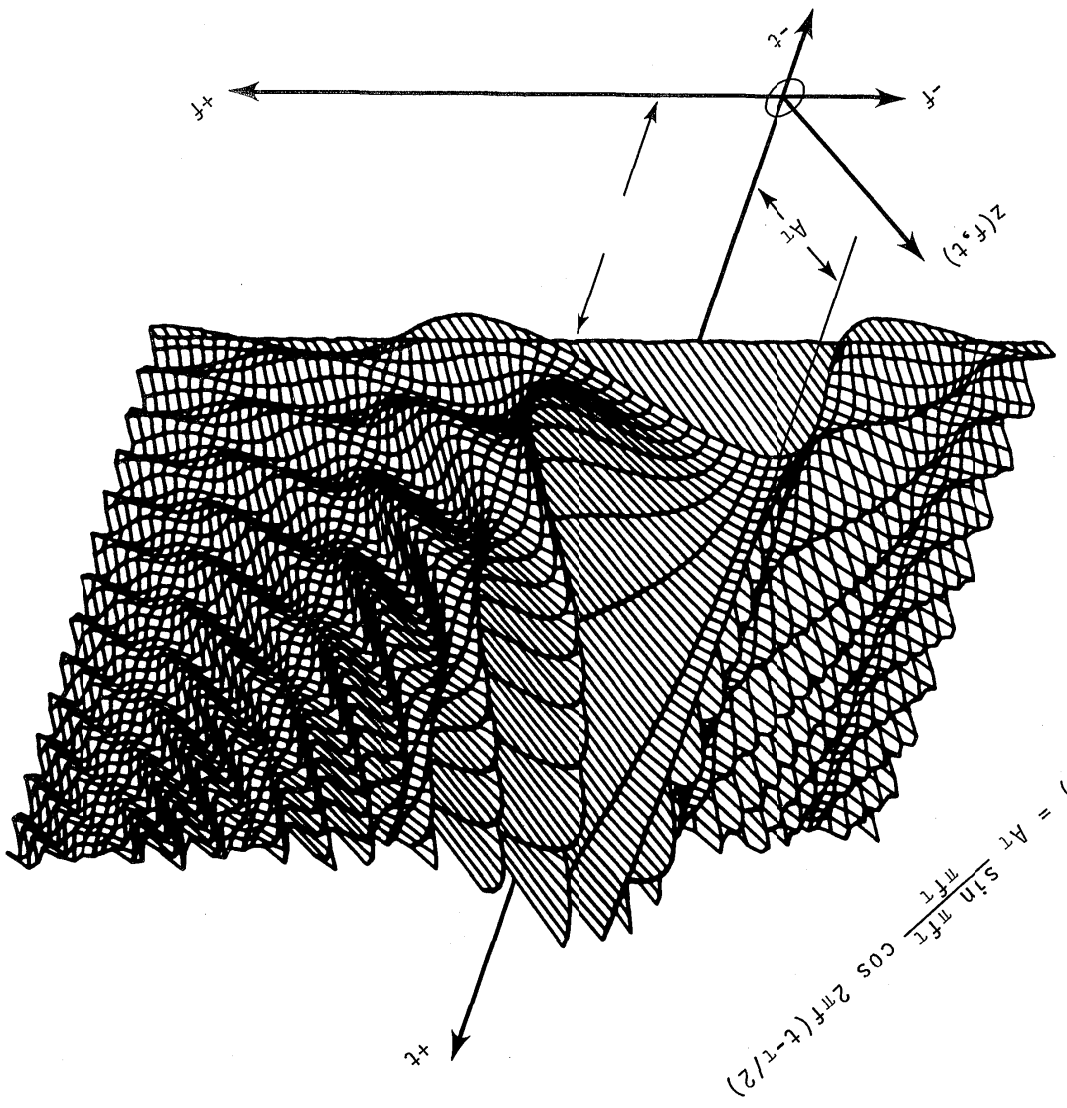

Figure 2-7. Three-dimensional plot of z(f,t).

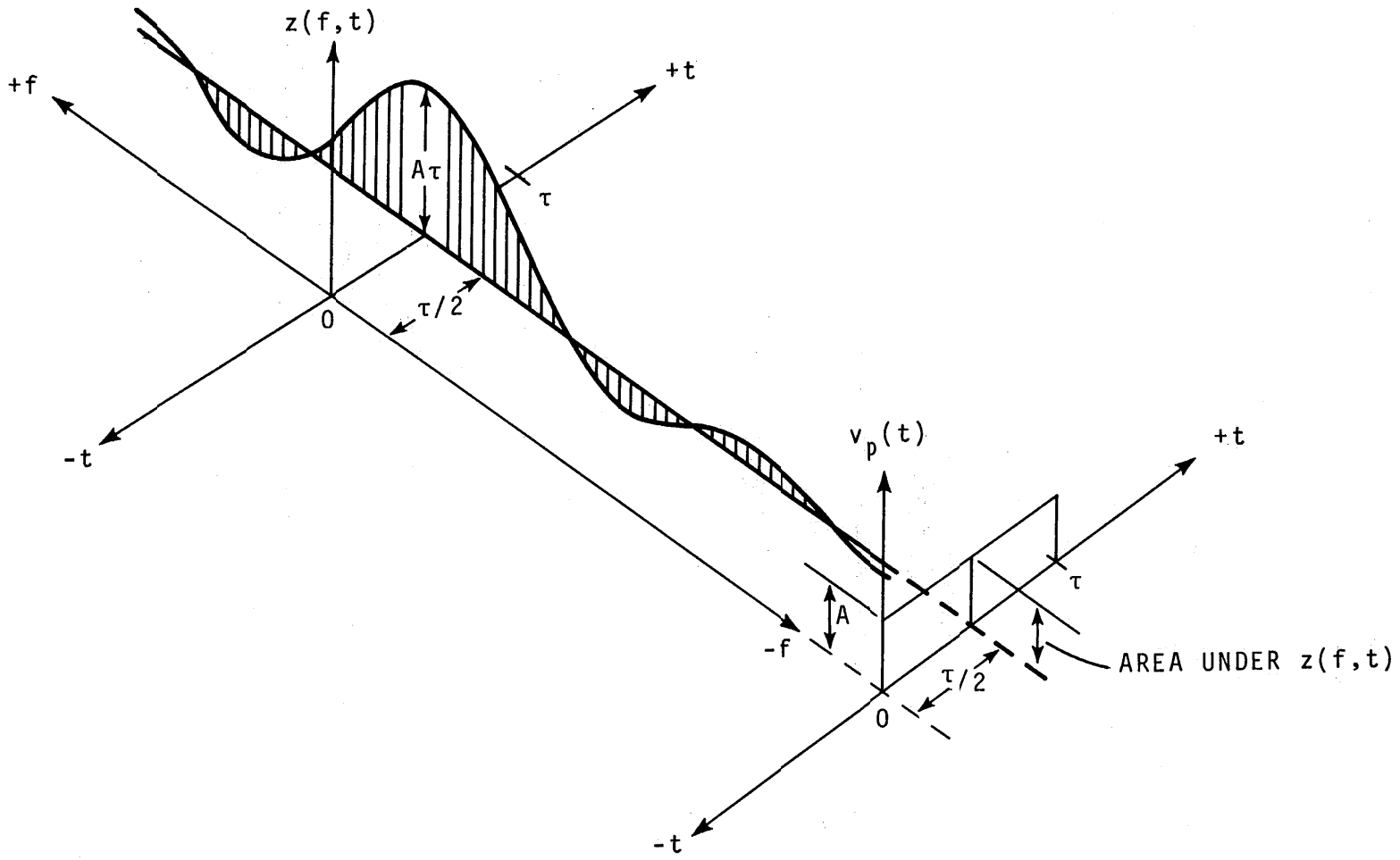

Figure 2-8. Illustrating the relationship between z(f,t) and $v_p(t)$.

2. Another example is the measurement of the impulse bandwidth, IBW, of an idealized bandpass filter [2] using the equation

$$IBW = \frac{R_{(max)}}{S(f)G_o} \tag{2-26}$$

where $R_{(max)}$ is the maximum value of the envelope of the network response r(t), and G_o is the network maximum gain.

3. The total energy, E_t, delivered by v(t) to a resistance R is given by the equations

$$E_t = \frac{1}{R} \int_{-\infty}^{\infty} v^2(t)\, dt = \frac{1}{R} \int_{-\infty}^{\infty} |V(f)|^2\, df \tag{2-27}$$

$$= \frac{1}{2R} \int_{o}^{\infty} S^2(f) df. \tag{2-28}$$

The part, E_b, of E_t, that lies in the frequency band from f_1 to f_2 is given by the equation

$$E_b = \frac{1}{2R} \int_{f_1}^{f_2} S^2(f) df. \tag{2-29}$$

The total energy, E_n, due to the output signal from a two-port network is given by the equation

$$E_n = \frac{1}{2R} \int_{o}^{\infty} S^2(f) \cdot |H(f)|^2\, df. \tag{2-30}$$

Signal power can be derived from these energy equations.

2.6 Summary

In summary, we have emphasized the following points:

First, the frequency-domain representation of a physical signal is a complex mathematical quantity with both a magnitude and a phase.

Second, this complex quantity, the Fourier transform, has dimensional units (e.g., volts per hertz) that are different from those of the time domain representation (e.g., volts) of the physical signal. Thus it is a type of density function that describes how the strength of the signal is distributed with frequency.

Third, the Fourier transform of every physical signal is continuously defined throughout the entire frequency domain. It is not a discrete or true line function of frequency.

Fourth, twice the magnitude of the Fourier transform is defined as the spectrum amplitude, and is a useful engineering quantity because it appears in this form in many useful algebraic relationships. Like the Fourier transform, it is a continuously defined function in the frequency domain, and not a discrete line spectrum nor a single-valued quantity independent of frequency. It may not of itself be sufficient to adequately describe a physical signal in the frequency domain. One may also need to know the phase of V(f).

Finally, the dimensional units of spectrum amplitude are both volt-seconds and volts per hertz, equivalently. However there may be practical reasons for using one set of units rather than the other.

2.7 Derivation of $V_r(f)$

For the finite regularly repeating function shown in figure 2-6(a), $v_r(t)$ is the convolution of the eternal periodic function, $v_e(t)$, and a gate function, $g(t)$,

$$v_r(t) = v_e(t) * g(t) \tag{2-31}$$

where

$$v_e(t) = A, \; -\frac{\tau}{2} < t < \frac{\tau}{2}$$

$$= 0, \begin{cases} \frac{\tau}{2} < t < \frac{1}{f_o} - \frac{\tau}{2} \\ -\frac{1}{f_o} + \frac{\tau}{2} < t < -\frac{\tau}{2} \end{cases}$$

$$= A, \begin{cases} \frac{1}{f_o} - \frac{\tau}{2} < t < \frac{1}{f_o} + \frac{\tau}{2} \\ -\frac{1}{f_o} - \frac{\tau}{2} < t < -\frac{1}{f_o} + \frac{\tau}{2} \end{cases}$$

$$= 0, \begin{cases} \frac{1}{f_o} + \frac{\tau}{2} < t < \frac{2}{f_o} - \frac{\tau}{2} \\ -\frac{2}{f_o} + \frac{\tau}{2} < t < -\frac{1}{f_o} - \frac{\tau}{2} \end{cases} \tag{2-32}$$

etc.,

and

$$g(t) = 1, \; -\frac{T}{2} < t < \frac{T}{2}$$

$$= 0 \text{ elsewhere.} \tag{2-33}$$

From the time-convolution theorem,

$$v_e(t) * g(t) \leftrightarrow V_e(f)G(f) \tag{2-34}$$

where $V_p(f)$ and $G(f)$ are the Fourier transforms of $v_e(t)$ and $g(t)$, respectively, and the symbol ($\leftrightarrow$) reads "is the transform of" in both directions.

The Fourier transform of $v_e(t)$ is [6]

$$V_e(f) = A\tau f_o \sum_{n=-\infty}^{n=\infty} \frac{\sin(\pi n f_o \tau)}{\pi n f_o \tau} \cdot \delta(f-nf_o) \tag{2-35}$$

where δ is the unit impulse function. The Fourier transform of $g(t)$ is

$$G(f) = T \frac{\sin(\pi fT)}{\pi fT} \tag{2-36}$$

which is similar to eq. (2-14) except that in this case the imaginary part is zero because of the choice of time origin. Therefore, the Fourier transform of $v_r(t)$ is

$$\begin{aligned} V_r(f) &= V_e(f)G(f) \\ &= A\tau f_o T \frac{\sin(\pi fT)}{\pi fT} \sum_{n=-\infty}^{n=\infty} \frac{\sin(\pi n f_o \tau)}{\pi n f_o} \cdot \delta(f-nf_o) \\ &= A\tau f_o T \left\{ \sum_{n=-\infty}^{n=\infty} \frac{\sin(\pi n f_o \tau)}{\pi n f_o \tau} \cdot \frac{\sin[\pi(f-nf_o)T]}{\pi(f-nf_o)T} \right\}. \end{aligned} \tag{2-37}$$

2.8 Derivation of $v_p(t)$

For the baseband pulse, figure 2-1, we use eqs. (2-2) and (2-14) to obtain

$$\begin{aligned} v_p(t) &= \int_{-\infty}^{\infty} V_p(f) e^{j2\pi ft}\, df \\ &= A\tau \int_{-\infty}^{\infty} \frac{\sin(\pi f\tau)}{\pi f\tau} e^{j(2\pi ft - \pi f\tau)} df \\ &= A\tau \int_{-\infty}^{\infty} \frac{\sin(\pi f\tau)}{\pi f\tau} \cos[2\pi f(t-\tau/2)] df, \end{aligned} \tag{2-38}$$

since

$$A\tau \int_{-\infty}^{\infty} \frac{\sin(\pi f\tau)}{\pi f\tau} \sin[2\pi f(t-\tau/2)] = 0.$$

3. SPECTRUM AMPLITUDE GENERATION

This chapter deals with the techniques commonly used to generate electrical signals which have a broadband spectrum amplitude. The first section presents a tabulation and figures of S(f) for various common waveforms. Section 3.2 describes mercury switch impulse generators while section 3.3 describes similar generators which use avalanche transistors. Section 3.4 describes a new solid state impulse generator developed at NBS which produces a useful spectrum to 6 GHz. Section 3.5 describes a useful technique for generating rf pulses. Finally, section 3.5 describes a broadband microwave impulse generator.

3.1 Amplitude Spectrum of Common Waveforms

In EMC pulse measurements, a limited number of waveforms are commonly encountered. They are the step, truncated ramp, impulse, rectangular pulse, triangular pulse, sine squared pulse, and the rf pulse. These waveforms are important because they can be described mathematically and their spectra can be readily calculated. Actual generators are capable of closely approximating these idealized waveforms.

Table 3-1 lists these various waveforms, their mathematical equations in the time domain, and the equations for their amplitude spectrum, S(f). Figures 3-1 through 3-6 show the waveforms and their respective S(f).

The unit step, figure 3-1, and the truncated ramp, figure 3-2, are power signals and as such do not possess Fourier transforms as defined earlier. They are not absolutely integrable as they do not satify the Dirchlet conditions. The spectral equations given in table 3-1 were obtained from the more general unified Fourier transform by deleting the delta functions [7]. For example, the unified Fourier transform of the unit step is

$$F[u(t)] = \frac{1}{j\omega} + \pi\delta(\omega) \tag{3-1}$$

$$|F[u(t)]| = \frac{1}{\omega}, \qquad \omega > 0. \tag{3-2}$$

The spectrum of the ideal step, figure 3-1, is inversely proportional to frequency. It is thus characterized by a constant slope of -20 dB/decade. The truncated ramp's spectrum, figure 3-2, is identical to that of the ideal step for low frequencies. However as the frequency increases and approaches $1/t_o$, S(f) departs from the -20 dB/decade slope and assumes more the characteristic of the triangular pulse, figure 3-4.

The rectangular pulse, figure 3-3, is seen to have a sin(x)/x variation (see also Chapter 2). A distinguishing feature of this pulse and most other impulsive shaped pulses, such as the triangular pulse, figure 3-4, and the sine squared pulse, figure 3-5, is the fact that the spectrum amplitude approaches a constant value $2\ v_o t_o$ at low frequencies. $v_o t_o$ is simply the area under the v(t) curve and is defined as the "Impulse Strength" [2]. The shape of the

Table 3-1. Amplitude Spectrum of Common Waveforms

Waveform	V(t)	S(f)
Step	$V_o u(t)$	$V_o/(\pi f)$
Truncated Ramp	$\frac{V_o}{t_o}[t\,u(t) - (t-t_o)u(t-t_o)]$	$\left\|\frac{V_o t_o}{\sqrt{2}\,\pi}\right\| \frac{[1-\cos(2\pi f t_o)]^{1/2}}{(t_o f)^2}$
Rectangular Pulse	$V_o[u(t) - u(t-t_o)]$	$2V_o t_o\left\|\frac{\sin(\pi f t_o)}{(\pi f t_o)}\right\|$
Triangular Pulse	$\frac{V_o}{t_o}[t\,u(t) - 2(t-t_o)u(t-t_o) + (t-2t_o)u(t-2t_o)]$	$2V_o t_o\left\|\frac{\sin(\pi f t_o)}{(\pi f t_o)}\right\|^2$
Sine Squared Pulse	$V_o\left[\sin^2\left(\frac{\pi t}{2t_o}\right)u(t) - \sin^2\left(\frac{\pi t}{2t_o}\right)u(t-t_o)\right]$	$2V_o t_o\left\|\frac{\sin(2\pi f t_o)}{(2\pi f t_o)[1-(2f t_o)^2]}\right\|$
RF Pulse	$V_o[\sin(2\pi f_c t)u(t+t_o/2) - \sin(2\pi f_c t)u(t-t_o/2)]$	$V_o t_o\left\|\frac{\sin(\pi\Delta f t_o)}{(\pi\Delta f t_o)} - \frac{\sin[\pi(2f_c+\Delta f)t_o]}{[\pi(2f_c+\Delta f)t_o]}\right\|$ where $\Delta f = f - f_c$

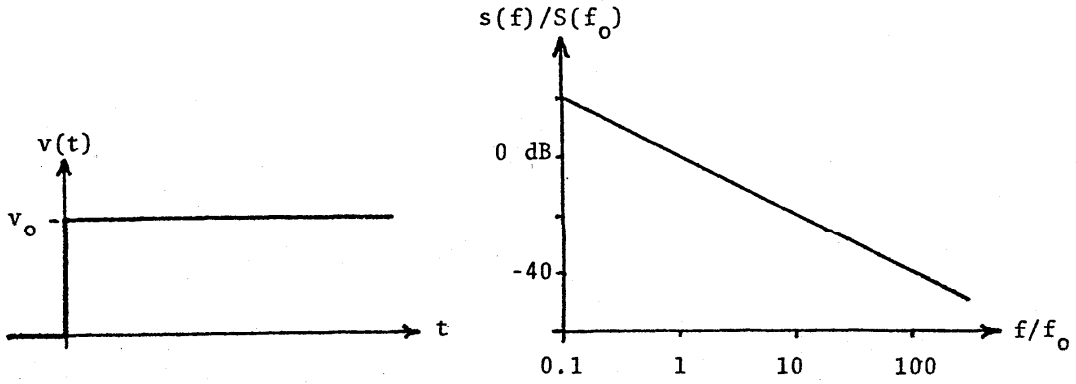

Figure 3-1. Step.

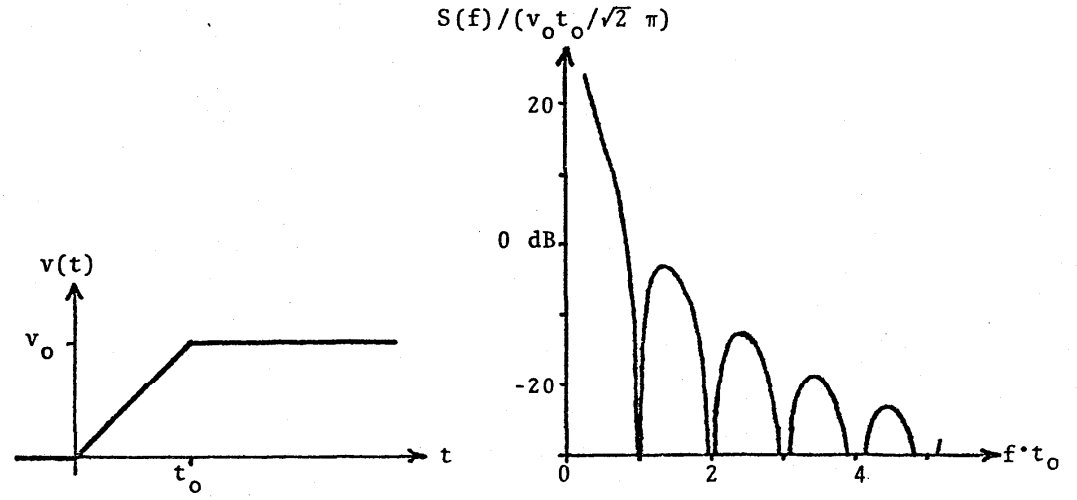

Figure 3-2. Truncated ramp.

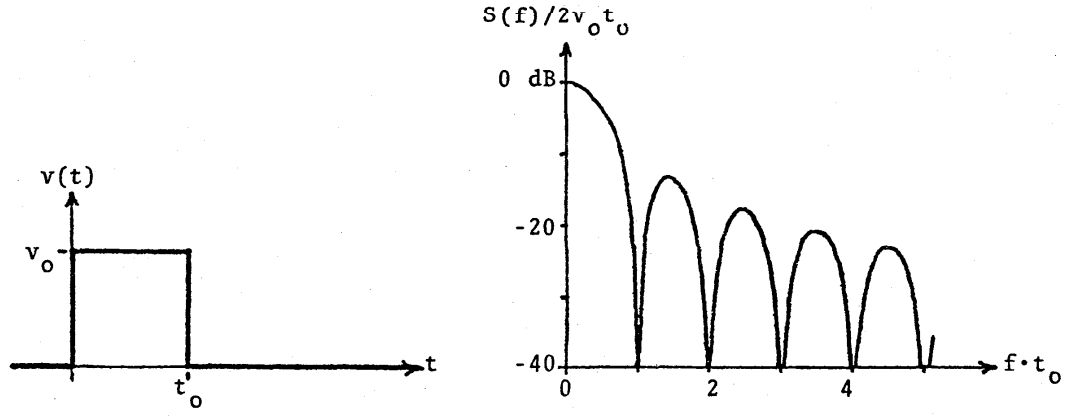

Figure 3-3. Rectangular pulse.

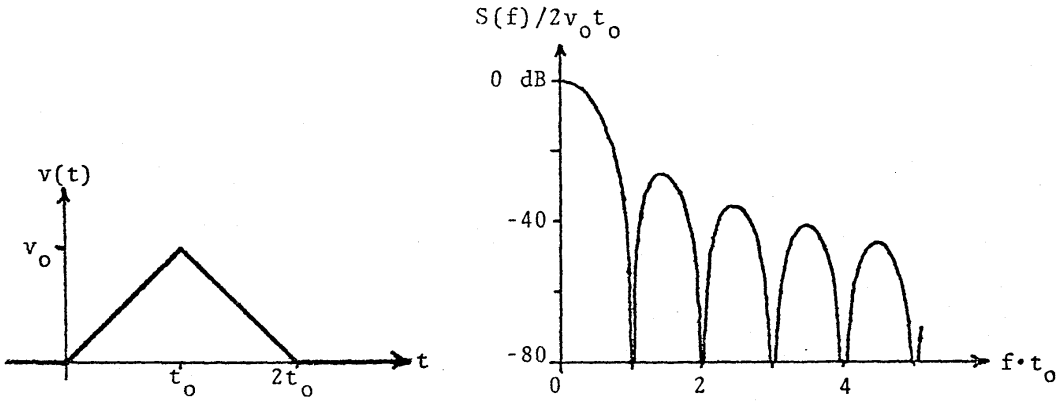

Figure 3-4. Triangular pulse.

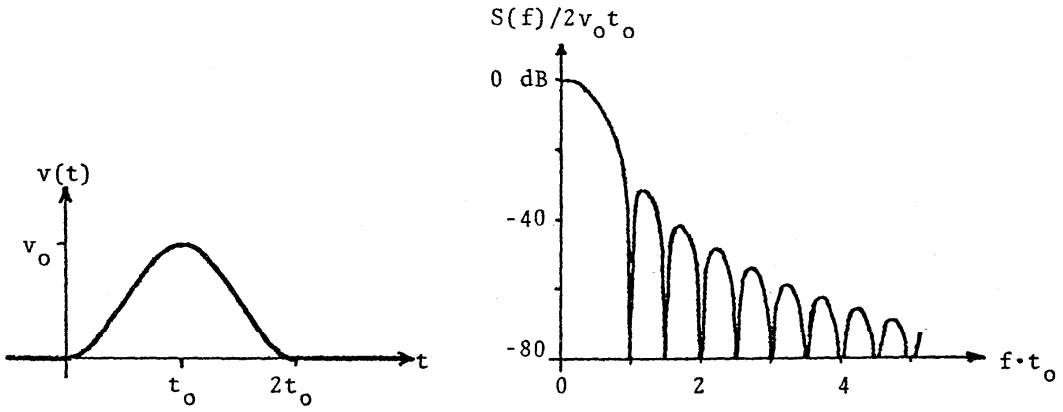

Figure 3-5. Sine squared pulse.

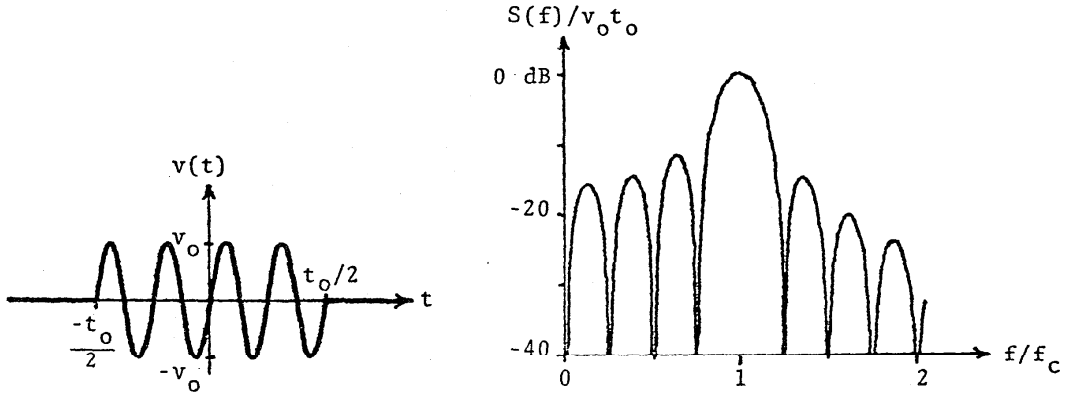

Figure 3-6. Rectangular rf pulse.

spectrum for the triangular pulse, figure 3-4, is identical to that of the rectangular pulse except that S(f) of the triangular pulse drops faster with frequency. Note that the vertical scale is 20 dB/div. instead of 10 dB/div. The sine squared pulse, figure 3-5, has its first spectrum zero at $1/t_o$ like earlier pulses. Its higher order zeros occur twice as often.

A special case of the rectangular pulse is the true impulse or as it is called in mathematics, the Dirac delta function, $\delta(t)$. It is defined as

$$\delta(t) = \lim_{a \to 0} \frac{u(t) - u(t-a)}{a} \tag{3-3}$$

$$\int_{-\infty}^{\infty} \delta(t) = 1 \tag{3-4}$$

This is seen to be a rectangular pulse of width a and height 1/a with a constant unit area. Its spectrum is like that of the rectangular pulse except that its first $\sin(x)/x$ zero occurs at infinity. In other words its spectrum amplitude is constant for all frequencies.

In practice a narrow rectangular pulse is often referred to as an impulse. This is done with the implicit understanding that its spectrum amplitude is essentially constant for all frequencies of interest.

The spectrum of the rectangular rf pulse, figure 3-6, is seen to be simply that of the rectangular pulse transposed in frequency by the carrier frequency, f_c. However, the sidebands are not symmetrical. The dissymmetry is caused by the second term involving $(2f_c + \Delta f)$. This second term accounts for the aliasing caused by the transposition of the rectangular pulse spectrum to both $+f_c$ and $-f_c$. When the rf pulse contains an integer number of cycles, i.e., $t_o = N/f_c$, then the number of zeros of S(f) between zero and f_c are equal to N. For frequencies near f_c (i.e., $\Delta f \simeq 0$), S(f) is essentially constant and approximately equal to $v_o t_o$.

3.2 Mercury Switch Impulse Generator

Most of the impulse generators used in the field for broadband calibration of field intensity meters (FIM) are of the mercury switch variety. They are attractive for several reasons including (1) low cost, (2) reasonably predictable output, and (3) easily adjustable output.

A mercury switch impulse generator is an extremely simple circuit, figure 3-7 [8]. It consists of a dc voltage source, V_{bb}, a charging resistor, R_c, a short coaxial transmission line of impedance R_o and length ℓ, and a mercury wetted mechanical switch. Initially with the switch open, the transmission line appears as a capacitor and is charged up to the supply voltage, V_{bb}, through the charging resistor, R_c. When the switch is closed the transmission line discharges into the load R_L. During discharge the line appears as a source of voltage V_{bb} and internal resistance R_o. If the load is matched to

the line,

$$R_L = R_o. \tag{3-5}$$

Then the output voltage, V_o, is simply

$$V_o = V_{bb}/2 \tag{3-6}$$

and the output pulse duration, t_o, is fixed at twice the electrical transit time of the line.

$$t_o = 2\ell/v_p. \tag{3-7}$$

v_p is the velocity of light in the line ($v_p \sim 3 \times 10^8$ m/s in air). Thus a 30 cm length of air line will produce a 2 ns pulse.

This generator thus produces a rectangular pulse of amplitude, V_o, duration, t_o, impulse strength, $V_o t_o$, and at low frequency, its spectrum amplitude is

$$S(f) = 2V_o t_o, \quad f << \frac{1}{t_o}. \tag{3-8}$$

If the supply voltage is adjustable then S(f) may also be varied.

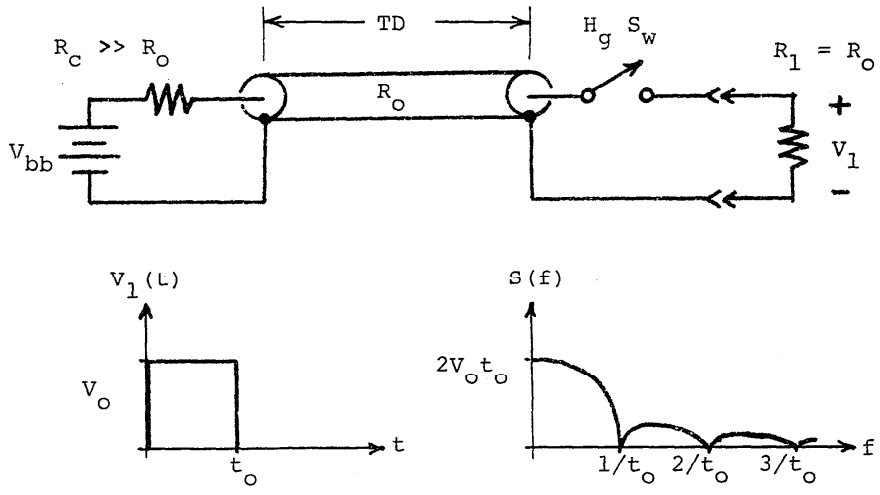

Figure 3-7. Mercury switch impulse generator.

For proper functioning the load resistance must equal the line impedance. To insure that this condition is met some manufacturers permanently install a coaxial attenuator between the switch and the output connector.

Typical pulse transition times (rise and fall times) are of the order of 0.5 ns. However, with microminiature mercury switches, transition times of 40 ps have been achieved [9]. Pulse amplitudes as large as 2 kV are possible with pressurized mercury wetted switches. Even higher voltages are possible if the mercury switch is replaced with a spark gap. Some spark gaps are triggered externally with a laser pulse.

Equation (3-7) is quite accurate for HF IG's with 10 ns or longer pulses. Its accuracy suffers for $t_o < 1$ ns, because the waveform is no longer rectangular. The transition (rise and fall) times are comparable to the duration. It also becomes difficult to model or measure accurately the actual time delay of the charge line and the switch.

The major disadvantage of the mercury switch is its mechanical nature which inherently limits its switching repetition rate to a few hundred hertz at most. Also due to its mechanical inertia, friction, etc., it is not possible to trigger the switch closure with better than a few hundred microseconds precision. This triggering uncertainty leads to much phase jitter.

3.3 Avalanche Transistor Impulse Generator

The trigger uncertainty and the low repetition rate disadvantage of the mercury switch can be eliminated by replacing the mercury switch in an impulse generator, figure 3-7, with an avalanche transistor. Trigger jitter of less than 10 ps and repetition rates of several MHz are possible. This section briefly describes an inexpensive, simple impulse generator developed at NBS several years ago [10]. The major disadvantage is its lower voltages compared to mercury switches (50-100 volts are typical).

Avalanche multiplication in reverse-biased pn junctions is a result of impact ionization produced by mobile charge carriers. If the electric field in the depletion region of the pn junction is large enough, an electron moving through the crystal lattice gains sufficient energy to release an additional electron and hole when it collides with an atom in the lattice. The two free electrons may then cause additional ionizations and an ever-growing cascade, or an avalanche of ionization occurs.

In transistors the avalanche breakdown [11] may be controlled through the injection of carriers by the base current, figure 3-8. Normal transistor operation lies in the region of collector-emitter voltages between 0 and BV_{CEO} and forward base currents. BV_{CEO} is the breakdown voltage from the collector to the emitter with the base open circuited. If a reverse base current is applied, then the collector-emitter voltage may be increased above BV_{CEO} before an avalanche breakdown is reached. The upper voltage limit BV_{CBO} is reached when $I_b = I_c$. BV_{CBO} is the breakdown voltage from the collector to the base with

the emitter open circuited. The avalanche region of the transistor lies between BV_{CEO} and BV_{CBO}. An important item to notice in figure 3-8 is the negative slope of the constant I_b curves in the avalanche region. The negative slope means that the small-signal resistance, $r_a = \Delta V/\Delta i$, is negative. A negative resistance implies unstable operation. Thus the avalanche transistor is useful as an oscillator or switching element. The switching speeds that can be obtained are quite fast because of the multiplying effect of the avalanche breakdown. Transition times of 500 picoseconds have been obtained.

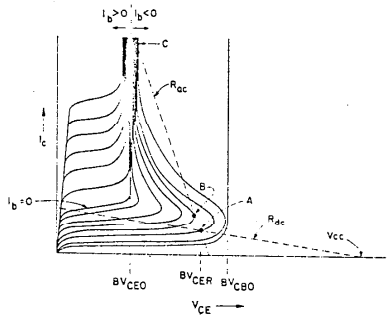

Figure 3-8. Transistor V-I characteristic curves including the avalanche region.

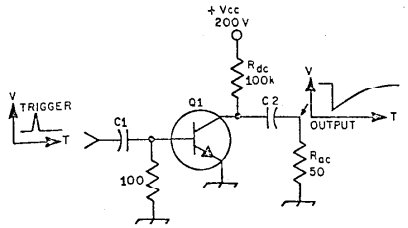

Figure 3-9. Typical avalanche-transistor switching circuit.

A typical avalanche transistor switching circuit is shown in figure 3-9. The large supply voltage, V_{cc}, and dc load resistor, R_{dc}, of figure 3-9 place the transistor at the stable operating point A, figure 3-8. The positive trigger pulse injects an additional quantity of base current causing the collector current to move along the ac load line, R_{ac}, to operating point B. Point B is in the negative resistance region and is an unstable point. Thus the operating point rapidly switches along the ac load line to the next stable location, point C.

Many transistors are capable of avalanche operation although very few are actually specified as avalanche transistors. If the specification sheet for a given transistor says the BV_{CBO} is greater than BV_{CEO}, it is probable that the transistor will avalanche, although the switching characteristic may not be fast. Very few pnp transistors have been found that will avalanche.

An impulse generator that will produce a usable frequency spectrum to beyond 1 GHz is shown in figure 3-10. The circuit is an avalanche transistor adaption of the classical mercury switch -- charged transmission-line pulse generator [12]. Charge line, DL1, is charged through R4 to BV_{CER} of Q1. When a positive trigger pulse is coupled through C1 and R1 into the base of Q1,

avalanche breakdown is initiated. Q1 rapidly switches to its lower breakdown voltage BV_{CEO} and allows the charge line, D11, to discharge into R3 and the external 50-ohm load. A square pulse is generated with transition times of the order of 500 picoseconds. The pulse duration is fixed at twice the electrical transit time of the charge line, DL1. An impulse can be formed by shortening the charge line until the desired impulse width is obtained. As soon as the charge line is discharged Q1 reverts to a low current state. The output delay line, DL2, is included so that reflections from the external load do not arrive back at Q1 until it has switched off. R3 is included to provide a 50-ohm reverse termination for reflections. This impulse generator is designed to be driven directly by TTL pulses. U1 is included to demonstrate this fact. It can be driven at repetition rates up to 1.5 MHz.

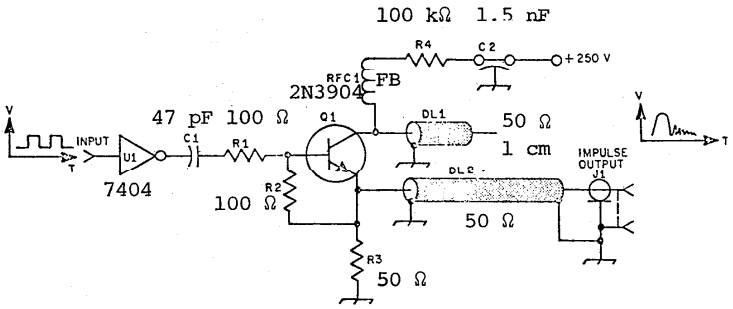

Figure 3-10. Avalanche transistor impulse generator.

Figure 3-11 shows the impulse output measured with a 50-ohm sampling oscilloscope with a 10- to 90-percent transition time of approximately 28 picoseconds. The impulse has a peak amplitude of 14 volts and an impulse duration of 420 picoseconds. Figure 3-12 shows the impulse spectrum as measured on a spectrum analyzer over the frequency range of 500 kHz to 1250 MHz. The spectrum is approximately 10 dB down at 1250 MHz. Usable 10-kHz markers were measured up to 1250 MHz. The amplitude of the 10-kHz markers was approximately 80 microvolts at 150 MHz, 64 microvolts at 450 MHz, and 30 microvolts at 1250 MHz.

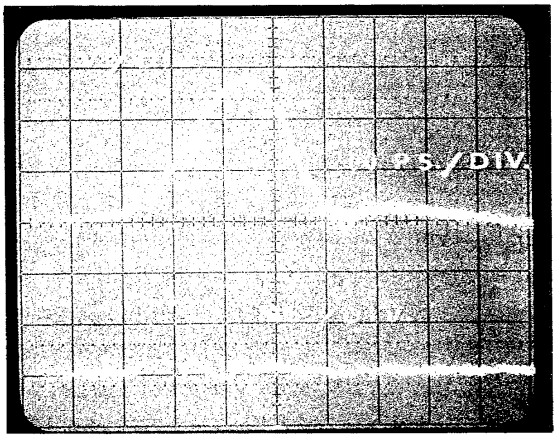

Figure 3-11. Avalanche transistor impulse generator output.

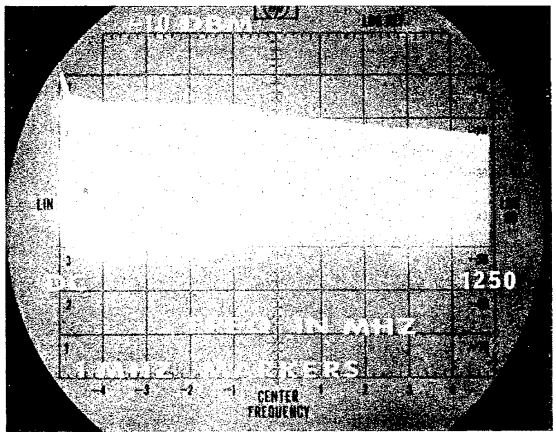

Figure 3-12. Avalanche transistor impulse generator spectrum.

3.4 NBS Step Recovery Diode Impulse Generator

Extremely fast transition times of the order of 100 ps can be obtained using step recovery diodes (SRD) to shape the output pulses from avalanche transistors. Voltage amplitudes of 10-30 volts are possible. Impulses with durations of 100 ps produce a useful spectrum well into the microwave region.

This section describes a baseband impulse generator recently developed at NBS [13]. The generator is completely solid-state. It uses avalanche transistors and step recovery diodes to generate a 100 ps duration impulse of 8 volts amplitude into 50 ohms. The spectrum amplitude of the impulse is greater than 60 dBμV/MHz at frequencies up to 5 GHz. The generator source impedance is a well matched 50 ohms. The repetition rate of the generator is controlled by a quartz crystal oscillator and is adjustable in a 1,2,5 sequence from 50 Hz to 100 kHz.

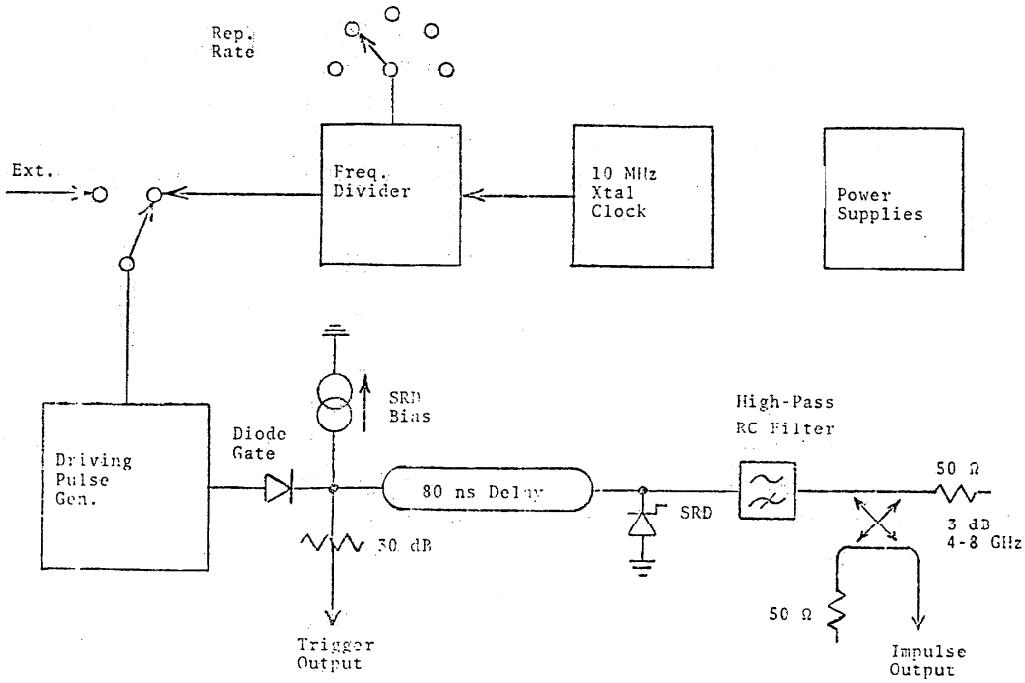

Figure 3-13. Block diagram of the NBS SRD impulse generator.

Figure 3-13 is the basic block diagram of the NBS impulse generator, series 3-75-X. The internal repetition rate is derived from a 10 MHz crystal controlled oscillator. The 10 MHz frequency is divided into lower frequencies from 100 kHz down to 50 Hz using TTL, ÷ 2, ÷ 5, and ÷ 10 dividers. The internal or external repetition rate source is used to trigger the driving pulse generator. This generator develops a 50 volt, 0.7 ns transition time pulse in a 25 ohm circuit using avalanche transistors and a step recovery diode. This pulse is driven through a diode gate onto two 50 ohm circuits in parallel. The first is a 30 dB attenuator the output of which is used as the trigger output. The second is an 80 ns coaxial delay line. At the output of the delay line is an extremely fast step recovery diode (SRD) which sharpens the leading edge of the driving pulse to a transition time less than 100 ps. Bias current for the SRD is supplied at the input to the delay line. This sharpened pulse is then differentiated in an R-C high pass filter and by passing it through a 4-8 GHz, 3 dB directional coupler, thus producing the desired output impulse. The purpose of the directional coupler is twofold. In addition to providing the necessary differentiation of the fast step from the SRD it also provides an excellent 50 ohm generator source impedance.

The primary purpose of the impulse generator is as a source of broadband impulse noise with as flat a spectrum as possible. To achieve the flat spectrum objective the output should be a pure impulse with no other spurious pulses present. Low-level, wide-spaced pulses will distort the spectrum particularly at low frequencies. To achieve this objective calls for design compromises that would not be made if the objective were simply to generate the highest amplitude, narrowest impulse possible.

To insure that only a single impulse is obtained, the driving pulse is shaped to be an exponential pulse with a fast leading edge transition time of 0.7 ns and an exponential decay time constant of 15 ns. After sharpening by the SRD, the differentiating action of the high pass filter and the directional coupler produce an impulse only on the fast rising leading edge of the driving pulse. A portion of the driving pulse incident upon the SRD is reflected back toward the driving pulse generator. If a portion of this reflected signal were allowed to eventually escape from the instrument through the impulse output port it would have the effect of distorting the impulse generator's spectrum particularly at low frequencies. The 30 dB trigger output attenuator is used to internally absorb this reflected signal. This reflection from the SRD is delayed in time by the delay line so that it arrives at the diode gate 160 ns after the driving pulse passed through the gate traveling in the opposite direction. The decay time of the driving pulse and the reverse bias on the gate are chosen so that the gate is nonconducting when the reflection arrives thus forcing the reflection to be absorbed in the 50 ohm, 30 dB attenuator.

The 80 ns delay line also serves an auxiliary purpose in providing an extremely stable time delay between the trigger and impulse outputs for sampling oscilloscope measurements of the impulse output.

Complete circuit description and schematic diagrams are found in appendix A.

Figure 3-14 is a typical waveform into a 50 ohm load from this generator. The impulse consists of a small precursor pulse, the main impulse, a negative undershoot and finally some low level damped perturbations on the baseline that last approximately 2 ns after the main impulse. There are no other signals emanating from the generator earlier or later in time than those shown with the exception of two low level impulses -36 dB and -46 dB below the main impulse occurring 80 ns and 160 ns respectively after the main impulse. The impulse amplitude is 8 volts and its 50% level duration is 100 ps.

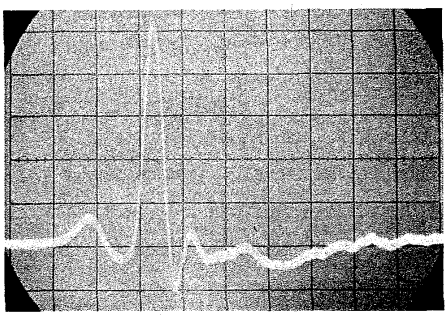

Figure 3-14. Typical output waveform of an NBS SRD impulse generator. Vertical: 50 mV/div. X 30 dB, Horizontal: 200 ps/div.

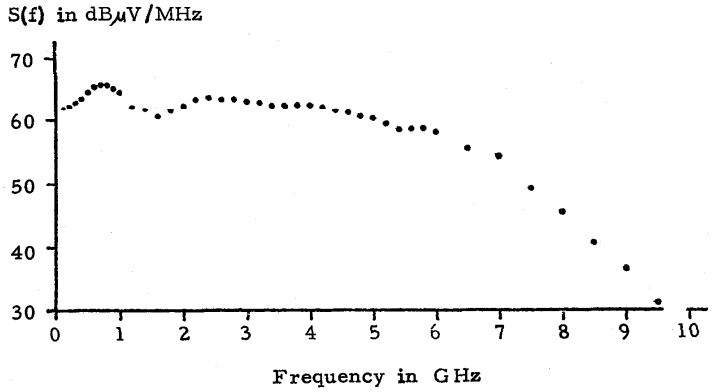

Figure 3-15. Typical spectrum amplitude of an NBS SRD impulse generator.

The spectrum amplitude, S(f), of the impulse is shown in figure 3-15. S(f) is seen to be relatively flat at approximately 62 dBμV/MHz out to 5 GHz with a +3 dB, -2 dB ripple. The peak in the ripple occurs at 0.75 GHz while the minimum occurs at 1.6 GHz. Beyond 6 GHz S(f) drops very rapidly at approximately 30 dB per octave. Due to the ac coupling inherent in the directional coupler, the spectrum amplitude is not flat to dc. It rolls off at frequencies below 20 MHz.

3.5 RF Pulse Generator

Potentially the most accurate method of generating a known spectrum amplitude at a particular frequency is the rf pulse technique [14]. The technique is quite simple. A cw signal generator provides a stable sine wave of known frequency and constant level. An rf switch is driven by a baseband pulse generator and is used to gate on and off the cw sine wave thus producing an rf pulse. This is the classical case of amplitude modulation. The spectrum of the modulation waveform is translated from a distribution about zero frequency to a distribution about the carrier frequency, f_c. As seen earlier, a rectangular pulse produces a sin(x)/x spectrum. Thus a rectangular pulse modulated rf burst produces a sin(x)/x spectrum centered at f_c. This technique has an advantage over baseband impulses in that it can concentrate most of the energy in the signal uniformly in the frequency region where a receiver to be calibrated is tuned.

As shown in table 3-1 the exact expression for S(f) contains two terms

$$S(f) = V_o t_o \left| \frac{\sin(\pi \Delta f t_o)}{(\pi \Delta f t_o)} - \frac{\sin[\pi(2f_c+\Delta f)t_o]}{[\pi(2f_c+\Delta f)t_o]} \right| \tag{3-9}$$

where

$$\Delta f = f - f_c. \tag{3-10}$$

The first sinc (sin(x)/x) term contributes most of the expressions value near the carrier, f_c, while the second sinc function, which is sometimes called the phase correction, will become significant at frequencies far removed from the carrier. The second sinc term becomes important if the rf pulse is short, i.e., if it only contains a small number of rf cycles. The example of figure 3-6 was for an extremely short pulse of only four cycles. For that case the sidebands were quite unsymmetrical. Reeve [14] has made calculations of the importance of the phase correction. For long rf pulses of fifteen or more rf cycles the spectrum amplitude may be approximated as

$$S(f) \simeq V_o t_o \left| \frac{\sin(\pi \Delta f t_o)}{(\pi \Delta f t_o)} \right|. \tag{3-11}$$

In the immediate vicinity of f_c

$$S(f) = S_o = V_o t_o, \quad \Delta f \sim 0. \tag{3-12}$$

As can be seen from eqs. (3-11) and (3-12), S(f) can be completely characterized by knowing the amplitude, V_o, and the duration, t_o. These values can be obtained by direct measurement. The amplitude can be obtained by measuring the output power, P, with the rf switch in the ON state.

$$V_o = \sqrt{2PR}. \tag{3-13}$$

R is the input impedance (typically 50 ohms) of the power meter. The duration, t_o, can be measured by using a calibrated oscilloscope. An alternate technique is to use a spectrum analyzer or receiver to determine the frequency, f_{null}, at which the first null occurs in the rf pulse spectrum. From eq. (3-11) t_o is given by

$$t_o = \frac{1}{f_{null} - f_c}. \tag{3-14}$$

The most critical component in the rf pulse generator is the rf switch. Of utmost importance is its on-off ratio. If the leakage in the off state is too large, then the continuous presence of the carrier will give undesirable results. For carrier suppression of 20 dB below S_o the rf switch on-off isolation must be

$$\text{isolation(dB)} > -20 \log(t_o f_o) + 20 \text{ dB} \tag{3-15}$$

where t_o is the pulse duration and f_o is the pulse repetition rate. As an example using typical numbers of 100 ns pulse duration and 100 Hz pulse repetition rate, a switch isolation in excess of 120 dB is required.

Another important parameter of the rf switch is its switching speed. Ideally, it would have zero switching times. In practice the switching times are limited, and they thus introduce some uncertainty in the pulse duration, t_o. PIN diodes provide excellent rf switches. They are capable of quite high isolation (90 dB) with switching times of the order of 5-50 ns. Another excellent rf switch is a Schottky diode balanced modulator. Switching times of the order of 1 ns are possible. Below 1 GHz balanced modulators are available with excellent isolation (60 dB). Quite fast balanced modulators are also available in the microwave region, but they typically have poor isolation of 20-30 dB.

P. Simpson of NBS has recently built a microwave pulse generator for calibrating microwave receivers [15]. A PIN diode modulator was used as the rf switch. This generator has the characteristics listed in table 3-2.

Table 3-2. NBS microwave pulse generator characteristics.

Frequency Bands:	1-2 GHz 2-4 GHz 4-8 GHz 8-12.4 GHz tunable
Max. cw Output Power into 50 Ohms:	1 mW, except 0.1 mW for 8-12.4 GHz
Pulse Duration:	∿ 20 ns
On and Off Transition Times:	2-5 ns
Max. Spectrum Amplitude into 50 Ohms:	∿ 76 dBμV/MHz except ∿ 66 dBμV/MHz for 8-12.4 GHz
Output Step Attenuator:	0 to 99 dB in steps of 1 dB
Pulse Repetition Rate:	10 Hz to 10 kHz

In addition to the microwave pulse generator [15], NBS has also built an rf pulse generator to cover the frequency range of 5 MHz to 500 MHz. Figure 3-16 is the block diagram of this generator, and table 3-3 lists the characteristics of this generator. An external signal generator is used to provide the cw sine wave. A low level signal of only -27 dBm is required. Broadband amplifiers A1 and A2 amplify the cw sine wave to +3 dBm to drive the double balanced mixers, DBM 1 and 2. A1 and A2 also provide isolation between the signal generator and the mixers. The mixers function as an rf switch. They are driven by simultaneous baseband pulses to turn on the sine wave. The baselines of the pulse generator outputs are independently adjusted to

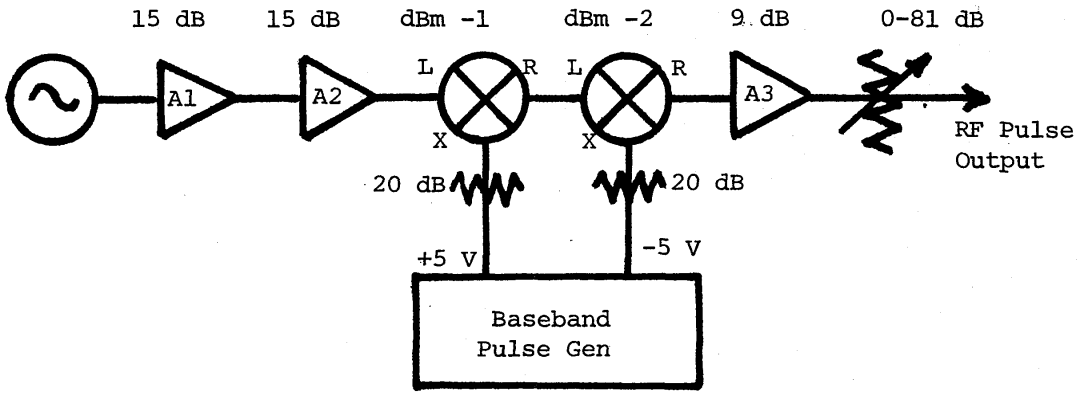

Figure 3-16. NBS rf pulse generator block diagram.

Table 3-3. NBS RF pulse generator characteristics.

Frequency Range:	5-500 MHz determined by ext. signal gen.
Max CW Output Power into 50 Ohms for linear Operation:	+ 5 dBm
On-Off Isolation:	115 dB @ 100 MHz
Pulse Duration:	set by baseband pulse gen.
On and Off Transition Times:	∿ 1 ns
Output Step Attenuator:	0 to 81 dB in steps of 0.1 dB
Pulse Repetition Rate:	set by baseband pulse gen.

optimize the on-off isolation of the mixers. By careful adjustment, isolations in excess of 115 dB have been achieved. The output of the second mixer is -5 dBm in the on state. Amplifier A3 is used to raise this level to +6 dBm. A3 also provides a well matched constant output impedance regardless of the state of the mixers. A set of 50 ohm step attenuators are provided on the output to allow precise setting of the output level. Figure 3-17 is the time domain waveform of a 100 ns, 100 MHz, rf pulse. Figure 3-18 is the spectrum as observed on a spectrum analyzer

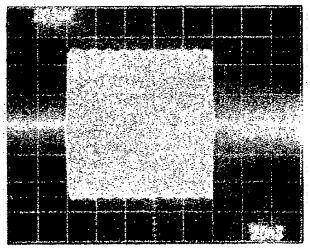

Figure 3-17. RF pulse generator output waveform. 100 ns, 100 MHz rf pulse. Peak power is +4 dBm.

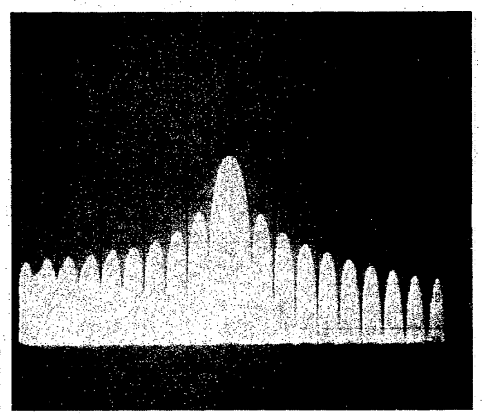

Figure 3-18. Spectrum of 0 dBm, 100 ns, 100 MHz rf pulse. Horizontal scan from 0 to 200 MHz.

3.6 Microwave Impulse Generator

The NBS microwave pulse generator built by P. Simpson [15] is an excellent source of relatively narrowband (< 10 MHz), known, impulsive noise. However, there are some microwave applications such as time domain antenna testing that require a very broadband (several GHz), high power, impulsive noise source. In these cases none of the previously described generators are adequate.

NBS has found that a useful technique of generating broadband, high power impulsive noise is to shock excite a high power traveling wave tube amplifier (TWTA). The TWTA is driven by an extremely narrow (< 100 ps) baseband impulse, such as the output of the NBS SRD impulse generator (section 3.4). The TWTA acts as both a wide bandpass filter (typically octave bandwidths, i.e., 1-2 GHz, 2-4 GHz, etc.) and a high gain amplifier. The output is a short rf pulse of a few rf cycles with a frequency near the low end of the TWTA pass band. Peak power comparable to the output power rating of the TWTA can be obtained. A broadband, adjustable, coaxial attenuator is required between the impulse generator and the TWTA to avoid driving the TWTA into saturation.

With the extremely short pulse duration of this type of generator, it is not possible to use the calibration technique employed for the rf pulse generators of section 3.5 to determine the spectrum amplitude. For this generator the time domain technique described later in section 4.9 is recommended.

Figures 3-19 and 3-20 show waveforms and spectra obtained from several pulsed TWTA's covering C, X and Ku bands, i.e., 4-8 GHz, 8-12.4 GHz, and 12.4-18 GHz. The TWTA's were driven by the NBS SRD impulse generator, figure 3-19(a). The variable attenuator was adjusted to drive the TWTA just below the saturation level. Saturation was evidenced by an abrupt change in the output waveform. The spectrum amplitudes of the TWTA's outputs were measured by the APMS (see section 4.9). As can be seen in figure 3-20, broadband spectrum amplitudes of the order of 80 dBμV/MHz can be obtained. The C band TWTA output is useful (20 dB range) from 2 GHz to 13 GHz. The X band TWTA useful range extends from 4 GHz to 15.5 GHz with the exception of a sharp notch at 9.4 GHz. The Ku band TWTA appears to be useful from approximately 10 GHz to 16 GHz.

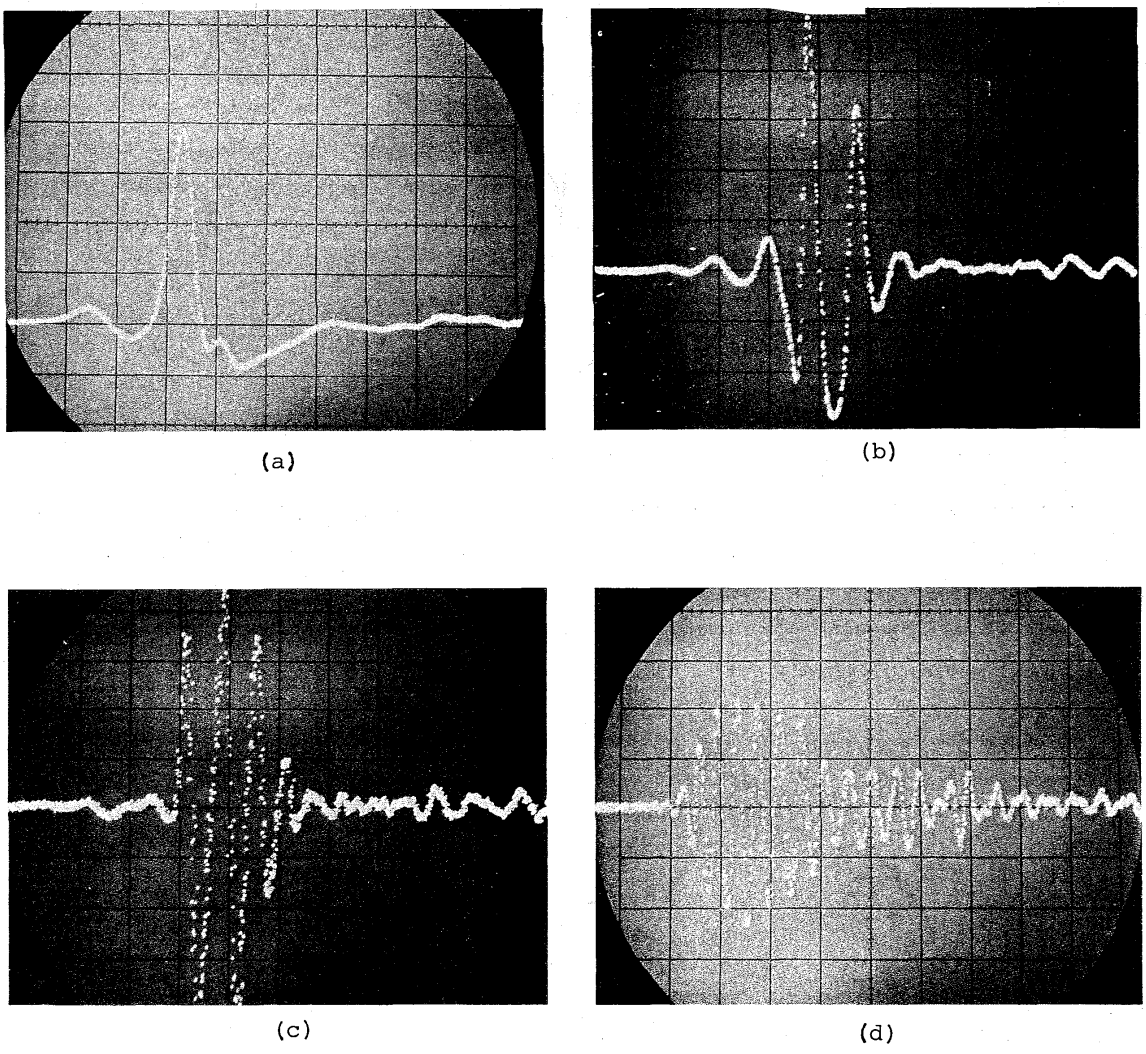

Figure 3-19. Impulse response of TWTAs. Vertical: 10 V/div. except (a) which is 3.2 V/div. Horizontal: 200 ps div. (a) NBS SRD impulse generator (SN 3-75-3) used as input to TWTA. (b) C band, 30 dB, 10 W TWTA. Input impulse attenuated 15 dB. (c) X band, 30 dB, 20 W TWTA. Input impulse attenuated 16 dB. (d) Ku band, 30 dB, 20 W TWTA.

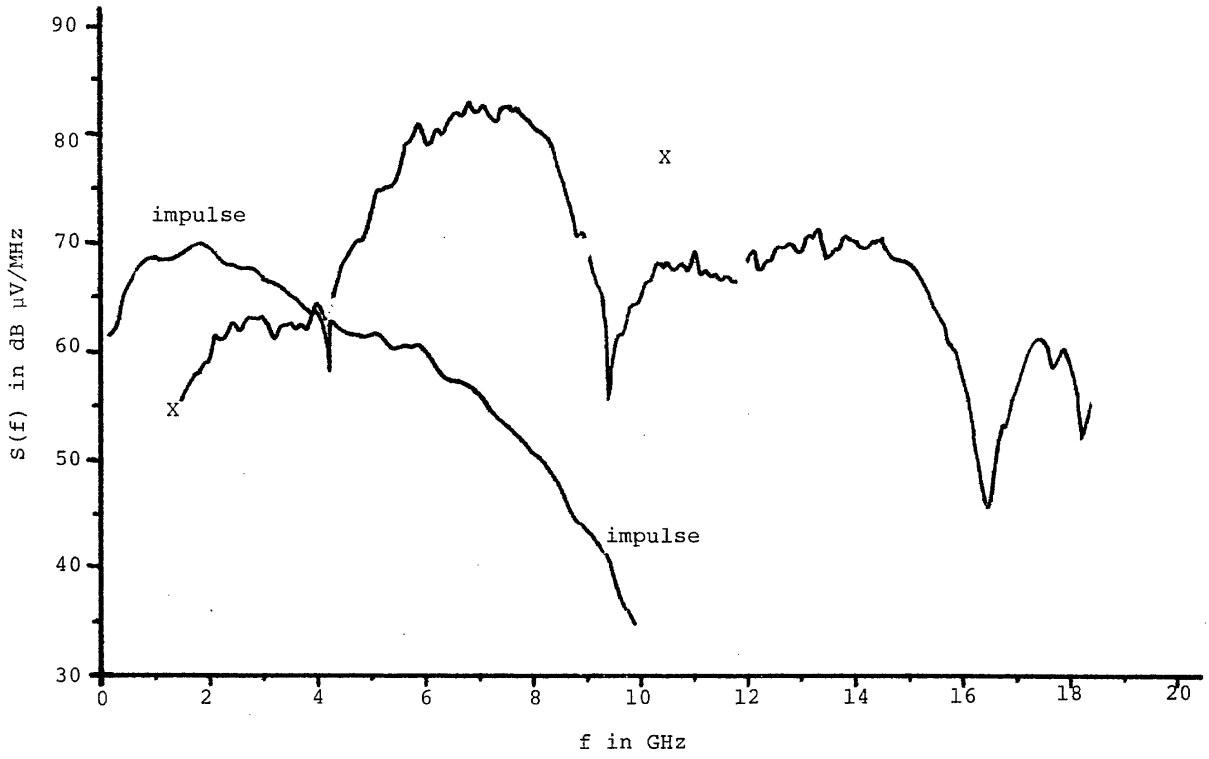

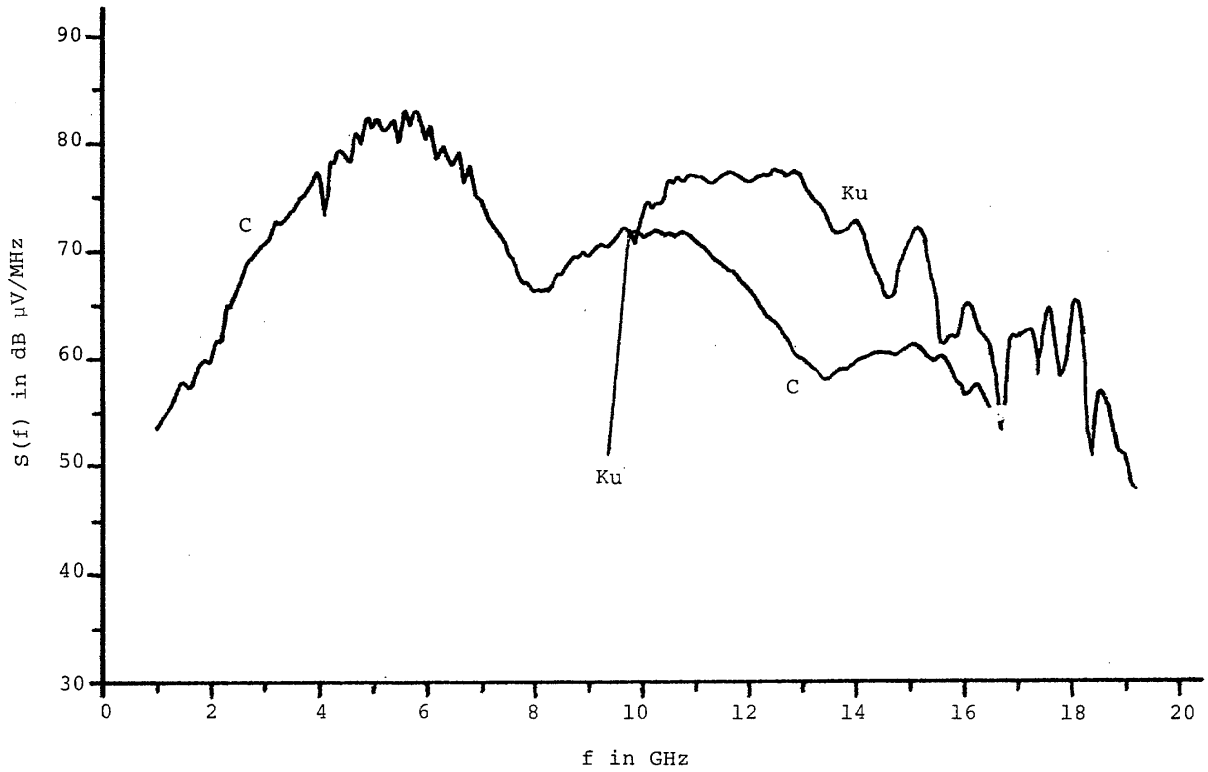

Figure 3-20. Spectrum amplitudes of TWTA impulse responses.

4. SPECTRUM AMPLITUDE MEASUREMENT TECHNIQUES

This chapter discusses the various techniques that have been used to calibrate impulse generators and to measure spectrum amplitude. The techniques included are (1) standard transmission line method, (2) harmonic measurement, (3) energy method, (4) sum and difference correlation radiometer, (5)Dicke type radiometer, (5) video pulse, Mil Std. 462, (7) spectrum analyzer, (8) standard pulse comparison, and (9) time domain measurement with Fourier transformation computation. Advantages and disadvantages of each technique are discussed.

4.1 Standard Transmission Line Method

This method is only applicable to the calibration of mercury switch impulse generators, such as discussed in section 3.2. As shown there the spectrum amplitude is given by eq. (3-8)

$$S(f) = 2V_o t_o, \qquad f << \frac{1}{t_o} \tag{4-1}$$

Substituting eqs. (3-6) and (3-7) into eq. (3-8) gives

$$S(f) = V_{bb}\ell/v_p, \qquad f << \frac{1}{t_o} \tag{4-2}$$

where V_{bb} is the dc supply voltage, ℓ is the transmission line physical length, and v_p is the propagation velocity of light in the transmission line.

V_{bb} can be measured quite accurately. More uncertainty exists in the measurement of v_p and ℓ because the actual generator structure includes not just a piece of uniform transmission line, but also the left half portion of the switch, figure 3-7. Rather than determining t_o from ℓ and v_p it can also be found from R_o and the total line capacitance, C_t.

$$t_o = 2R_o C_t \tag{4-3}$$

R_o can be determined either from the geometrical dimensions of the charge line or from time domain reflectometry (TDR) measurements. C_t can be measured on a capacitance bridge. It is also possible to determine t_o directly from TDR measurements.

4.2 Harmonic Measurement

If one has an extremely narrow bandwidth receiver, an impulse generator can be calibrated by measuring a single spectral line in the impulse generator's spectrum, figure 4-1, and comparing it against a known CW voltage standard. The spectrum amplitude is then given by

$$S(f,k) = \frac{V_k}{f_o} \quad , \tag{4-4}$$

where

$$f = kf_o \tag{4-5}$$

and f_o is the pulse repetition rate of the impulse generator. V_k is the voltage amplitude of the k^{th} harmonic of f_o. f_o can be measured very accurately with a digital frequency counter. V_k can also be measured accurately if the pulse repetition rate is much greater than the receiver bandwidth, BW.

$$f_o >> BW \tag{4-6}$$

If this condition is not met then the bandpass characteristics of the receiver must be well known. Palladino [16] has given a good discussion of this measurement technique along with an error analysis.

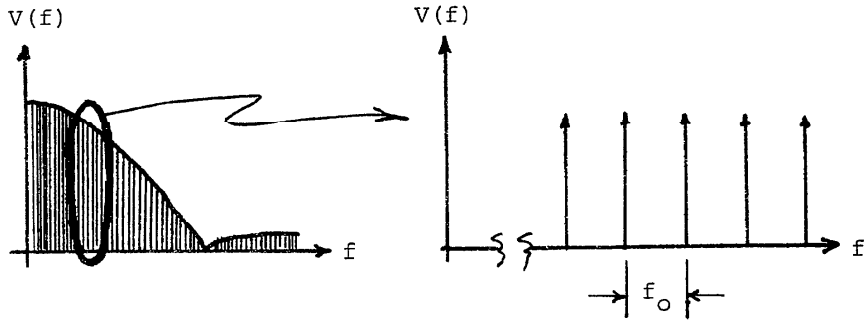

Figure 4-1. Harmonic measurement.

4.3 Energy Method

R. B. Andrews [17] has developed a spectrum amplitude measurement technique based upon the measurement of spectrum intensity. Spectrum intensity is defined [2] as the ratio of the power contained in a given frequency range to the frequency range as the frequency range approaches zero. This technique requires a power meter and a bandpass filter centered at the frequency of interest between the impulse generator and the power meter, figure 4-2.

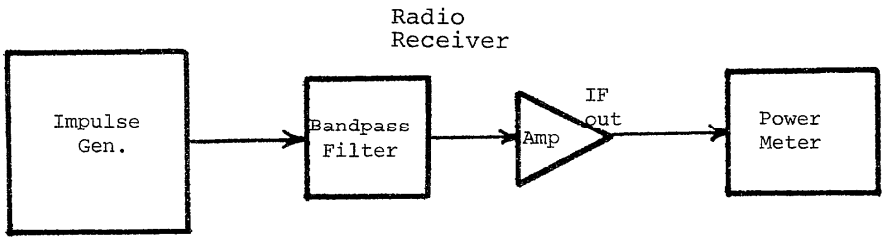

Figure 4-2. Energy method.

The energy relations derived in chapter 2 are used here. The total energy delivered to a load resistor, R_L, was given by eqs. (2-27) and (2-28). The average power delivered to the resistor by a series of impulses, v(t), periodically applied at the repetition rate f_o and period $T = 1/f_o$ is given by

$$\overline{P} = \frac{1}{TR_L} \int_o^T v^2(t)dt \tag{4-7}$$

and also

$$\overline{P} = \frac{f_o}{2R_L} \int_o^\infty S^2(f)df \tag{4-8}$$

If the impulse is applied to a bandpass filter with a voltage transfer function H(f), the average power delivered to a resistor R_L at the output is obtained from eq. (2-30).

$$\overline{P} = \frac{f_o}{2R_L} \int_o^\infty S^2(f)|H(f)|^2 \, df \tag{4-9}$$

If the spectrum amplitude is flat over the bandwidth of the filter then

$$\overline{P} \simeq \frac{f_o S^2(f)}{2R_L} \int_o^\infty |H(f)|^2 \, df \tag{4-10}$$

The power bandwidth, PBW, of the filter is given by

$$PBW = \frac{1}{H_o^2(f_{cf})} \int_o^\infty |H(f)|^2 \, df \tag{4-11}$$

where $H_o(f_{cf})$ is the maximum gain of the network which occurs at the center frequency, f_{cf}. From eqs. (4-10) and (4-11) the spectrum amplitude is obtained.

$$S(f_{cf}) = \left(\frac{2R_L \overline{P}}{f_o PBW \, H_o^2(f_{cf})} \right)^{1/2} \tag{4-12}$$

This technique has the advantage that it uses ordinary metrology lab equipment to measure frequency and power. The bandpass filter commonly used is a radio receiver. The major disadvantages are: (1) the necessity of measuring Δf_p and H_o at each frequency of interest which can be a laborious procedure, (2) the power meter must be able to respond accurately to waveforms having a high peak to average ratio and the low repetition rate of the impulse generator, and also (3) the background noise from the receiver between pulses may drastically corrupt the measurement of the pulse power. Receiver gating can be used to reduce the effect of this last item.

4.4 Sum and Difference Correlation Radiometer

In the late 1960's, NBS developed a sum and difference correlation radiometer (SDCR) to calibrate impulse generators [18,19,14]. The SDCR is similar to the previously described energy method in that S(f) is obtained by measuring the spectrum intensity (watts/hertz). The unknown impulse is compared against a known thermal white noise source.

The SDCR basically measures the available power spectrum intensity, $P_a(f)$, of a Thevenin equivalent generator of internal source generator voltage, $V_s(t)$, and internal source resistance R_s. The maximum available power is obtained from this generator when the external load resistance R_L matches the internal source resistance.

$$R_L = R_s \tag{4-13}$$

For this case the output voltage, v_a, across the load is

$$v_a(t) = \frac{R_s}{R_s + R_L} v_s(t) = \frac{v_s(t)}{2} . \tag{4-14}$$

The available average power, $\overline{P}_a$, of an impulse generator of pulse repetition rate f_o and period $T = 1/f_o$ is (see eqs. (2-27) and (2-28))

$$\overline{P}_a = \frac{1}{TR_s} \int_o^T v_a(t)^2 \, dt \tag{4-15}$$

Using the Fourier integral theorem $\overline{P}_a$ is also given by

$$\overline{P}_a = \frac{f_o^2}{R_s} \int_o^\infty V_a(f)^2 \, df \tag{4-16}$$

or

$$\overline{P}_a = \frac{f_o}{2R_s} \int_o^\infty S_s^2(f) df \tag{4-17}$$

where

$$S_a(f) = 2|V_a(f)| \tag{4-18}$$

is the available spectrum amplitude. Equation (4-17) can also be written in terms of the available power spectrum intensity, $P_a(f)$.

$$\overline{P}_a = \int_o^\infty P_a(f) df \tag{4-19}$$

$$P_a(f) = \frac{f_o^2 S_a^2(f)}{2R_s} \tag{4-20}$$

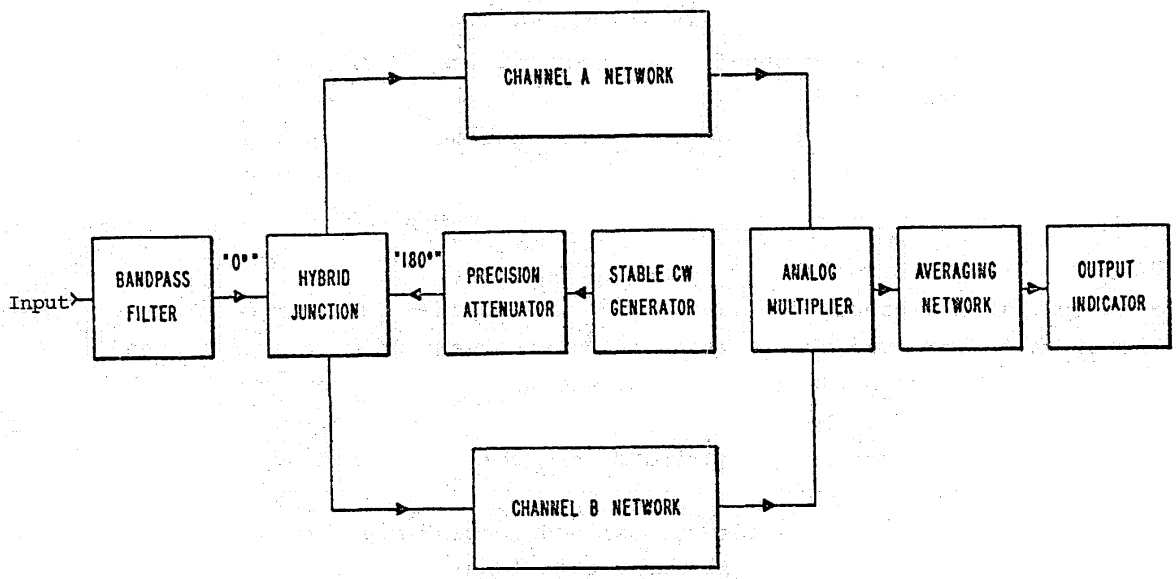

Figure 4-3. Sum and difference correlation radiometer.

The spectrum amplitude, $S_a(f)$, can be obtained from eq. (4-20).

$$S_a(f) = \left[\frac{2R_s P_a(f)}{f_o}\right]^{1/2} \tag{4-21}$$

To determine $S_a(f)$ from eq. (4-21) the source resistance, R_s, is measured with an impedance bridge or other suitable means, the pulse repetition rate, f_o, is measured with a frequency counter, and the available power spectrum intensity, $P_a(f)$ is measured with the sum and difference correlation radiometer (SDCR).

Figure 4-3 is the block diagram of an SDCR [20,21]. The impulsive signal is applied to the SDCR input through a narrow bandpass filter to reduce the peak amplitude of the pulses, and to increase the duration of each pulse. This allows the SDCR to operate within its linear range.

The SDCR is designed so that a null voltage output is obtained from the system when the power from an external signal generator, connected to the input port of the SDCR, is balanced against the power from internal sources within the SDCR. The internal sources of the SDCR consist of a) a stable cw generator and b) the unavoidable internal noise sources of the networks within the system. The power level of the cw generator is adjusted by a calibrated precision attenuator that is a part of the SDCR.

When the impulse generator under test is connected to the input port of the SDCR, the precision attenuator is adjusted to obtain zero output voltage from the system (null condition). The attenuator dial reading is recorded for

this condition. Then the impulse generator is disconnected, and a thermal noise generator of known noise temperature, T_n, is connected to the input port of the SDCR. The precision attenuator is readjusted to obtain a null condition, and its reading is recorded.

Arthur has shown in a lengthy derivation in reference [19], that the impulse generator available power spectrum intensity, $P_a(f)$, is given by

$$P_a(f) = kT_n \, 10^{\frac{1}{10}\Delta A} - kT_e(1 - 10^{\frac{1}{10}\Delta A}) \qquad (4\text{-}22)$$

where k is Boltzmann's constant (1.38×10^{-23} watt-second per degree kelvin), T_n is the noise temperature of the calibrated noise generator, and ΔA is the difference, in dB, between the precision attenuator settings that produce the two null conditions stated above. T_e is the effective input noise temperature of the SDCR. The procedure for measuring T_e has been described by Arthur, et al. [21].

The SDCR technique measures the composite spectrum intensity of the impulse generator under test which includes both impulsive noise and Johnson thermal noise. To separate the two noise contributions, it is necessary to measure the Johnson noise alone with the impulse generator's impulse output turned off, but with the generator still connected to the SDCR.

Two SDCR radiometers for impulse signals have been built [14]. Their operating frequencies are 30 MHz and 1 GHz, and the impulse bandwidth is 30 kHz for each system. The measurement uncertainties of these instruments appear to be no greater than approximately 1 dB. The measurement uncertainty depends upon the spectrum amplitude level and the pulse repetition rate. Figure 4-4 shows the ranges of these two quantities within which the 30 MHz system can be used with stated accuracy. For levels less than the values along the bottom edge of the "band of operation," the system performance becomes poor because of the small signal-to-noise ratio of impulse power to system noise power. For levels greater than the values along the top edge of the "band of operation," the system performance becomes poor because of non-linear amplification in the system. However, levels greater that those bounded by the "band of operation" can be measured by attenuating the impulsive signal before applying it to the SDCR system. The 1 GHz system has a similar "band of operation," except that the lower edge of the band is raised approximately 10 dB because of the larger internal noise level.

The SDCR radiometer technique has the potential of great accuracy. In addition it does not require a precise measurement of the SDCR impulse bandwidth and bandpass characteristics as this parameter doesn't appear directly in the relevant equations (4-21 and 4-22). There are however several major disadvantages. First it provides data at a single fixed frequency. Second, the SDCR is a quite sophisticated and expensive instrument. Its primary usefulness is as an independent measurement technique in a national standards laboratory. Third, eq. (4-21) requires that the impulse generator source impedance be

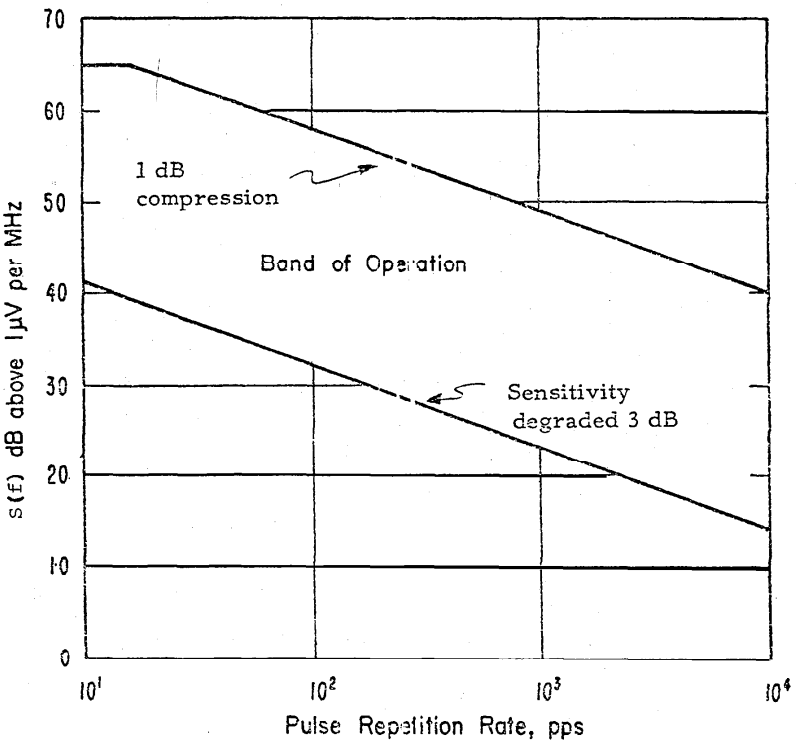

Figure 4-4. Useful range of operation of 30 MHz SDCR.

measured. This is not always an easy task as the source impedance of some generators is a time varying quantity. The simple mercury switch impulse generator (see section 3.2 and figure 3-7) is the worst case. During the initial pulse generation time ($0 < t < t_o$) the generator can be represented as a Thevenin source voltage V_{bb} and source resistance R_o. However, after the transmission line is discharged ($t > t_o$ when $R_L = R_o$) the generator's equivalent circuit is a source voltage V_{bb} and source resistance R_c which is much larger than Z_o. Even later in time when the switch opens, the generator's equivalent circuit is simply an open circuit. Some manufacturers attempt to reduce this problem by installing a coaxial attenuator (typically 6 dB) between the switch and the output connector.

4.5 Dicke Radiometer

In 1974, Oranc [22] proposed using a Dicke radiometer [23] to calibrate impulse generators. The Dicke radiometer measures the noise temperature of an input broadband signal. It is a linear radio receiver in which the input is switched alternately between the unknown signal source and a known thermal noise source. A synchronous detector locked to the input switching frequency is used to detect the difference between the two input noise temperatures.

For this radiometer measurement the equivalent circuit of an impulse generator consists of the internal impulse voltage source, $v_{si}(t)$, the internal source resistance, R_s, and a Johnson thermal noise source, $v_{sn}(t)$, associated with the resistor, R_s.

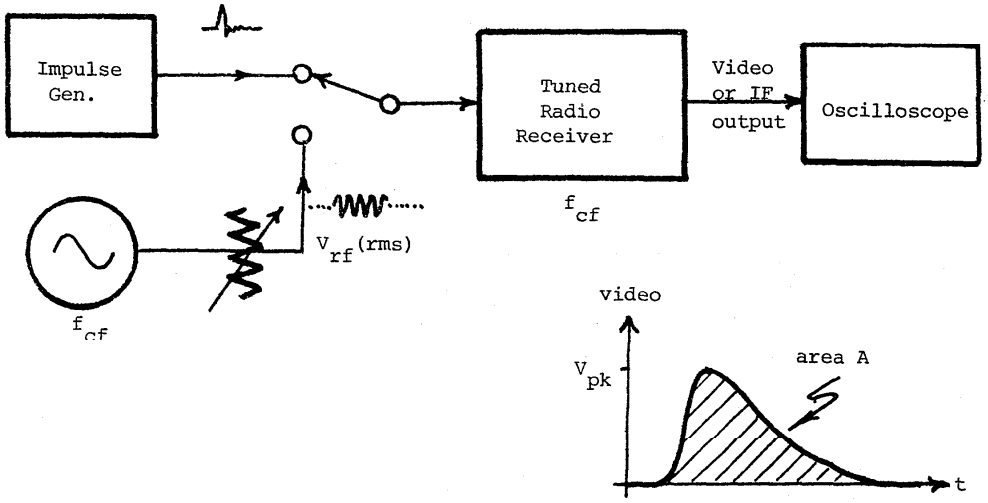

Figure 4-5. Video pulse - Mil. Std. 462.

4.6 Video Pulse -- Mil. Std. 462

The video pulse technique, figure 4-5, is the one currently accepted by the U.S. military for the calibration of impulse generators [24]. The IEEE also recognizes it as a valid measurement technique [2]. The technique consists essentially of connecting the impulse generator to a narrowband filter (such as a radio receiver) and observing with an oscilloscope the envelope response (i.e. video pulse) of the filter output and comparing the peak amplitude to that obtained from a known cw sine wave signal generator. The impulse bandwidth, IBW, of the filter must also be known and there are several measurement techniques to determine IBW [25,26].

U.S. Military Standards 461, 462, and 463 set forth the specifications, definitions, and calibration procedures for impulse generators. Those portions pertinent to this topic are reproduced here.

Mil-Std-461A, 1 Aug. 1968, p. 11

5.4 Impulse Generators. -- Impulse generators shall conform to the following requirements:

(a) Calibrated in terms of output to a 50 ohm load.

(b) Spectrum shall be flat ± 2 dB over its frequency range.

(c) Amplitude accuracy shall be ± 2 dB.

Mil-STD-462, 31 July 1967, p. 4

4.2.3.6 Impulse Generators. -- Impulse generators shall be calibrated as follows:

(a) Apply the output of an impulse generator to the input of an amplitude-linear receiver having synchronously tuned, less than critically coupled circuits. EMI receivers are satisfactory for this purpose if their impulse bandwidth is at least five times the repetition rate of the impulse generator. Any AGC system, shall be disabled and the AGC line firmly referred to ground with a low impedance voltage source of appropriate value.

(b) Obtain an oscilloscope pattern of the overall receiver response at the IF output. The oscilloscope controls shall be so adjusted that the pattern is as large as possible within the calibrated area on the face plate. Either photograph or trace the pattern. Record the oscilloscope sweep speed setting. (The sweep speed shall be calibrated accurately.)

(c) Use a planimeter or other integrating device to determine the area of the pattern. This operation shall be carried out at least 10 times and the average of the readings taken as the area.

(d) Calculate the impulse bandwidth of the receiver in accordance with the following formula:

$$\text{IBW in Hz} = \frac{\text{(Pattern height in cm)}}{\text{(Pattern area in cm}^2\text{) (Sweep speed in sec/cm)}}$$

(e) Connect a sinewave generator to the receiver and at f_o and adjust the output until the peak pattern height is the same as that obtained with the impulse generator.

(f) Connect an r.f. power meter to the signal generator and measure the power output. Calculate the r.m.s. voltage on the sinewave signal.

(g) The output of the impulse generator is now calculated by taking the r.m.s. voltage calculated in step (f) divided by the impulse bandwidth determined in step (d).

Mil-Std-462, Notice 2, 1 May 1970, Appendix A

30. Impulse Generators

30.1 By definition, the calibration for broadband measurements is referenced to the RMS value of an equivalent sine wave. Correct calibration of impulse generators is subject to verification by witnessing officials, in accordance with Mil-Std-462.

Mil-Std-463, 9 June 1966, p. 5

4.18 Impulse Bandwidth. The peak value divided by the area of the impulse response envelope.

4.20 Impulse Strength. The rms unmodulated sine wave voltage required to produce in a circuit a peak response equal to that produced by the impulse in question, divided by the impulse bandwidth of the circuit. For the purpose of this standard it is expressed in terms of μV/MHz or dBμV/MHz.

The video pulse method is probably the most widely used due to the fact that is is specified by Mil. Std. 462 and because it uses common laboratory instruments such as a calibrated cw signal generator, a tunable receiver, and an oscilloscope. There are however several difficulties associated with this technique. The major problem lies in the determination of the narrowband filter impulse bandwidth. E.B. Larsen [25] of NBS has written an exhaustive report on the many problems that are encountered in accurately determining the impulse bandwidth of a radio receiver. He reports that the results can vary widely depending upon the actual shape of the filter passband, both in amplitude and phase. Overcoupled or stagger tuned networks or mechanical filters are definitely undesirable for this purpose. Problems also arise in trying to determine the impulse bandwidth from the envelope response area per Mil. Std. 462 due to noise distortion of the envelope response and accuracy problems in measuring the area.

Larsen [25] and Simpson [15] have recommended that the most accurate method of determining impulse bandwidth is to use a known rf pulse. Their recommended procedure is listed in table 4-1.

As can be seen from eq. (1) in table 4-1 under No. 8, only two parameters affect the accuracy of measuring the impulse bandwidth by this standard pulse/cw signal generator method. They are the pulse duration t_o and the difference in two attenuator settings.

4.7 Spectrum Analyzer

A spectrum analyzer is perhaps the easiest instrument to use for making broadband spectrum amplitude measurements. It gives an immediate visual display of relative spectrum amplitude versus frequency. Some spectrum analyzers of recent design are also capable of making quite accurate S(f) measurements [14]. Of major importance is that the input impedance, gain, and bandwidth of the instrument be constant and not a function of frequency. It must also be free of spurious and image responses. Reeve [14] has found that some FIM and EMI receivers currently in wide use are not suitable because of impedance, gain, and bandwidth variations with frequency.

To use a spectrum analyzer, it must first be calibrated as a tuned voltmeter at several selected frequencies using a standard cw sine wave generator of known output. The impulse bandwidth must also be calibrated at the same frequencies. The technique described in table 4-1 is recommended.

Table 4-1. Impulse bandwidth calibration procedure for field intensity meter receivers.

1. Assemble a standard pulsed/cw signal generator consisting of a cw sine wave generator, baseband pulse generator, modulator, and a calibrated attenuator. See section 3.5 for complete description.

2. Set the standard signal generator controls as follows:

   a. mode -- pulse

   b. carrier frequency, f_c -- same as FIM

   c. repetition rate, f_o -- as desired, with the restriction $f_o < \frac{BW}{5}$, where BW is the nominal 3 dB bandwidth of the FIM

   d. rf pulse duration, t_o -- as desired with the restrictions [11]

$$\frac{15}{f_c} < t_o < \frac{1}{10\ BW}$$

   e. duty cycle -- $t_o f_o < 0.05$.

3. Set the FIM controls as follows:

   a. amplifier mode -- linear

   b. AGC -- off

   c. detector -- peak

   d. video filter -- off

   e. frequency tuning -- centered on f_c, the standard signal generator frequency

   f. bandwidth -- as desired.

4. Connect the standard signal generator output to the FIM antenna input.

5. Adjust the attenuator to obtain a reading on the FIM peak detector that is near full scale and well above the FIM noise level. Check that the FIM is operating in the linear region by increasing and decreasing the input signal to the FIM by several dB and noting whether the peak detector follows linearly the input variation. Reset the attenuator to the desired level and record the attenuator setting, A_1, in dB and the peak detector reading, PD_1.

6. Set the standard signal generator mode control to cw.

7. Adjust the attenuator to obtain the same peak detector reading, PD_1, as obtained in step 5. Record the attenuator setting, A_2.

8. Calculate the impulse bandwidth, IBW, from the following equation:

$$IBW = 1/t_o\ 10^{[(A_1-A_2)/20]} \qquad (1)$$

Spectrum amplitude can then be measured directly from the CRT display using

$$S(f) = V_{in}(f)/IBW \qquad (4\text{-}23)$$

where $V_{in}(f)$ is the equivalent input voltage as indicated on the spectrum analyzer CRT screen. Most spectrum analyzers use a peak detector to determine V_{in}; however, the CRT display is usually calibrated in terms of rms volts for sine wave measurements. Thus S(f) from eq. (4-23) is a root mean square spectrum amplitude. To convert to standard spectrum amplitude the results from eq. (4-23) should be multiplied by $\sqrt{2}$ or if S(f) is given in dBμV/MHz, 3 dB should be added.

Below 1 GHz there are several excellent spectrum analyzers commercially available that are capable of making accurate spectrum amplitude measurements. However above 1 GHz the currently available spectrum analyzers' performances are not as good as the < 1 GHz models. If an analyzer is to be used above 1 GHz for S(f) measurements, considerably more care must be exercised in the measurement.

A major problem in using a spectrum analyzer for S(f) measurements is its susceptibility to overload. Most modern spectrum analyzers apply the input signal directly to the input mixer. If the peak input voltage exceeds 150-200 mV, signal compression occurs, while voltages in excess of a volt will destroy the mixer diodes. This poses a severe limitation when attempting to measure an extremely narrow (< 1 ns) impulse of several tens or hundreds of volts. If the impulse is attenuated to the 150 mV peak level by a broadband attenuator then the resultant spectrum amplitude is found to be comparable to or below the noise level of the spectrum analyzer. The solution lies in the use of preselector bandpass filters between the impulse generator and the input to the mixer. The filter acts to reduce the peak voltage applied to the mixer without reducing the spectrum amplitude at the measurement frequency. It is good practice to use broadband attenuators of typically 6 to 10 dB on either side of the filter to provide proper impedance matching. The preselector filter bandwidth should be at least ten times larger than the spectrum analyzer's impulse bandwidth. Otherwise the impulse bandwidth of the preselector/spectrum analyzer combination must be calibrated at every measurement frequency. The attenuation of the preselector and the external attenuators must be included in the measurement calculations.

4.8 Standard Pulse Comparison

Reeve [14] has proposed a sophisticated scheme for automatically calibrating an impulse generator using a comparison against a known standard pulse such as an rf pulse. His proposed system would use a programmable spectrum analyzer, a tracking cw generator, a network analyzer, a standard pulsed/cw signal generator, and a minicomputer to control all the various instruments to perform the measurement and the necessary computations. Such a system would

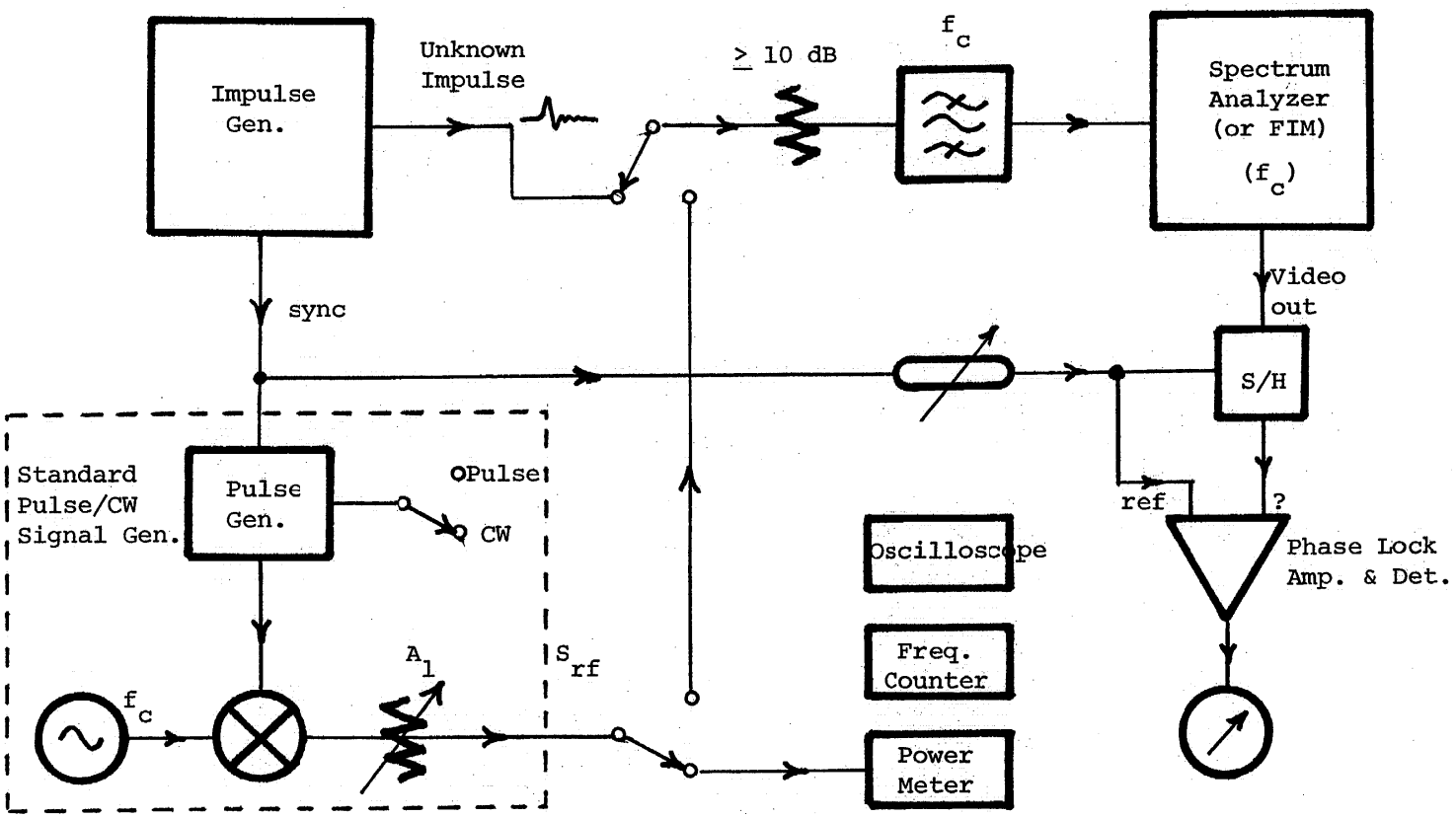

Figure 4-6. Standard pulse comparison block diagram.

incorporate the best features of modern measurement technology and probably offers the ultimate in precision and accuracy. The cost of such a system would be quite high and for this reason it has not been built.

The basic ideas of Reeve's system can be incorporated in a manually operated standard pulse comparison system. Such a system is shown in figure 4-6 which uses ordinary instruments normally found in a calibration laboratory. Basically, the technique involves adjusting the level of the rf pulse from the standard pulsed/cw signal generator until the same video pulse output is obtained from the narrow band filter (a spectrum analyzer or FIM) as is obtained when the unknown impulse generator is connected to the narrow band filter input.

A phase lock amplifier/detector may also be used in conjunction with a peak sample/hold and delay circuit to recover very low level video pulses from the spectrum analyzer's peak detectors that would otherwise be buried in the system noise. This permits a considerable increase in dynamic range of S(f) measurements over simply using the spectrum analyzer's CRT display. A variable delay circuit is triggered by a sync pulse from the impulse generator. The delay is adjusted to correspond to the delay in the spectrum analyzer between the impulse input and the peak of the output video pulse. The peak sample/hold circuit is gated to sample and hold the peak value of the video pulse. The sync pulse is used as a reference signal and the peak sample/hold output is the unknown input to a phase lock amplifier. The standard pulsed/cw signal generator is externally triggered by the impulse generator to establish its repetition rate, f_o. In this manner by using the impulse generator to establish f_o it is possible to directly intercompare the two generators without readjusting any of the phase lock video pulse detector circuits. The load impedance is fixed at 50 ohms by using a fixed coaxial attenuator of at least 10 dB at the spectrum analyzer input. A preselector filter is used as discussed previously. The oscilloscope and frequency counter are additional instruments required for setting and calibrating the equipment.

In operation the impulse generator is first connected to the spectrum analyzer. All of the controls of the analyzer and phase lock detector are optimized to obtain a maximum indication on the phase lock detector meter. This meter reading is recorded. The standard pulse/cw signal generator is then connected to the spectrum analyzer and the amplitude of the rf pulse is adjusted with the calibrated attenuator until the same phase lock detector meter reading is obtained as previously with the impulse generator. The attenuator setting in dB, A_1, is recorded. In this setting the rf pulse spectrum amplitude, $S_{rf}(f_c)$, is equal to the impulse generator spectrum amplitude $S_i(f_c)$.

$$S_i(f_c) = S_{rf}(f_c) \tag{4-24}$$

S_{rf} is given in dBμV/MHz by

$$S_{rf}(f_c) = S_o(f_c) - A_1(\text{dB}) \quad . \tag{4-25}$$

$S_o(f_c)$ is determined with the attenuator set to 0 dB and measuring the cw output power and the rf pulse duration, t_o, as described in section 3.5.

4.9 Time Domain Measurement/Fourier Transformation Computation

With the exception of the standard transmission line method (section 4.1) the previous techniques for measuring spectrum amplitude have all been some variation of a frequency domain measurement using a narrow bandpass filter. An alternate technique is to measure the time domain waveform, $v_i(t)$, of the signal to be measured. From $v_i(t)$ the spectrum amplitude, $S_i(f)$, can then be computed using the basic definition of spectrum amplitude, eqs. (1-1) and (1-2).

$$S_i(f) = 2|V_i f)| \tag{4-26}$$

$$V_i(f) = \int_{-\infty}^{\infty} v_i(t) e^{-j2\pi ft}\, dt \tag{4-27}$$

This technique has been known for a long time, but it has not been widely used because it has been very time consuming. It has required photographing an oscilloscope CRT display of the signal to be analyzed. Many data points must then be read by eye from the photograph, typed onto paper tape or computer cards, and then processed (eqs. (4-26) and 4-27)) on a time share or large central computer. The process easily consumed an entire working day.

With the advent of inexpensive (< 10 K$) minicomputers, this has all changed. The cost of computing capability is now comparable to that of a high performance oscilloscope, and it is now cost-effective to dedicate a minicomputer to be hard-wired to an oscilloscope. In addition, sampling oscilloscopes are commercially available with bandwidths as great as dc-18 GHz which permit v(t) and hence S(f), via eqs. (4-26) and (4-27), to be measured over this very broad range with a single instrument.

In 1974, NBS built such a time domain measurement system. It is called the Automatic Pulse Measurement System (APMS). As shown in the block diagram of figure 4-7, the APMS consists basically of a dc-18 GHz sampling oscilloscope directly interfaced with and controlled by a minicomputer. The APMS is described in full detail in NBS Tech Note 672 [27]. It was originally developed as a Time Domain Automatic Network Analyzer (TDANA) [28] but has several other capabilities as tabulated below:

1. Acquisition and storage in memory of a time domain waveform. Data arrays as large as 2048 points can be accommodated.
2. Signal averaging for greatly improved signal to noise ratio and the recovery of low level signals buried in the noise.
3. Spectrum analyzer using the Fast Fourier Transformation (FFT) of time domain waveforms.
4. Computation of time domain waveform parameters such as pulse amplitude, risetime, overshoot, duration, distortion, etc.

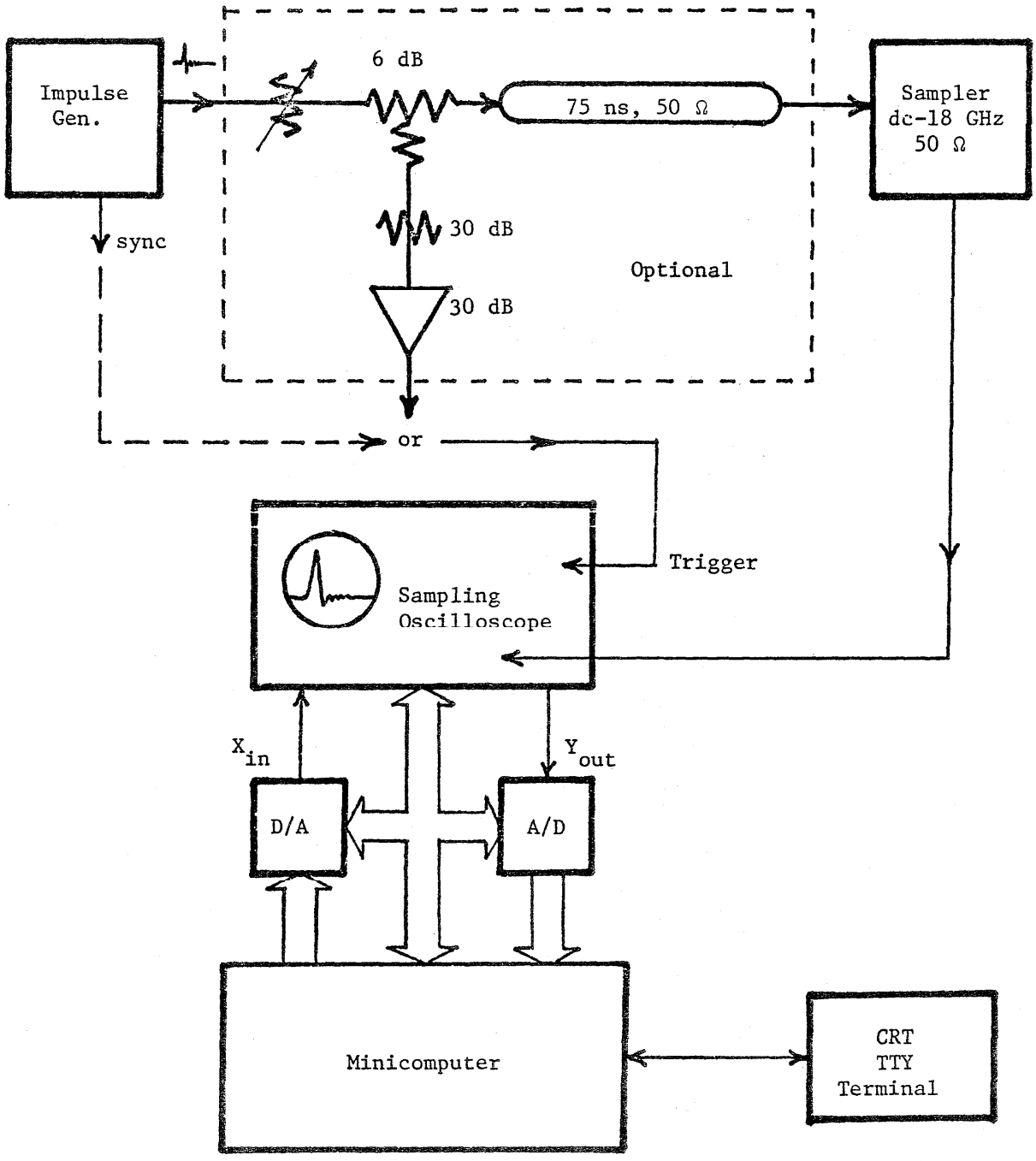

Figure 4-7. NBS automatic pulse measurement system.

5. Network analyzer measurements of the S parameters (transmission and reflection), in both magnitude and phase, of rf and microwave networks. Present limits are a dynamic range of 40 dB and frequency coverage from dc to X band but will be increased in the future.

6. Availability of a minicomputer within the laboratory with both BASIC and FORTRAN capability for solving many mathematical problems.

When the APMS is used to measure the spectrum amplitude of an impulse generator, it gives excellent results. Chapter 5 presents the results of the APMS with other measurement techniques. In operation, the impulse to be measured is applied to the input of the sampler. If the impulse amplitude is greater than ± 400 mV then broadband coaxial attenuators must be used between the impulse generator and the sampler. The impulse generator must also supply a suitable stable trigger pulse to the sampling oscilloscope approximately 75 to 100 ns prior to the impulse. Some electronic impulse generators normally supply such a trigger pulse. However the vast majority of impulse generators use mercury switches or spark gaps and are not capable of being triggered reliably. The sync pulse from these generators cannot be used. For these generators a trigger pick off and coaxial delay line, figure 4-7, must be used to provide the necessary trigger for the sampling oscilloscope.

When a delay line is necessary the overall system bandwidth is degraded below the sampler 18 GHz bandwidth. The major limitation is due to skin effect in the coaxial delay line. With ordinary coaxial cables the arrangement of figure 4-7 is useful only up to 1 or 2 GHz. For higher frequencies and impulse durations less than 250 ps a superconducting coaxial delay line is used [9,29].

The APMS time domain method of calibrating impulse generators has the advantages of: (1) very broad frequency coverage (dc-18 GHz), (2) rapid measurement time of typically two minutes, and (3) providing a large amount of data (typically several hundred data points). It does have some disadvantages however. The major one is that it cannot measure v(t) over the complete interval $-\infty < t < +\infty$. It can only acquire a limited finite amount of data points. Thus a time window of finite extent is used to observe the impulse. Any signals emanating from the impulse generator other than the main impulse and positioned in time outside of the time window are ignored. Their contribution to the composite spectrum amplitude is not accounted for in the FFT computation. Another problem which arises when either external attenuators and/or a trigger pick off delay line arrangement is used, is the necessity to also calibrate the attenuation versus frequency of these additional components to provide correction factors for the measured S(f). This is not a major problem however because the APMS can also be used as a TDANA to determine the "S" parameters of these components. The major effect is a reduction in the overall accuracy.

5. EXPERIMENTAL COMPARISON OF VARIOUS S(f) MEASUREMENT TECHNIQUES

This chapter presents the results of a set of experiments to compare the various spectrum amplitude measurement techniques that were discussed in chapter 4. The energy method and the Dicke radiometer techniques were not used. The other techniques were investigated and were found to all give consistent results.

5.1 Standard Transmission Line Experiment

A mercury switch impulse generator was constructed consisting of a small mercury switch mounted in a 3 mm coaxial housing; a 5 ns, 50 ohm, 3 mm semi-rigid coaxial cable; a stable dc voltage supply; and a digital voltmeter. The transition time (10%-90%) of the mercury wetted reed switch was 0.21 ns [9]. The exact value of t_o was determined from eq. (4-3) using a TDR measurement of R_o and a capacitance bridge measurement of C_T. R_o was 50.5 ohms and C_T was 102.333 pF.

With a supply voltage of 1.6 volts and an impulse duration of 10.336 ns, the low frequency spectrum amplitude, S_o, is 84.37 dBμV/MHz. Being almost a perfect rectangular pulse, the spectrum should theoretically follow the $\sin(\pi f t_o)/(\pi f t_o)$ equation. For a 10.336 ns pulse the first zero in the spectrum occurs at 96.749 MHz.

Table 5-1 is a comparison of the theoretically predicted spectrum for this generator and measurements made on the NBS APMS using the time domain measurement/fast Fourier transform computation (hereafter abbreviated as TD/FFT) technique. There is agreement within ± 0.6 dB over the low frequency portion of the spectrum up to 85 MHz which covers a 15 dB range. The spectrum nulls near the frequencies $f_n = n \cdot 1/t_o$ are extremely sharp and as expected the agreement between theory and experiment is very poor. However, good agreement is obtained for the peaks on the higher order lobes of the spectrum.

5.2 Sum and Difference Correlation Radiometer Experiment

Experiments were performed in 1972 by Reeve [14] to measure spectrum amplitude using the NBS sum and difference correlation radiometer (SDCR). He used an NBS step recovery diode impulse generator develped in 1970 by Ondrejka [30] as the broadband impulsive noise source to be tested. The same generator was measured in 1976 using the TD/FFT technique using the NBS APMS. The results are compared in table 5-2. At 30 MHz the results obtained by the two techniques differed only by 0.35 dB. At 1 GHz the agreement was not as good. G. Reeve [31] cautions that the 1972 SDCR results are not to be considered as an absolute calibrated measurement as a complete error analysis of the SDCR has never been made. However, he feels that the 30 MHz SDCR is much more accurate than the 1 GHz instrument. The 1 GHz SDCR was plagued with a reduced sensitivity and a phase instability. Thus considerable doubt exists concerning the validity of the 1 GHz measurements.

Table 5-1. Comparison of S(f) measurement using TD/FFT technique versus standard transmission line theory.

S(f) in dBμV/MHz

Frequency in MHz	TD/FFT	Std. Line Theory	Difference
9.96	83.87	84.22	0.35
19.92	83.32	83.76	0.44
29.88	82.44	82.96	0.52
39.84	81.20	81.80	0.60
49.80	79.59	80.19	0.60
59.76	77.46	78.00	0.54
69.72	74.77	74.99	0.22
79.68	70.69	70.54	-0.15
89.64	63.87	62.28	-1.59
99.56	40.65	53.37	12.7
119.5	67.34	69.16	1.82
139.4	69.90	71.10	1.20
159.4	68.71	69.13	0.42
179.3	63.31	62.05	-1.26
199.2	38.21	53.45	15.2
259.0	64.39	64.46	0.07

Table 5-2. Comparison of S(f) measurements using the SDCR and TD/FFT techniques.

S(f) in dBμV/MHz

Frequency in MHz	SDCR	TD/FFT	Difference
30	37.15	37.5	-0.35
1000	35.35	33.9	1.45

5.3 Experiments with Commercial Mercury Switch Impulse Generators

Four different measurement techniques were used in experiments to measure the spectrum amplitude of two commercial* mercury switch impulse generators. The techniques were: (1) TD/FFT; (2) standard pulse comparison; (3) video pulse -- Mil. Std. 462; and (4) spectrum analyzer. The first generator produced a 10 ns impulse with a spectrum amplitude specified by the manufacturer to be flat within ± 1 dB from 500 Hz to 35 MHz. The output was adjustable from 0 to 121 dBμV/MHz (RMS) in 0.25 dB steps. The second generator was specified by the manufacturer to produce a spectrum output flat within ± 1 dB from 60 kHz to 1000 MHz. The output was adjustable from 10 to 101 dBμV/MHz (RMS) in 0.25 dB steps. The results of these experiments are summarized at a few representative frequencies in tables 5-3 and 5-4.

Table 5-3. Comparison of S(f) measurements on a commercial mercury switch HF impulse generator.

	S(f) in dBμV/MHz				
Frequency in MHz	Manufacturer's Spec.(1)	TD/FFT	Std. Pulse	Mil. Std. 462	Spectrum Analyzer
5	83.0(1)	83.1	83.1	83.8	82.8
10	83.0	83.0	82.6	83.3	83.5
20	83.0	83.0	82.8	83.4	83.2
40	NA(2)	82.3	82.3	82.8	82.5
60	NA	78.9	79.0	79.7	78.9

(1) Output amplitude controls set at +80 dBμV(RMS)/MHz.

(2) Output specified flat within ± 1.0 dB maximum from 500 Hz to 35 MHz.

*It is NBS policy not to mention manufacturers nor commercial products in its publications. This is done to avoid giving unfair economic advantage to any manufacturer which might occur through a real, implied, or imagined endorsement.

Table 5-4. Comparison of S(f) measurements on a commercial mercury switch UHF impulse generator.

	S(f) in dBμV/MHz				
Frequency in MHz	Manufacturer's Spec.	TD/FFT (2)	Std. Pulse	Mil. Std. 462	Spectrum Analyzer
20	83.0 (1)	83.9	83.4	83.9	82.8
60	83.0	83.6	83.8	84.4	83.5
100	83.0	83.6	84.0	84.2	82.7
200	83.0	83.4	83.5	84.0	84.0
500	83.0	82.3	83.2	83.2	82.7
1000	83.0	82.0	84.4	85.1	84.8

(1) Output amplitude controls set at +80 dBμV(RMS)/MHz.

(2) Output amplitude controls set at +50 dBμV(RMS)/MHz for measurement. Data corrected to +80 dB level.

The TD/FFT measurement of S(f) was performed by the NBS APMS. These ercury switch impulse generators did not supply the necessary trigger pulse :or the oscilloscope. Thus the arrangement shown in figure 4-7 was used to obtain the necessary trigger signal. A broadband (dc-18 GHz) 6 dB coaxial power divider is used as a trigger pick-off. The power divider is impedance matched, i.e. when its two output ports are terminated in 50 ohms it presents a 50 ohm load to the impulse generator. The trigger input of the sampling oscilloscope is only nominally matched to 50 ohms. The VSWR is high enough to upset precision measurements if the output of the 6 dB power divider were connected directly to the trigger input. To provide impedance matching and VSWR isolation a broadband (dc-12 GHz), 30 dB, 50 ohm attenuator terminates the trigger output port of the power divider. To compensate for the trigger signal amplitude loss due to the attenuator, a broadband (5-500 MHz) 30 dB amplifier is used. The other output of the power divider is connected to a 75 ns, 50 ohm coaxial delay line, which in turn is connected to the remote sampler. The delay line has a 3 dB bandwidth of 3 GHz. The actual waveform measured by the APMS is the input to the remote sampler. This waveform is attenuated and distorted due to transmission through the power divider and the delay line. Thus, the APMS measurement must be corrected for the insertion loss versus frequency of the power divider and delay line to give the correct spectrum amplitude of the impulse generator under test. The necessary correction factors are obtained by operating the APMS as a TDANA to measure S_{21} of the power divider/delay line network.

The frequency domain measurements, namely the standard pulse comparison, the video pulse, and the spectrum analyzer all used a commercial spectrum analyzer as the measuring instrument. It tunes from 100 kHz to 1250 MHz with a specified flatness of ± 1 dB. The bandwidth is adjustable from 300 Hz to 300 kHz in a 1,3 sequence. There is no preselector in this instrument. The input signal is applied directly to the first mixer through an adjustable input attenuator. Prior to making any measurements the spectrum analyzer was calibrated against cw signal sources of known power and frequency.

The impulse bandwidth of the spectrum analyzer was measured at 30 MHz using several different methods that have been reported in the literature [25]. This was done to compare the relative accuracies of the various methods. The results are tabulated in table 5-5. The nominal bandwidth is the value engraved on the front panel of the instrument. The standard pulse impulse bandwidths were determined as described in section 4.8 and table 4-1. The difference between the two measurements was the output indicator which was the spectrum analyzer CRT display in one case and an external oscilloscope display of the video output pulse in the other. The video pulse impulse bandwidth is determined from the area under the video output pulse time domain response as described in section 4.6. The 6 dB bandwidth is simply the bandwidth between the -6 dB points on the frequency response curve. The area bandwidth is that of an equivalent rectangular frequency response with an area equal to the area under the linear frequency response curve. The power bandwidth (sometimes called random noise bandwidth) is that of an equivalent rectangular frequency response with an area equal to the squared voltage frequency response curve. In the 100 kHz and lower positions the frequency response appeared to be almost perfectly gaussian while the video pulse response was also gaussian-like. In the 300 kHz position the frequency response was slightly nonsymmetrical and the video pulse response included a minor secondary pulse 4 μs after the primary pulse. For the 100 kHz position with its gaussian-like response, extremely good correlation was obtained between the video pulse IBW, standard pulse IBW, and the area BW. For the non-gaussian 300 kHz position the correlation between various bandwidths was not as good. The difference in the two standard pulse measurements illustrate some of the problems that can be encountered in making measurements at two supposedly identical measurement ports. The difference noted here is attributed to the video signal output amplifier bandwidth. The video pulse technique correlates within 1 dB of the standard pulse method. The 6 dB bandwidth also gave good agreement for this set of measurements, however, Larsen [25] cautions that it is subject to large errors for extremely non-gaussian responses. The area bandwidth gives a good correlation for a gaussian response but introduces a large error for a slightly non-gaussian response. The power bandwidth should not be used for the impulse bandwidth.

Table 5-5. Comparison of various impulse bandwidth measurement methods.

Impulse Bandwidth Measurement Method	300 kHz Nominal Bandwidth IBW kHz	300 kHz Nominal Bandwidth IBW-IBW(std) dB MHz	100 kHz Nominal Bandwidth IBW kHz	100 kHz Nominal Bandwidth IBW-IBW(std) dB MHz
Standard Pulse per Table 4-1 (CRT Display)	371	0	157	0
Standard Pulse per Table 4-1 (video signal output)	360	-0.26	152	-0.28
Video Pulse per Mil. Std. 462	341	-0.73	158	0.05
6 dB Bandwidth	362	-0.22	144	-0.75
Area Bandwidth	473	2.11	158	0.05
Power Bandwidth	295	-1.99	106	-3.41

5.4 Experiment with Step Recovery Diode Impulse Generator

A set of experiments were also run to measure the spectrum amplitude of a step recovery diode impulse generator using five different measurement techniques. The techniques were: (1) TD/FFT; (2) standard pulse comparison; (3) video pulse -- Mil Std. 462; (4) spectrum analyzer; and (5) harmonic measurement. The results are tabulated at a few representative frequencies in table 5-6. The generator used was NBS impulse generator S/N 3-75-1. It is identical to the one described in section 3.4 and appendix A with the exception that the RC high-pass filter is not included in the SRD module as was done with later models.

The TD/FFT measurement of S(f) was performed by the NBS APMS. The generator impulse output was connected directly to the sampler through a broadband (dc-12 GHz), 30 dB, 50 ohm, coaxial attenuator. The sampling oscilloscope was triggered directly from the trigger output from the generator. The APMS S(f) measurement was corrected for the attenuation versus frequency characteristic of the 30 dB attenuator which was obtained by a S_{21} measurement using the APMS as a TDANA.

The frequency domain measurements all used the same commercial spectrum analyzer described previously in section 5.3 with the exception that the measurements at 1, 2, and 5 GHz were made with a different rf tuning unit plug-in. Various combinations of attenuators and low-pass or band-pass filters were used at different frequencies. The standard rf pulse generators used were previously described in section 3.5 and tables 3-2 and 3-3. The standard pulse comparison, video pulse, and spectrum analyzer measurement techniques used are the same as used in the previous section. In addition to these it was

also possible to use the harmonic measurement technique as this impulse generator was capable of operating at high repetition rates up to 100 kHz. A 300 Hz bandwidth was used for this measurement and the harmonic amplitude was read directly from the spectrum analyzer CRT.

The results of this experiment, table 5-6, all show good agreement. The worst case difference is 2.1 dB at 500 MHz. The frequency domain measurements at 500 MHz had the poorest accuracy due to the 700 MHz preselector low pass filter used which resulted in a poor signal to noise ratio. The spectrum analyzer detected a small 1 dB, 3 MHz ripple in the spectrum at frequencies up to 200 MHz. This was due to a small 60 mV secondary pulse 330 ns after the main impulse. This secondary pulse was not included in the TD/FFT measurement time window which helps explain part of the differences noted at low frequencies. Particularly encouraging were the mirowave results between 2 and 5 GHz. For these measurements the impulse generator was applied directly to the spectrum analyzer through a tracking YIG preselector with a 70 MHz bandwidth.

The results of the experiments on the two mercury switch impulse generators are listed in tables 5-3 and 5-4. The frequency domain measurements were made using the 300 kHz bandwidth of the spectrum analyzer and 10 dB of input attenuation. For the Mil. Std. 462 data the impulse bandwidth used was 341 kHz. For the spectrum analyzer results the spectrum amplitude was obtained from the peak deflection noted on the calibrated CRT screen divided by an impulse bandwidth of 371 kHz. The data was corrected for a 3 dB difference due to the RMS calibration of the spectrum analyzer. The standard pulse data was obtained by adjusting the output attenuator of the standard rf pulse generator (see section 3.5 and table 3-3) to obtain the same peak deflection on the CRT as from the unknown impulse generator. The majority of these tests were made using a 0.5 μs rectangular rf pulse. The maximum cw output was +4 dBm. The unknown generator's spectrum amplitude was obtained directly from the attenuator setting in dB, A, and the following equation

$$S \approx 108 - A \text{ dB}\mu\text{V/MHz}. \qquad (5\text{-}1)$$

For the tests with the 10 ns, HF generator, a 6 dB attenuator was used at the input to the spectrum analyzer to provide a dc return for the impulse generator. The insertion loss of the attenuator was calibrated at each measurement frequency and was used as a correction factor. For the UHF impulse generator various attenuators, low pass or band pass filters, and generator output amplitudes were used to obtain the optimum peak impulse amplitude into the spectrum analyzer. The insertion loss of the various external components and the output amplitude change are all included as correction factors to normalize the data to the nominal 83 dBμV/MHz level. The measurements at 500 and 1000 MHz have the poorest accuracy due to a poor signal to noise ratio.

The measurements on the 10 ns, HF impulse generator all show excellent agreement. The worst case is 1 dB between the Mil. Std. 462 and the spectrum analyzer at 5 MHz. Between the TD/FFT and the standard pulse the largest difference is 0.4 dB at 10 MHz.

The results of the measurements on the 1/2 ns, UHF impulse generator showed a fair amount of spread. The large spread in the results at 500 and 1000 MHz is attributed to the poor signal plus noise to noise ratio of 14 dB in the frequency domain measurements. In other words the random noise on the spectrum analyzer CRT display was 20% of the signal level. This made it difficult to make precise measurements within closer than ± 1 dB at best. These problems could have been alleviated if narrowband preselector filters had been available at the time of the measurements. At 500 MHz, a 700 MHz loss pass filter was used, while at 1000 MHz a 900 to 1200 MHz bandpass filter was used. At frequencies up to 200 MHz the agreement between the TD/FFT and the standard pulse measurements was quite good. The largest difference was 0.5 dB at 20 MHz.

Table 5-6. Comparison of S(f) measurements on an NBS step recovery diode impulse generator (S/N 3-75-1).

	S(f) in dBμV/MHz				
Frequency in GHz	TD/FFT (1)	Std. Pulse	Mil. Std. 462	Spectrum Analyzer	Harmonic
0.05	72.9	72.1	72.4	71.8 (2)	71.2
0.10	72.2	72.4	73.2	71.6 (2)	71.8
0.20	71.6	72.5	73.1	72.9 (2)	72.3
0.50	70.7	68.9	68.6	70.4	70.7
1.0	68.7	68.7	69.2	69.6	68.3
2.0	68.4	68.1	68.8	68.9	68.4
5.0	58.6	58.0	58.6	59.0	57.8

(1) TD measurement made using a 30 dB external attenuator.

(2) One dB, 3 MHz ripple noted in spectrum due to small secondary pulse 330 ns after main impulse.

6. ERROR ANALYSIS OF S(f) MEASUREMENT USING TD/FFT

NBS calibrations of the spectrum amplitude output of impulse generators are made on the NBS Automatic Pulse Measurement System (APMS) using the time domain measurement/Fourier transformation computation (TD/FFT) method described previously in section 4.9. It is the purpose of this chapter to discuss the various sources of errors in this method.

An impulse can be characterized to the first order by (1) its peak amplitude, V_{pk}; (2) its duration, τ; and (3) its low frequency spectrum amplitude, $S_o = 2V_{pk}\tau$. Thus the two major sources of error in S(f) are uncertainty in the measurement of voltage and time.

6.1 Sampling Oscilloscope Errors

The vertical, voltage axis of a typical sampling oscilloscope can be calibrated using accurately known dc voltages to a typical uncertainty of ± 3% for full scale (or 10 cm) deflection on the CRT. The vertical linearity is quite good (< ± 1%) over the normal range of operation. The major nonlinearity is severe signal compression for amplitudes greater than ± 0.7 V [32]. ± 4% vertical uncertainty contributes ± 0.36 dB.

The time base in a typical sampling oscilloscope can be calibrated to within ± 4% uncertainty for a 10 cm horizontal deflection. The time base may have a nonlinearity of ± 6% within any one cm. Thus a time base uncertainty of ± 10% contributes ± 0.92 dB.

The voltage and time uncertainties in an ordinary calibrated sampling oscilloscope are unacceptable for accurate impulse generator calibrations. Thus prior to each IG calibration the APMS sampling oscilloscope is calibrated on the particular vertical and horizontal scale factors actually used in the S(f) measurement. Typically the impulse amplitude is adjusted to be approximately 300 mV and the 50 mV/cm vertical scale is used. Under control of a computer program an accurately known dc voltage is applied to the sampler and incremented in 50.00 mV steps. The computer determines the resultant oscilloscope deflection and computes the average scale factor. For a 0.5 ns impulse the 5 ns/cm time base is used. The time base is calibrated by applying an accurately known 200.00 MHz sine wave. The computer analyzes the resultant displayed waveform and determines either the positive or negative slope zero crossing intercepts of the sine wave. From this data it then prints out a scale factor for each centimeter of horizontal deflection along with the average sweep rate. In a typical IG calibration, the operator selects for later computational use the scale factor of the particular centimeter in which the impulse waveform under test is located. Using these computer assisted calibrations, it is possible to reduce the vertical and horizontal uncertainties to less than ± 1% each, or ± 0.09 dB.

In addition to the error contribution to the value of S(f), the time base uncertainty of ± 1% translates directly to a ± 1% uncertainty in the actual frequency, f_i.

The calibration of an impulse generator is in terms of the voltage delivered to a resistive 50 ohm load. Any deviations in the actual load impedance from 50 ohms are an additional source of error. The maximum measured VSWR over the frequency range .1 to 6 GHz for the APMS sampler is 1.278 at 4.6 GHz [33]. For this VSWR the uncertainty contribution is ± 1.13 dB. Another source of uncertainty is the frequency response of the sampling gate. Based upon risetime measurements the -3 dB bandwidth of the sampling gate is of the order of 18 GHz. Frequency domain measurements on similar samplers tend to confirm this value [32,33,34]. Thus at 6 GHz an error of 0.33 dB would be contributed.

A source of random error is the sampling oscilloscope noise. There are two distinct types, namely vertical amplitude fluctuations and horizontal timing jitter. Noise experiments [27] on the APMS have determined that the short term noise has a normal distribution with a standard deviation of 1.9 mV (3σ = 5.7 mV). For a single measurement of a 300 mV impulse this gives a signal to noise ratio ($V_{pk}/3\sigma$) of 34.4 dB or an error of ± 0.17 dB. With the computer it is possible to do digital signal averaging to improve the signal to noise ratio. For a typical mercury switch IG calibration 50 waveforms are measured and averaged which gives a 17 dB improvement in signal to noise ratio reducing the vertical noise error contribution to ± 0.023 dB.

The short term timing jitter was also found to have a normal distribution with a standard deviation of 3 ps under the most optimum conditions. When additive vertical signal averaging is used on a signal with time jitter, the effect is the same as passing the signal through a low-pass filter [27]. Three picoseconds of jitter is equivalent to a 44 GHz low-pass filter. Thus the effective -3 dB bandwidth is reduced from a nominal 18 GHz to 16.7 GHz.

6.2 Computer Errors

The APMS computer interface is another potential source of errors. The X coordinate or point in time of a measurement is determined by the computer. The computer generates a digital X address which is then converted to an analog voltage via a 14 bit D/A. This analog voltage drives the X axis of the sampling oscilloscope. The sampling oscilloscope then samples the input signal at the addressed position in time, t_i. The sampled value, $V_s(t_i)$, is an analog voltage. It is then converted into a digital number via a 14 bit A/D for storage and later processing in the computer. Thus the A/D and D/A conversions are performed with a precision of 1 part in 16384. For a typical calibration the 50 mV/cm and 5 ns/cm scales are used. Thus the vertical precision is 30 μV and the horizontal precision is 3.1 ps. For a 300 mV, 0.5 ns impulse these amount to uncertainties of ± 0.001 dB and ± 0.054 dB, respectively.

For machine computation purposes, errors may be thought of as being inherent errors, truncation errors, or roundoff errors. Inherent errors in data are errors introduced into the data before it reaches the computer. These data errors may be caused by such things as systematic and random measurement

errors, measurement recording errors, and data input errors (caused by a faulty papertape reader, for example). Truncation errors are caused by the necessity of truncating an infinite series representation of a function for computational purposes. For example, calculation of the sine of x from the infinite series,

$$\sin x = x - \frac{x^3}{3!} + \frac{x^5}{5!} - \frac{x^7}{7!} + \ldots \qquad (6\text{-}1)$$

leads to truncation errors because an exact answer can be obtained only by computing the values of an infinite number of terms.

Roundoff errors are caused by memory limitation in the computer. Depending on the machine design, only so much memory is allocated for storage of a number. Also, arithmetic processes are limited in the size of numbers upon which they can operate. Thus, only an approximation for such irrational numbers as π and e may be stored and used in a computer. The APMS system minicomputer, operating in FORTRAN, is capable of storing and operating upon numbers up to seven decimal digits in length. Remaining least significant digits are simply discarded.

It is known that both truncation and roundoff errors are generated by an FFT computation, but an exhaustive attempt to establish bounds on these errors remains for necessary future work.

Another source of computational error that must be considered is the error introduced by the FFT algorithm. Use of this algorithm not only generated errors of truncation and roundoff, as mentioned above, but also errors due to aliasing and windowing may be introduced.

As discussed in reference [27] aliasing errors occur whenever the frequency content of the acquired time domain waveform exceeds $1/2\Delta t$ where Δt is the time sampling interval. For the most part, these errors may be effectively eliminated by use of bandpass or low-pass filters, either analog or digital, that remove any frequency components of the time domain waveform at or above the Nyquist or folding frequency, or by a proper selection of Δt relative to the waveform under test. In a typical measurement of a 0.5 ns triangular impulse the 5 ns/cm time scale is used. One thousand twenty four data points are acquired over the 50 ns time window. Approximately 20 data points describe the major features of the impulse. The sampling interval Δt is 48.8 ps. Thus the Nyquist frequency is 10.24 GHz. The first zero in the spectrum of a 0.5 ns impulse is in the vicinity of 2 GHz which is approximately a factor of 5 below the Nyquist frequency. Thus the maximum aliasing overlap into the first spectrum lobe (dc-2 GHz) is 67 dB below S_o. This contributes 0.004 dB error. The FFT computes the spectrum at harmonics of the reciprocal of the time window, T_w. For a 50 ns time window the results are given at harmonics of 20 MHz.

Errors introduced by windowing are more difficult to resolve. The problem faced is that leakage errors will occur in the FFT computation if the time domain waveform to be transformed does not start and stop at exactly the same value of amplitude. This primarily requires the operator to select an appropriate time window to insure that the impulse waveform has returned to

the zero baseline. It also requires that the time window be wide enough to include all secondary pulse emissions or reflections from the impulse generator. This does not pose a problem with mercury switch impulse generators. This is a problem with many solid-state generators which often produce spurious low level secondary pulses. If the secondary pulse problem is too severe, the TD/FFT cannot be used to determine S(f).

6.3 Nonrepeatability

Another uncertainty introduced into an impulse generator calibration is the nonrepeatability of the measurement. The effects of long term drift, particularly in the vertical and horizontal axis of the sampling oscilloscope, greatly influence this. In a normal IG calibration the APMS is programmed to automatically repeat the measurement several times. The final output listing is a tabulation of the mean and standard deviation of S(f) versus frequency. This allows the operator to maintain statistical control of the calibration. For an extremely stable impulse generator that can be operated at a high repetition rate, such as the NBS step recovery diode generator, standard deviations of 0.06 dB are obtained over the frequency range of 1.3 to 4.4 GHz The worst cases are at the low and high frequency end of the calibration, with 0.34 dB at the lowest frequency, 50 MHz. A similar effect is also noted with mercury switch impulse generators; however, the standard deviation is 0.15 dB over the middle portion of the main spectrum lobe. The higher standard deviations obtained at low frequencies are attributed to slow drift in the vertical axis, while the high frequency effect is attributed to timing drift.

6.4 Error Tabulation

The results of the error analysis in the previous sections is summarized in table 6-1. The results are tabulated in columns according to frequency band. The VSWR, bandwidth, and measurement standard deviation are the frequency dependent error sources. The uncertainty associated with the measurement consists of two parts: (1) the total systematic error obtained by taking the root sum of the squares of the various systematic errors; and (2) the measurement standard deviation. The total uncertainty is obtained by taking the root sum of the squares of the total systematic error and three times the measurement standard deviation (3σ).

Table 6-1. Uncertainties in spectrum amplitude measurement.

(TD/FFT Method)

Type of Error	Common	Frequency Range in GHz					
		.005-1	1-2	2-3	3-4	4-5	5-6
DC Voltage Calib.	0.087 dB						
Time Base Calib.	0.087 dB						
VSWR (dB)		0.12	0.61	0.68	0.69	1.13	1.11
Sampling Gate Bandwidth & Averaged Jitter (dB)		0.02	0.05	0.10	0.17	0.26	0.39
Averaged Vertical Noise	0.023 dB						
A/D Quantization	0.001 dB						
D/A Quantization	0.054 dB						
FFT Aliasing	0.004 dB						
Total (RMS) Systematic Error (dB)		0.18	0.63	0.70	0.72	1.17	1.18
Measurement Standard Deviation (dB)*		0.15	0.06	0.06	0.06	0.06	0.20
Total (RMS) Uncertainty (dB)		0.48	0.66	0.72	0.74	1.18	1.32

*The measurement standard deviation in the .005 to 1 GHz range is for a typical mercury switch IG, while the remaining values are for a solid-state ps IG.

6.5 Comparison with Other Measurement Techniques

Chapter 5 gave the results of a set of experiments designed to compare the results obtained with the TD/FFT and various other S(f) measurement techniques. They were: (1) standard transmission line; (2) sum and difference correlation radiometer; (3) standard pulse comparison; (4) video pulse -- Mil. Std. 462; (5) spectrum analyzer; and (6) harmonic measurement. From this set of experiments and the previous error analysis, conclusions were reached regarding the total uncertainty that should be assigned to the NBS calibration service for IG's. In weighing the results from the various experiments, the heaviest emphasis was given to the differences between the standard pulse comparison and the TD/FFT. From this analysis the total uncertainty assigned to the NBS IG calibration service is as listed in table 6-2.

Table 6-2. Uncertainties for the NBS Impulse Generator Spectrum Amplitude Calibration Service.

Frequency Range	S(f) Total Uncertainty
5 MHz $\leq$ f $\leq$ 1 GHz	± 0.6 dB
1 GHz < f $\leq$ 4 GHz	± 1.2 dB
4 GHz < f $\leq$ 6 GHz	± 2.0 dB

6.6 Calibration of Other Components

For some impulse generator calibrations it is necessary to use additional components to attenuate the amplitude and/or to provide the necessary trigger signal. For amplitude attenuation, broadband, 50 ohm coaxial attenuators are used. To obtain a trigger signal a power divider and delay line are used. In either case it is necessary to calibrate the attenuation versus frequency characteristic of the components used in a particular measurement. The uncertainty of this attenuation calibration must then be added to the uncertainty of the APMS S(f) measurement to arrive at the final uncertainty assigned to an impulse generator calibration. The attenuators, power divider, and delay line used in IG calibrations are calibrated for S_{21} with the APMS operating in the TDANA mode. The uncertainty, U, of the TDANA S_{21} measurements has been evaluated by a set of comparisons with other standards and measurement techniques [24]. The uncertainty equation is

$$U(dB) = 0.02 + 0.015\ A + 0.0015\ Af \qquad (6\text{-}2)$$

where A is attenuation in dB and f is frequency in GHz. For example, the 6 dB power divider and delay line combination has an attenuation of 6.24 dB at dc and 8.43 dB at 2 GHz with respective uncertainties of 0.11 dB and 0.14 dB. A 30 dB attenuator will have uncertainties of 0.47 dB at dc and 0.74 dB at 6 GHz.

7. NBS IMPULSE GENERATOR SPECTRUM AMPLITUDE CALIBRATION SERVICE

In response to calibration needs from the electromagnetic interference (EMI) community, NBS has developed a measurement service to calibrate the broadband spectrum amplitude output from impulse generators. Such a generator can then be used as a transfer standard of broadband impulsive noise for field calibration of spectrum analyzers and field intensity meters (FIM). This chapter describes the currently offered NBS measurement service for calibrating the spectrum amplitude output of impulse generators. It includes NBS definitions, measurement technique, and a tabulation of the capabilities and limitations of the service.

7.1 Spectrum Amplitude Definition

Spectrum Amplitude, S(f), is defined by NBS and the IEEE [2] as two times the magnitude of the Fourier transform, $|V(f)|$, of a time domain signal function, v(t).

$$V(f) = \int_{-\infty}^{\infty} v(t) e^{-j2\pi ft}\, dt, \tag{7-1}$$

$$S(f) = 2|V(f)|. \tag{7-2}$$

The unit of S(f) is volt-second or equivalently volts per hertz. The unit in common usage is microvolts per megahertz (μV/MHz). Also in common usage is a decibel expression, decibel microvolts per megahertz (dBμV/MHz), above 1 μV/MHz.

$$S(dB) = 20 \log_{10}\left(\frac{S(\mu V/MHz)}{1\ \mu V/MHz}\right) \tag{7-3}$$

In the time domain voltages are measured in terms of absolute SI volts. In the frequency domain however power is usually a major consideration and as a result voltages are usually expressed in RMS voltage. For a sine wave the peak voltage is $\sqrt{2}$ times the RMS voltage. On a power basis where the voltages are squared this becomes a factor of 2 or expressed in dB, 3 dB. When a peak responding receiver that has been calibrated in terms of the RMS value of a sine wave is used to measure S(f) the measurement results will be 3 dB lower than if it were calibrated in terms of the peak value.

The NBS and IEEE definition of S(f), eqs. (7-1) and (7-2) uses absolute SI volts and seconds with NBS measurements expressed in dBμV/MHz, eq. (7-3). NBS customers using peak responding, RMS calibrated receivers to measure S(f) are cautioned to apply the 3 dB correction factor to their measurements.

7.2 NBS S(f) Measurement Technique

Several techniques are available for measuring spectrum amplitude. They were discussed in detail in chapter 4. They are also summarized in a paper [35] presented at CPEM-76 by J. R. Andrews entitled "Impulse Generator Spectrum Amplitude Measurement Techniques." It was published in the December 1976 issue of the IEEE Transactions on Instrumentation and Measurement.

The NBS calibration service uses the time domain measurement/Fourier transformation computation (TD/FFT) method for calibrating of impulse generators. This is done using the NBS Automatic Pulse Measurement System (APMS), figure 7-1. The APMS consists of an 18 GHz bandwidth, 20 ps risetime, 50 ohm sampling oscilloscope directly interfaced with and controlled by a minicomputer. The APMS measures an impulse generator's time domain waveform which is digitized and stored in the minicomputer memory. By acquiring an ensemble of many waveforms it is possible to perform signal averaging within the minicomputer to improve the signal to noise ratio in the measurement. The minicomputer then computes the spectrum amplitude from the digitized, averaged waveform using the Fast Fourier Transform (FET) and eqs. (7-1), (7-2) and (7-3). As a matter of policy, the spectrum is also checked on a spectrum analyzer to detect any gross anomalies which might be caused by small secondary pulses that were not included in the APMS measurement time window. Depending upon the severity of the secondary pulses either the calibration error limits are expanded or the generator is rejected as unsuitable for calibration.

7.3 Limitations and Capabilities of S(f) Measurement Service

The APMS sampling oscilloscope imposes some requirements on the impulse to be measured. Peak voltages in excess of ± 3 volts will destroy the sampling diodes. Severe waveform compression occurs in the region ± 1 volt. Best results are obtained with peak voltages of ± 300 mV. The high level signal compression is minimized while maintaining a good signal to noise ratio.

Impulses with peak voltages greater than ± 400 mV are attenuated to this level using broadband, coaxial, 50 ohm attenuators. There are also peak voltage limitations on the coaxial attenuators. Therefore, NBS will not accept any impulse generator with an output greater than ± 1.2 kV.

The APMS sampling oscilloscope time base must be triggered at least 75-100 ns in advance of the impulse to be measured. It is preferable if the impulse generator itself provides a stable trigger pulse. When this is not possible then the oscilloscope will be triggered from the impulse itself using a coaxial, 6 dB, 50 ohm power divider tee. One output of the tee connects to the trigger input of the oscilloscope. The other output of the tee is connected to a 50 ohm coaxial delay line, the output of which is connected to the sampling head. A time window of 200 ns is the broadest that can be used with this arrangement. This sets the 5 MHz lower limit on the advertised IG calibration service. This limit can be extended to broader time windows and

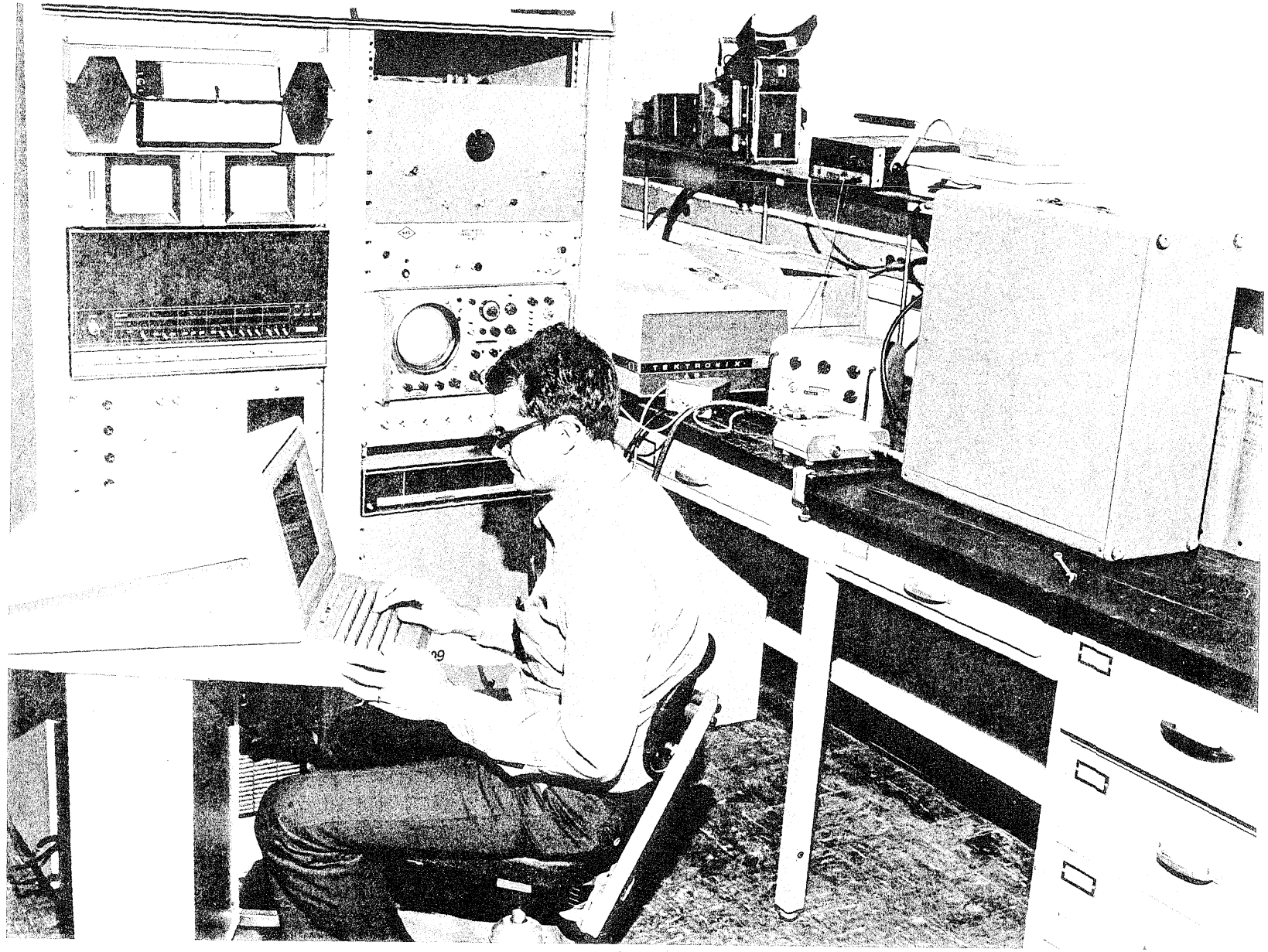

Figure 7-1. The NBS automatic pulse measurement system for calibrating impulse generators

lower frequencies if the generator is an electronic generator with a suitable trigger pulse and adjustable delay.

When it is necessary to use external attenuators for peak voltage reduction and/or the 6 dB tee and delay line for obtaining a trigger pulse, then these components must also be calibrated for wideband attenuation over the same frequency range that the impulse generator is calibrated over. The total external attenuation in dB is added to the spectrum amplitude computed from the measured waveform to give the actual spectrum amplitude of the generator's impulse output. Likewise, the uncertainty of the attenuator calibration is added to the basic uncertainty of the actual waveform measurement and S(f) computation. The attenuators, tee and delay line are calibrated by operating the APMS in the TDANA mode [27,28].

The following table along with qualifying notes lists NBS's current capabilities for impulse generator spectrum amplitude calibration. Table 7-2 lists the wide band attenuation capability.

Table 7-1. Impulse generator spectrum amplitude measurement service capabilities.

Parameter	Limits	Notes
Maximum Impulse Amplitude without attenuators	± 400 mV	1,2,3
Maximum Impulse Amplitude with external attenuators	± 1.2 kV	3,4
Spectrum Amplitude	-15 dBμV/MHz < $[S(f)-S_o]$ < ± 5 dBμV/MHz	5,6,7
S(f) Uncertainty	$f \leq 1$ GHz, ± 0.6 dB 1 GHz < $f \leq 4$ GHz, ± 1.2 dB 4 GHz < $f \leq 6$ GHz, ± 2.0 dB	5,6,7,8&9
Frequency Range	5 MHz to 6 GHz	5,6,7,&10
Frequency Spacing	Δf = 5,10,20,50, or 100 MHz	5,10
Frequency Uncertainty	± 1%	7
Load Impedance	50.0 ohms	
Load Impedance Uncertainty	± 0.1 ohm at dc VSWR < 1.3 up to 6 GHz	8,11
Trigger Pulse Magnitude	> 100 mV	12
Trigger Pulse Transition Time	< 5 ns	12
Trigger to Impulse Delay	75 ns < t_t < 100 ns	12
Trigger to Impulse Jitter	< 20 ps	12

Table 7-1. Continued.

Notes

1. The impulse generator is characterized by its impulse output waveform into 50 ohms of peak amplitude (V_{pk}), 50% level duration (τ), and low frequency spectrum amplitude ($S_o \sim 2 V_{pk}\tau$).

2. Impulse generator with an adjustable amplitude impulse output will be calibrated with the generator adjusted to give a peak amplitude in the range of 200 mV to 400 mV.

3. Impulse generators with fixed outputs greater than ± 400 mV must have the impulse attenuated to the 200 mV - 400 mV level by 50 ohm wideband coaxial attenuators.

4. Either customer supplied or NBS attenuators may be used.

5. Depends upon actual generator characteristics.

6. Data will not be given in the first spectrum null or at frequencies above. Typically 100 data points are supplied.

7. Subject to revision.

8. Only for impulse amplitudes less than ± 400 mV.

9. If external attenuators and/or a 6 dB tee and delay line are used then the uncertainty associated with the attenuator calibration is added to these values.

10. Lower frequencies (< 5 MHz) are available as a special test.

11. Depends upon input impedance of external attenuators when used.

12. If the impulse generator does not supply a trigger output or if the trigger output does not have the proper characteristics then a 6 dB tee and a delay line will be used to provide a suitable trigger pulse.

Table 7-2. Wide band attenuation/gain measurement service capability.

Parameter	Limits	Notes
Attenuation/Gain	40 dB	1
Attenuation/Gain Uncertainty	U = 0.02 + 0.015 A + 0.0015 Af in dB	1,2,3
Frequency	$\leq$ 12.5 GHz	1
Frequency Uncertainty	± 1%	1
Frequency Range in MHz	50 + i x 100, $0 \leq i \leq 124$ or i x 50, $1 \leq i \leq 120$	1,4,5
Source and Load Impedance	50 ohms, nominal	
Connectors	Coaxial	6

Notes

1. Subject to revision.

2. A is attenuation in dB, f is frequency in GHz.

3. Applies only for APC-7 sexless connectors.

4. Lower frequency ranges are also available.

5. Lower frequencies and smaller frequency spacing is also available.

6. All measurements are made by the substitution method, which requires that the connectors used be sexless or that the network under test have a male connector at one port and a female connector at the other. If an adapter is required to comply with the foregoing, it must be supplied with the network. The combination will be calibrated as one unit.

Many of the limitations concerning the frequency range and spacing are related to the FFT. With an oscilloscope it is not possible to observe waveforms from $t = -\infty$ to $+\infty$. One can only observe a waveform within a limited time window. For this particular measurement service time windows of 10 ns, 20 ns, 50 ns, 100 ns and 200 ns are available. Within the time window the sampling oscilloscope measures 1024 separate uniformly spaced, values of the waveform. This sampled data is then transformed to the frequency domain using the FFT. Due to the mathematics of the FFT, the lowest frequency resulting from the computation is the reciprocal of the time window (i.e., 50 ns → 20 MHz). The other frequency components are harmonics of the fundamental (i.e., 20, 40, 60, 80 MHz ...). The highest frequency component is $1/(2\Delta t)$ where Δt is the time domain sample spacing and $\Delta t = T_{window}/N$. For the 50 ns window Δt is 48.8 ps and f_{max} is 10.24 GHz. Due to various accuracy considerations the time window is chosen such that at least ten data points are obtained on the major feature of the impulse waveform. Fewer data points rapidly introduce significant errors in the computations. As an example an impulse of 500 ps duration would be measured over a 50 ns time window with a Δt of 48.8 ps and a resulting spectrum amplitude data table starting at 20 MHz. Another significant limitation on the choice of the time window is the requirement that no other spurious pulses occur outside of the window and that the waveform be completely relaxed and resting on the baseline at the beginning and end of the time window. If these criteria cannot be met then the generator is rejected for calibration.

Eighty percent of the impulse generators calibrated at NBS are of the mercury switch variety with an impulse duration of 1/2 ns and adjustable amplitude. For this type of generator the calibration fee at the time of publication of this technical note was $475 for a single unit and $385 for additional identical items. The current fee schedule can be determined by consulting the most recent appendix to the NBS SP-250 [36]. Generators with different characteristics are not covered by this fee schedule. Individual fee quotations are given for these generators.

7.4 Calibration Report

A "Report of Calibration" is furnished to a customer upon completion of calibration of his impulse generator. A typical report includes: (1) spectrum amplitude definition, (2) a description of the calibration procedure, (3) the specific control settings and operating conditions of IG at the time of calibration, (4) a computer generated plot of the IG's waveform, (5) a table listing the spectrum amplitude, S(f), versus frequency, (6) a statement regarding the standard deviation of the particular calibration, (7) a statement of the total uncertainty, including the standard deviation, associated with the particular calibration, and (8) a list of pertinent references.

APPENDIX A -- NBS IMPULSE GENERATOR SPECIFICATIONS, CIRCUIT DESCRIPTION AND SCHEMATICS

This appendix describes in more detail the NBS Impulse Generator, series 3-75-X, that was discussed in section 3.4 in the main text. Figure A-1 is a photograph of the actual instrument. Specifications, circuit descriptions and schematics are included in this appendix.

A-1. Specifications

Impulse Output

Source Impedance:	50 ohms, ± 1 ohm at dc. ± 0.1 ρ maximum reflection as measured by a 30 ps risetime TDR.
Impulse Amplitude:	8 volts, ± 25%, into 50 ohms.
Polarity:	Positive.
Baseline:	0 volts.
Impulse Duration (50%):	100 ps, ± 25%.
Spectrum Amplitude, S(f):	> 60 dBμV/MHz.
Frequency Range for S(f) Spec.:	20 MHz to 3 GHz.

Repetition Rate, Trigger and Timing

Internal Rep. Rate:	50 Hz to 100 kHz in a 1,2,5 sequence. Quartz crystal controlled. (± 0.001%.)
External Rep. Rate Input:	
Frequency:	DC to 100 kHz max. Repetition rates in excess of 100 kHz may damage the impulse generator.
Pulse Required:	Standard TTL pulse 0 V < "0" < 0.8 V 2 V < "1" < 5 V.
Polarity:	Triggering occurs on positive going transition.
Input Loading:	Single TTL 74H00 gate.
Delay:	Nominal 25 ns lag at trigger output port referred to the external input port.
Trigger Output Pulse:	
Source Impedance:	50 ohms.
Amplitude:	1.5 volts, ± 25%, into 50 ohms.
Polarity:	Positive.
Baseline:	0 volts.
Risetime:	0.7 ns, ± 25%.

Duration (50%):	10 ns, ± 25%.
Timing:	Leading edge of trigger pulse is 80 ns, ± 5 ns, in advance of impulse output.
Jitter:	< 5 ps jitter in the delay between the trigger output pulse and the impulse output.

Note: Second pulse of + .8 V amplitude occurs 160 ns after the main trigger output pulse.

General

Supply Voltage:	117 volts, ± 10%, 60 Hz.
Power Consumption:	30 watts, nominal.
Size:	43 cm x 45 cm x 26.5 cm.
Weight:	11.8 kg · Less Accessories.

Accessories Furnished

1. Power cord, 2.4 m.
2. Output cable, 1 m, RG-9B/U, type N male connectors.
3. BNC, 50 ohm termination for trigger output.
4. Mounting hardware for standard 48 cm relay rack.
5. Operating and service manual.
6. Calibration certificate.

A-2. Circuit Description

Figure A-2 is the chassis wiring schematic. Practically all of the electronic circuits are on printed circuit cards which are described below.

Card 1 - Low Voltage

Printed circuit card number 1 contains the low voltage power supplies. Figure A-3 is the schematic diagram. +15 V, +5 V, -15 V, and -18 V are supplied by this card. Most components are mounted directly on the card with the exception of the power transformer, the -15 V regulator and the +5 V pass transistor. Integrated circuit voltage regulators are used throughout with the exception of the -18 V which is obtained using a zener diode.

Card 2 - High Voltage

Figure A-4 is the schematic for the high voltage power supply. The high voltage transformer is mounted on the chassis. The circuit is quite conventional. With the resistor combination the output voltage is nominally 240 to 250 V at normal line voltage. The zeners are not used for regulation but are included to limit the maximum output voltage to +250 V under conditions of high line voltage. This is done to protect the transistors in the high voltage regulator, card 3.

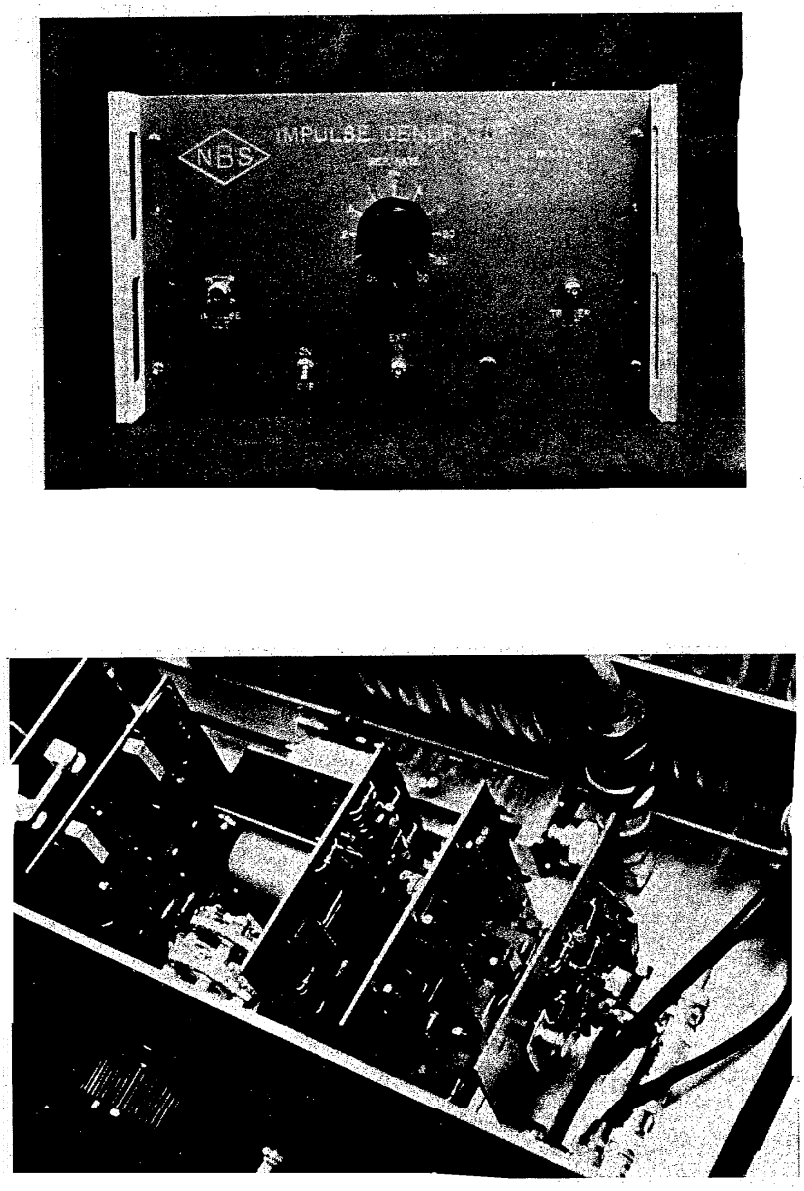

Figure A-1. NBS impulse generator exterior and interior view.

Card 3 - High Voltage Regulator and SRD Bias Current Regulator

Printed circuit board 3, figure A-5, contains two separate circuit functions, namely the high voltage regulator and the SRD bias current regulator. The driving pulse generator requires well-regulated +100 V and +200 V for its avalanche transistor circuits. The +250 V raw dc from the high voltage card is dropped to +200 V by the series pass transistor Q2. R4, R7, and R8 provides a sample of the +200 V output to the (+) input of the operational amplifier IC1. A fixed +6.8 V reference voltage is supplied to the (-) input by the zener diode, CR2. IC1, Q4, Q3, and Q1 form the feedback error amplifier to drive the series pass transistor Q2. R3 and Q5 are used to provide current limiting protection. The +100 V is obtained from the +200 V by the 2:1 divider, R9-R10, and the emitter follower Q6.

The remaining components of board 3 are the SRD bias current regulator. The collector of Q8 acts as a high impedance current source for the SRD. Operational amplifier, IC2, and Q7 function as the feedback error amplifier for Q8 to regulate the SRD bias current. The emitter current of Q8, which is approximately the same as its collector current, is regulated by IC2 by comparing the voltage drop across R12 with the adjustable reference voltage set by R13 and zener diode CR3. By connecting Q7 in a Darlington configuration with Q8, a super-high beta transistor results so that the SRD bias current is essentially identical to the emitter current of Q8 which is regulated by IC2. The diodes CR4-7 are included to provide an alternate path for the SRD bias current in the event that the SRD is not connected. They also provide overvoltage limiting protection for the SRD.

Card 4 - 10 MHz Clock

Printed circuit card 4, figure A-6, contains the 10 MHz crystal controlled oscillator and the ÷ 1, ÷ 2, ÷ 5 frequency divider for the internal repetition rate source. Q1 is the oscillator. Q2 is a high input impedance FET buffer amplifier, while Q3 is an overdriven squaring amplifier to provide a TTL logic level, 10 MHz square wave to the TTL frequency dividers. The 7400 quad, dual input NAND gate is included to allow digital selection of either the internal 10 MHz source or an external clock. This feature is not used in this impulse generator. The card was designed for some previous NBS pulse generators which used this feature. For this generator the INT line, pin 25, is permanently connected to the +5 V while the EXT line, pin 5, is grounded. The 7490 is connected to function as independent ÷ 2 and ÷ 5 frequency dividers driven by a common 10 MHz clock. Thus from the 7490 three frequencies, namely 10 MHz, 5 MHz, and 2 MHz, are available. The 7454 functions as a digitally controlled switch to select one of these frequencies. "Cold" switching is used, i.e., only dc control voltages are selected by the repetition rate switch, figure A-7, with the actual signal switching being performed on the circuit board. +5 V is required to activate the desired switch.

Card 5 - Frequency Divider

Printed circuit card 5, figure A-8 contains a chain of TTL frequency dividers. IC1-5 are 7490, ÷ 10 dividers connected in series to reduce the frequency from the clock card in steps of 10. The 7454 and 7451 are used for "cold" switch selection of the desired frequency in the same manner as on the clock card. The 7402 is used as an OR gate to combine the outputs of the 7454 and 7451.

Card 6 - Driving Pulse Generator

The driving pulse generator circuit is found on card 6, figure A-9. The rep. rate pulse, either internal or external, from the rep. rate switch is applied to two 74H00 NAND gates to sharpen up the positive going transition. The positive going pulse from the output of the second 74H00 gate is differentiated by C3 and is then used to trigger the first avalanche transistor, Q1. When Q1 avalanches, it very rapidly discharges C4 through pulse transformer T1. The output of T1 provides a large pulse to trigger Q3 into avalanche breakdown. Q2 is connected in series with Q3 and it also goes into avalanche breakdown simultaneously. The breakdown of Q2 and Q3 discharges a short 25 ohm transmission line, DL1, and C5 and C6 which had previously been charged to +200 V. The output of Q3, i.e., the emitter, is connected to a 25 ohm transmission line circuit, DL2. Thus when Q2-Q3 breakdown a high amplitude, fast rising, positive going pulse is launched onto DL2.

The pulse from the avalanche transistors Q2-Q3 has its leading edge sharpened by the step recovery diode, CR7. CR7 is normally forward biased by the -15 V supply and R9. The positive pulse from Q2-Q3 attempts to reverse bias CR7. However, CR7 continues to conduct in the reverse direction until its stored charge is depleted. At the instant when all the stored charge has been removed CR7 switches rapidly to a nonconducting state. It is this fast transition that decreases the rise time of the pulse.

The fast rising pulse from CR7 is then passed through the diode gate consisting of CR5 and CR6 in parallel. CR5-6 are reverse biased at -15 V. The pulse from CR7 is large enough to forward bias the gate and pass through it. On the other side of the gate the pulse encounters two 50 ohm circuits in parallel which provide a 25 ohm load to match the 25 ohm impedance of the driving pulse generator. The generator is also backmatched to 25 ohms by resistors R6 and R7 to absorb internal reflections. The purpose of the gate and the two paralleled 50 ohm circuits was discussed earlier. Bias current for the external, ultra-fast SRD module is inserted through L8. C11 provides a dc block.

SRD Module and Impulse Forming Network

Figure A-10 is the schematic diagram for the ultrafast step recovery diode and the impulse forming network. The leading edge of the driving pulse after transmission through the delay line is sharpened to less than 100 ps risetime by the ultrafast SRD. The SRD is a special device consisting of two separate identical step recovery diode chips connected in series and mounted in the same package. This allows the device breakdown voltage to be twice that of an individual chip while maintaining essentially the same step recovery transition time of a single chip. The ultrafast step transition from the SRD is formed into an impulse by the 3 dB directional coupler. R1-C1 form a high pass filter to provide additional pulse shaping for the purpose of giving a flat spectrum. It is possible to obtain a larger amplitude impulse without R1-C1 in the circuit but the penalty paid is a nonuniform spectrum. The circuit requires microwave construction techniques and is built in a 3 mm, 50 ohm coaxial housing, figure A-11. The SRD package has been modified by cutting off a portion of the cathode stud with a fine jewelers saw.

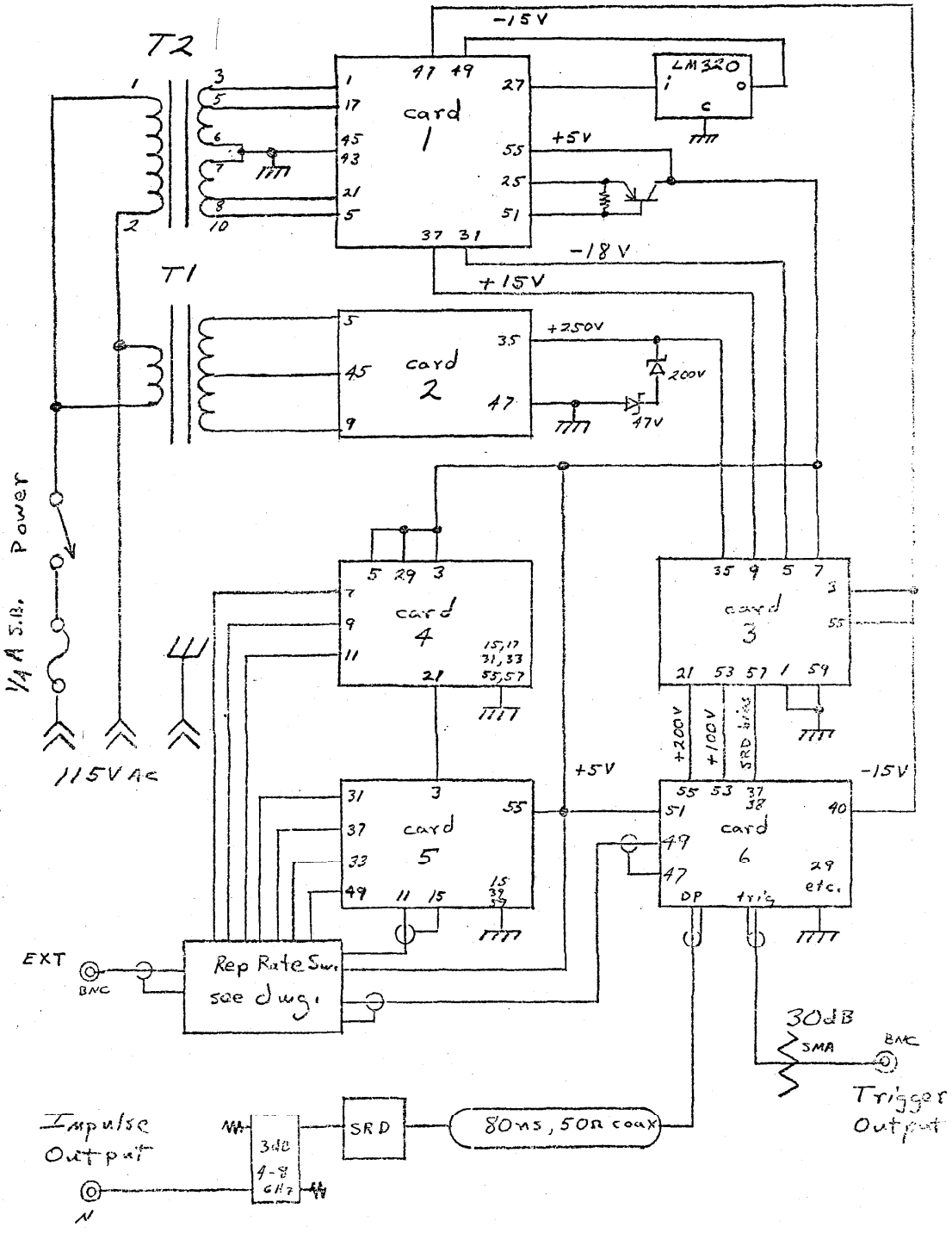

Figure A-2. Chassis wiring schematic.

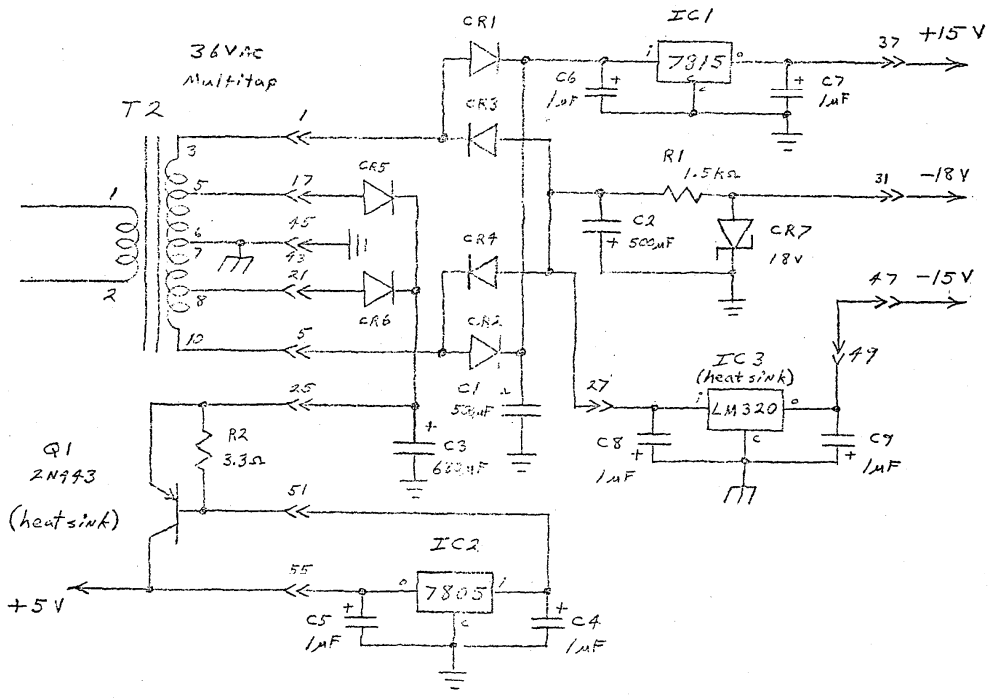

Figure A-3. Card 1 - low voltage.

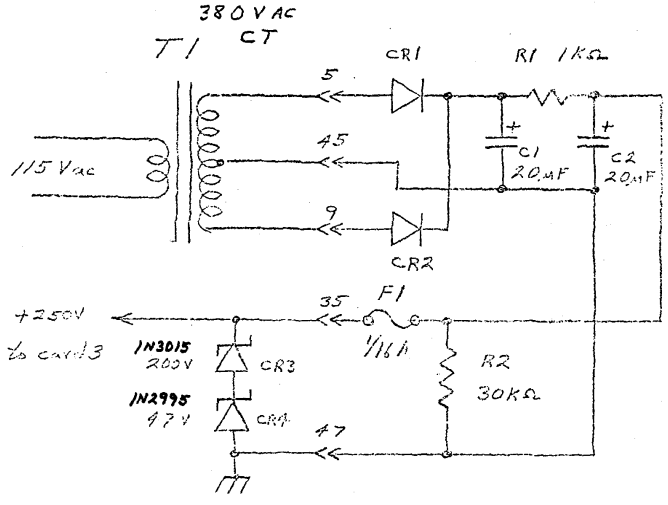

Figure A-4. Card 2 - high voltage.

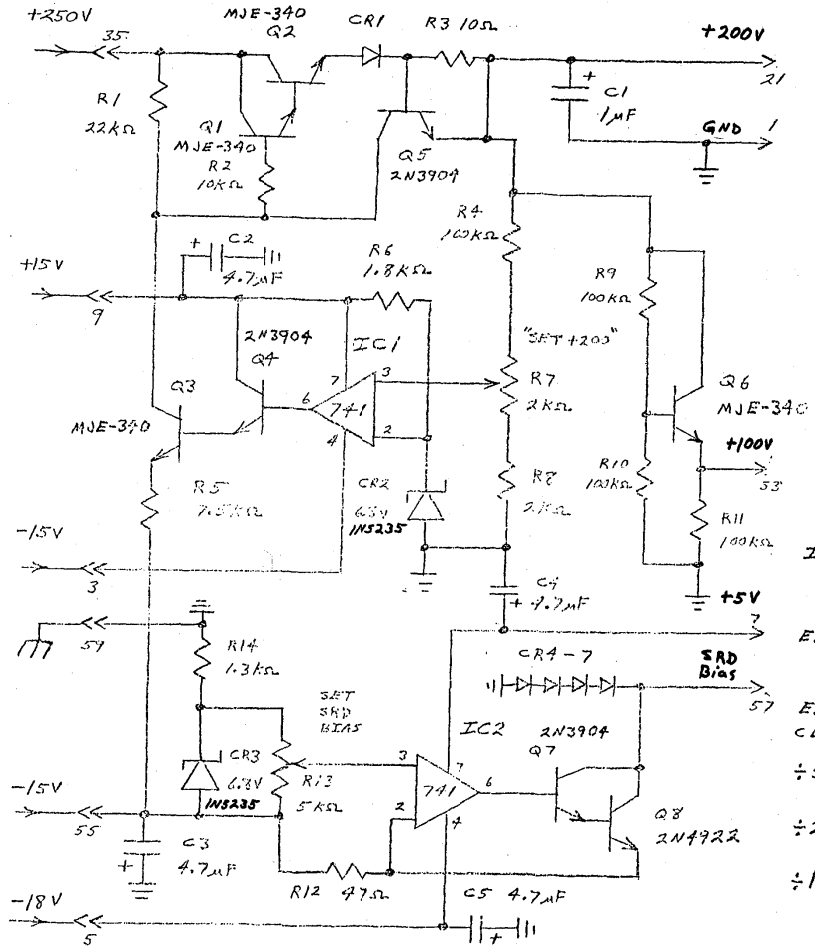

Figure A-5. Card 3 - high voltage regulator and SRD bias current regulator.

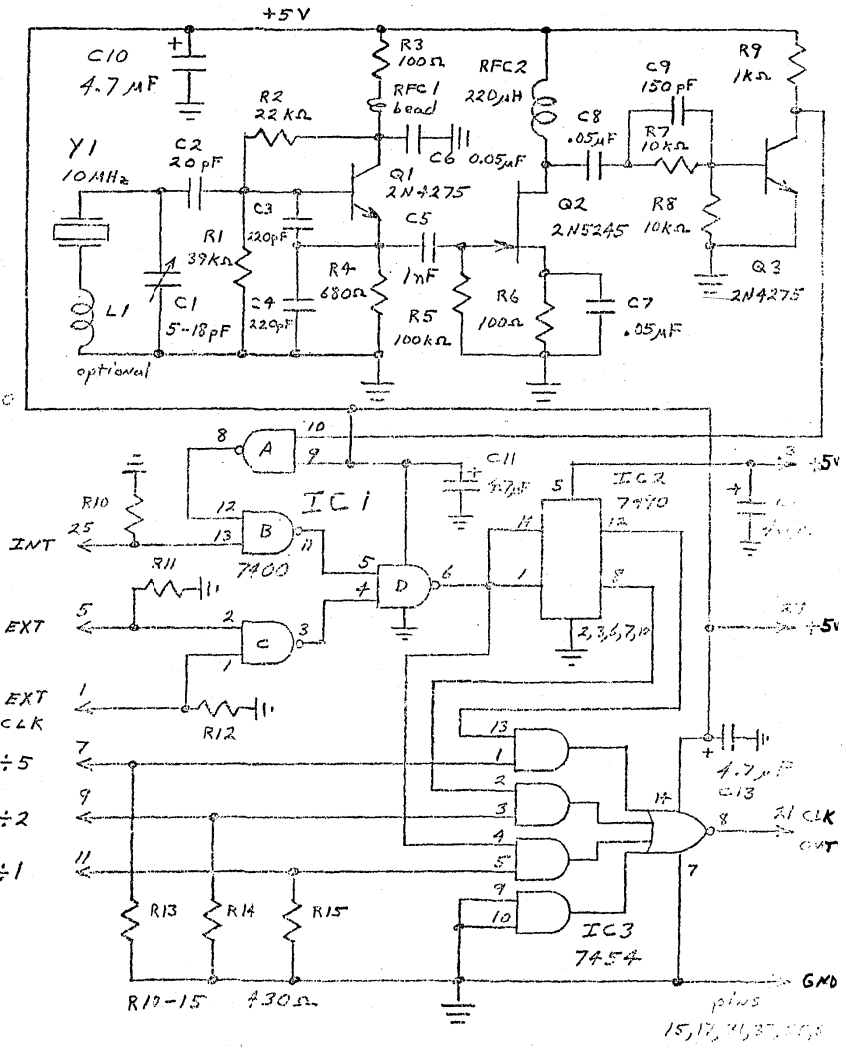

Figure A-6. Card 4 - 10 MHz clock.

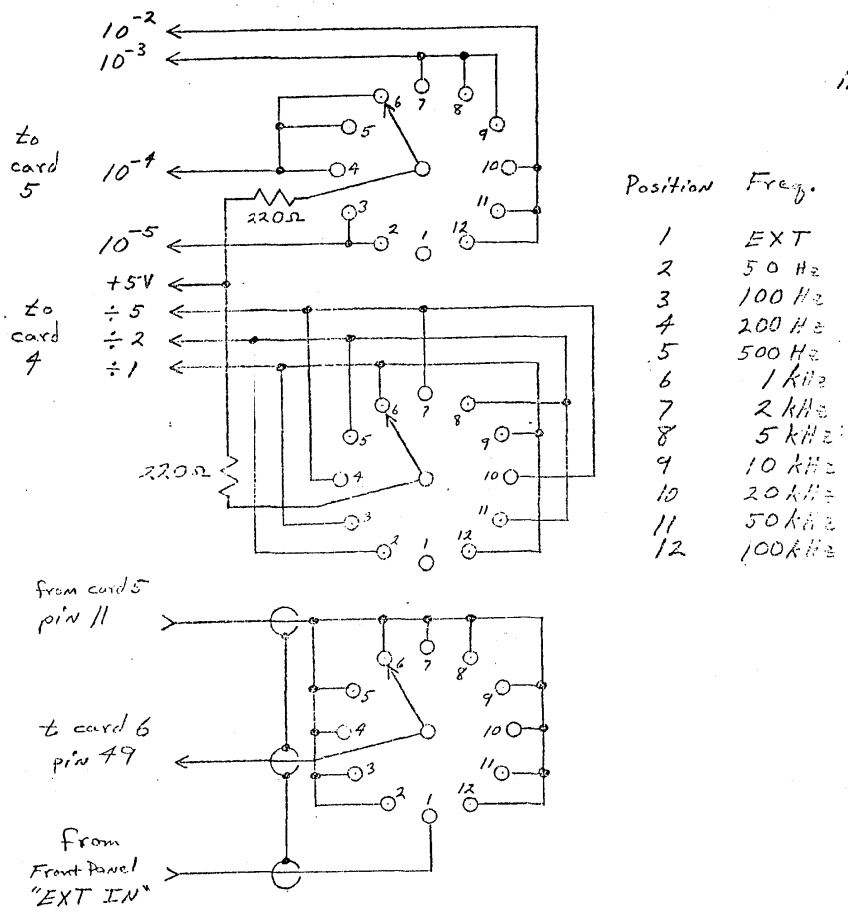

Figure A-7. Repetition rate switch.

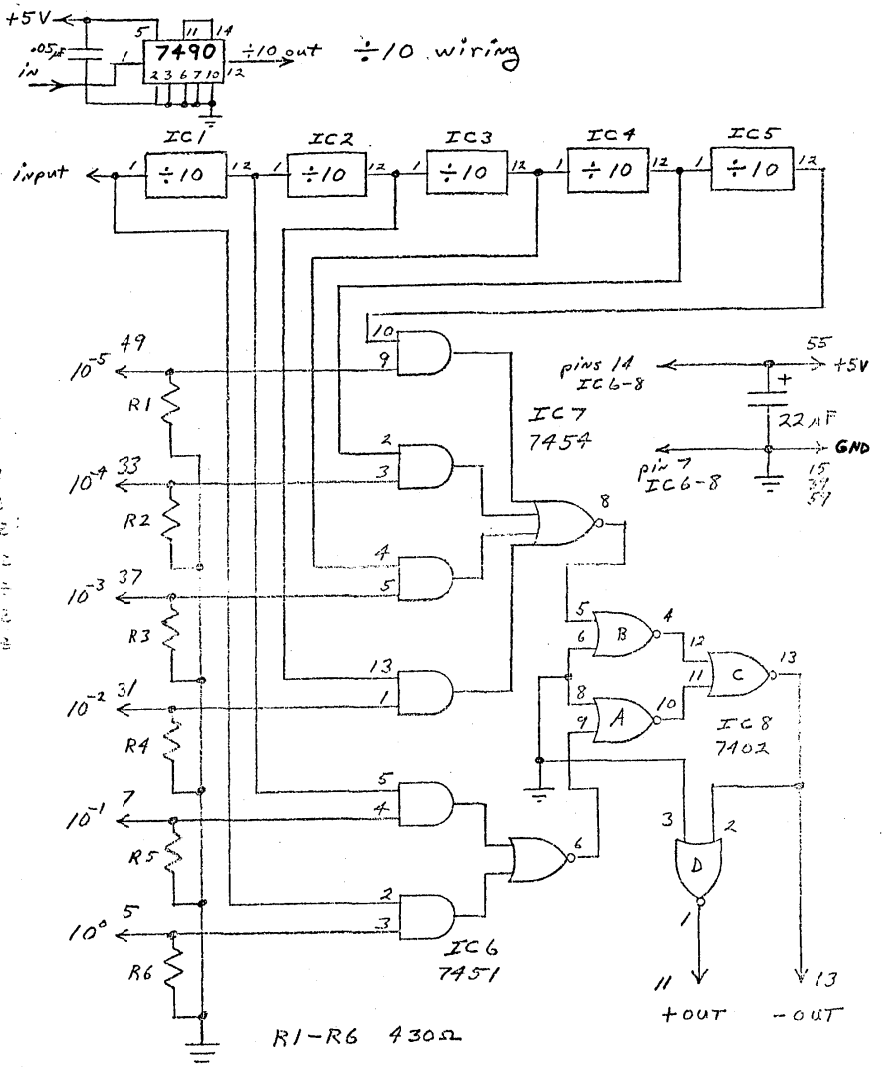

Figure A-8. Card 5 - frequency divider.

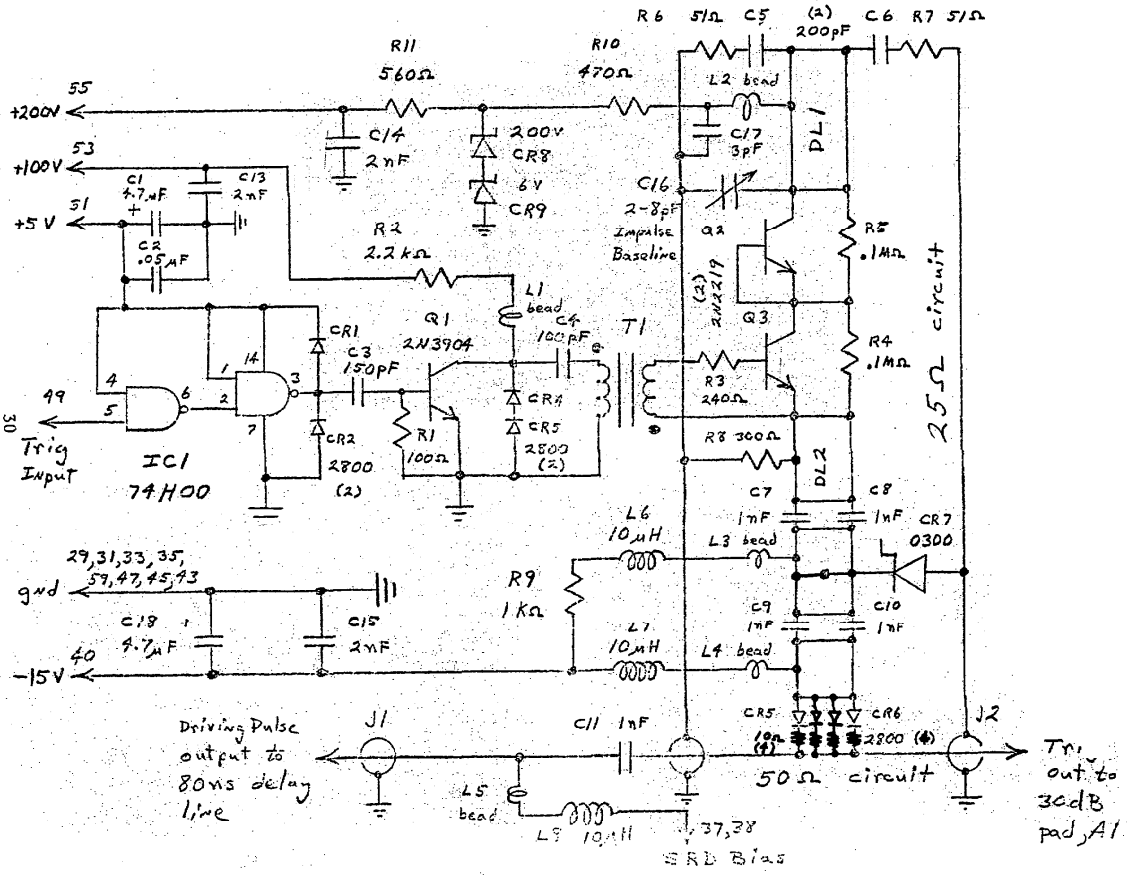

Figure A-9. Card 6 - driving pulse generator.

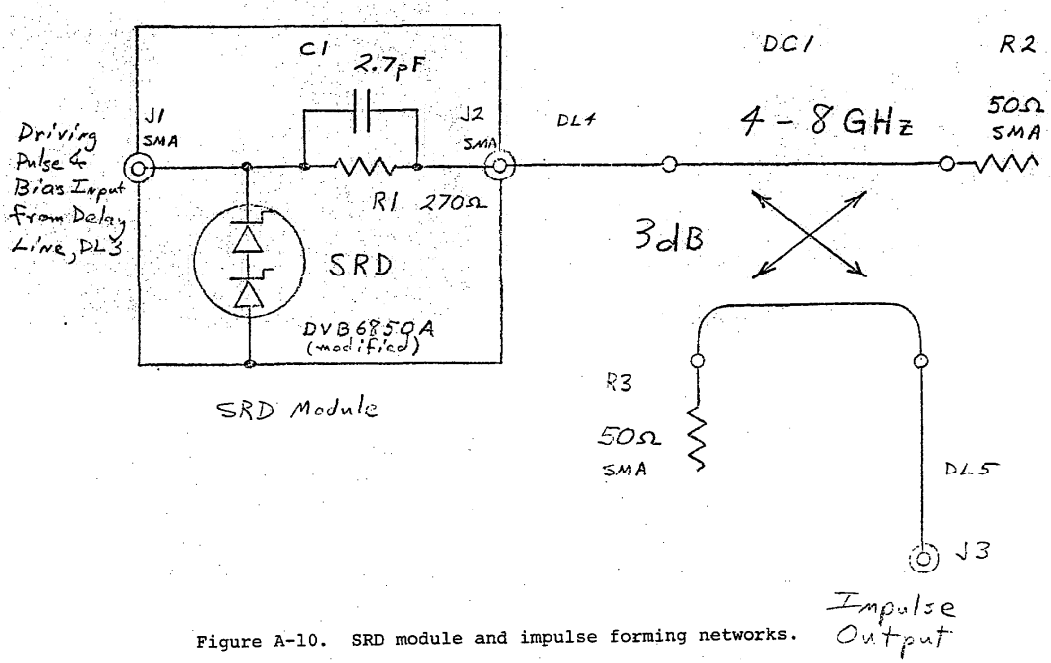

Figure A-10. SRD module and impulse forming networks.

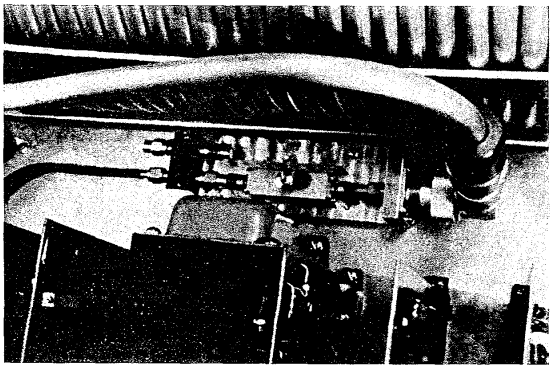

(a)

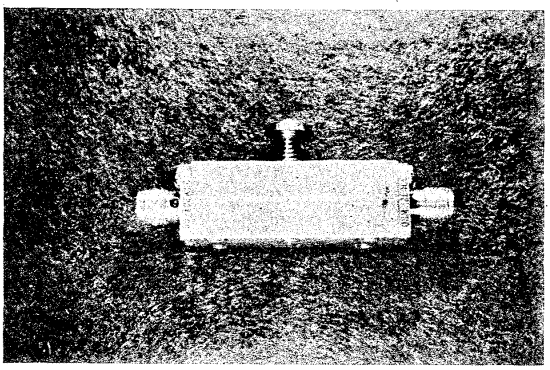

(b)

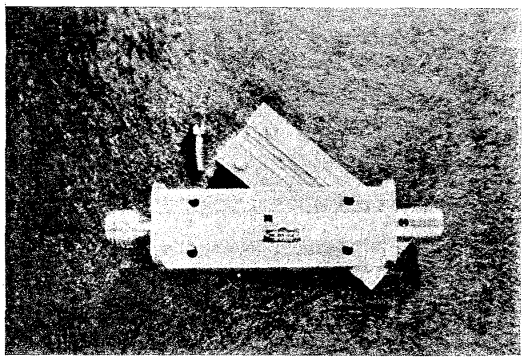

(c)

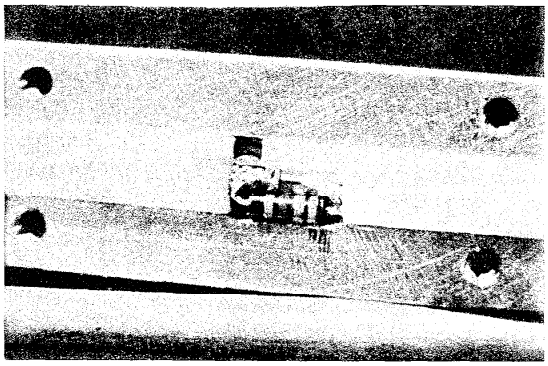

(d)

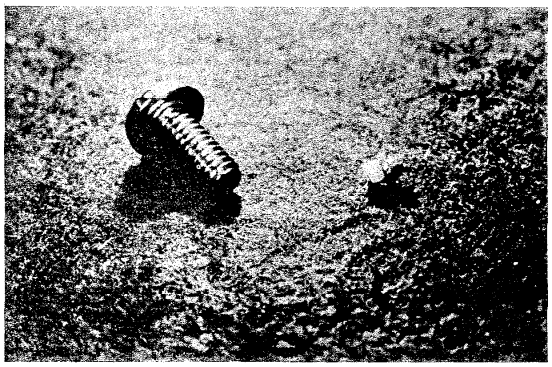

(e)

Figure A-11. SRD module and impulse forming network. (a) SRD module and directional coupler installed in generator and connected to coaxial delay line. (b) SRD module assembled. (c) SRD module, disassembled. (d) Close-up showing placement of SRD,. C1, and R1. (e) Modified SRD package and mounting screw.

REFERENCES

[1] IEEE Standard Dictionary of Electrical and Electronics Terms, IEEE Std. 100-1972, p. 549 (John Wiley & Sons, Inc., New York, 1972).

[2] IEEE Standard for the Measurement of Impulse Strength and Impulse Bandwidth, IEEE Std. 376-1975 (IEEE, New York, 1975).

[3] Westman, H.P. (editor), Reference Data for Radio Engineers, Fifth Edition, Chapter 42 (Howard W. Sams & Co., Inc., New York, 1968).

[4] Bracewell, R., The Fourier Transform and its Applications, pp. 8-13 (McGraw-Hill Book Company, New York, 1965).

[5] Middleton, D., An Introduction to Statistical Communication Theory, pp. 88-90 (McGraw-Hill Book Company, New York, 1960).

[6] Lathi, B.P., Signals, Systems and Communications, p. 130 (John Wiley & Sons, Inc., New York, 1965).

[7] Cooper, G.R. and McGillem, C.D., Methods of Signal and System Analysis, sec. 5-10, (Holt Rinchart & Winston, Inc., New York, 1967).

[8] Millman, J. and Taub, H., Pulse, Digital and Switching Waveforms, pp. 101-104 (McGraw-Hill, Inc., New York, 1965).

[9] Andrews, J.R., Picosecond pulse generators using microminiature mercury switches, NBSIR 74-377, NBS, Boulder, Colo. (1974).

[10] Andrews, J.R., A frequency calibrator for UHF using an avalanche transistor, QST, 16-18 (May 1972).

[11] GE Transistor Manual, 7th Edition, pp. 516-620 (1964).

[12] Millman, J. and Taub, H., op. cit. [8], pp. 510-512.

[13] Andrews, J.R. and Baldwin, E.E., Baseband impulse generator useful to 5 GHz, 1975 IEEE Electromagnetic Compatibility Symposium Record, 6BIdl-4 (Oct. 7-9, 1975).

[14] Reeve, G.R., Calibration of impulse noise generators, NBSIR 73-343, NBS, Boulder, Colo. (Oct. 1973).

[15] Simpson, P.A., Broadband pulsed/cw calibration signal standard for field intensity meter (FIM) receivers, NBSIR 74-371, NBS, Boulder, Colo. (June 1974).

[16] Palladino, J.R., A new method for the spectral density calibration of impulse generators, IEEE Trans. EMC, Vol. EMC-13, No. 1, 2-7 (Feb. 1971).

[17] Andrews, R.B., Jr., An impulse spectral intensity measurement system, IEEE Trans. on I&M, Vol. IM-15, No. 4, 299-303 (Dec. 1966).

[18] Arthur, M.G., Impulse spectral intensity calibration at the National Bureau of Standards, Proc. 1969 Dept. of Defense Electromagnetic Compatibility Symposium, 133-138 (1969).

[19] Arthur, M.G., Standards and measurement of impulse spectral intensity, unpublished NBS report to sponsor (1969).

[20] Allred, C.M., A precision noise spectral density comparator, J. Res. NBS, 66C, 323-330 (Oct.-Dec. 1972).

[21] Arthur, M.G., Allred, C.M., and Cannon, M.K., A precision noise power comparator, IEEE Trans. on Instr. & Meas., IM-13, 301-305 (Dec. 1964).

[22] Oranc, H.S., Calibration of impulse generators by using Dicke-type radiometers, IEEE Trans. Instr. & Meas., Vol. IM-23, No. 3, 232-234 (Sept. 1974).

[23] Dicke, R.H., The measurement of thermal radiation at microwave frequencies, Review of Scien. Instru., Vol. 17, No. 7, 268-275 (July 1946).

[24] Mil. Std. 462.

[25] Larsen, E.B., Calibration of radio receivers to measure broadband interference, NBSIR 73-335, NBS, Boulder, Colo. (Sept. 1973).

[26] EMI measurement procedure, HP-Appl. Note 142, Chapter II and Appendix A (July 1972).

[27] Gans, W.L. and Andrews, J.R., Time domain automatic network analyzer for measurement of RF and microwave components, NBS Tech. Note 672, NBS, Boulder, Colo. (Sept. 1975).

[28] Andrews, J.R. and Gans, W.L., Time domain automatic network analyzer, Proceedings of the Colloque International sur l'Electronique et la Measure, Paris, France, 258-267 (May 26-30, 1975) and also L'Onde Electrique, Vol. 55, No. 10, 569-574 (Dec. 1975).

[29] Andrews, J.R., Precision picosecond pulse measurements using a high quality superconducting delay line, IEEE Trans. on I&M, Vol. IM-23, No. 4, 468-472 (Dec. 1974).

[30] Ondrejka, A.R., Development and evaluation of a solid state impulse generator, unpublished NBS Report to Sponsor (1970).

[31] Reeve, G.R., private communication.

[32] Nahman, N.S. and Jickling, R.M., Frequency domain measurement of baseband instrumentation, NBSIR 73-330, NBS, Boulder, Colo. (1973).

[33] Andrews, J.R., Whittemore, T.R., and McCaa, Jr., W.D., Survey of present waveform sampling system limitations, unpublished NBS Report to Sponsor (1972).

[34] Lennon, C., Measurement of Microwave Sampling Gates, M.S. Thesis, Univ. of Toledo, Toledo, Ohio, 1975.

[35] Andrews, J.R., Impulse generator spectrum amplitude measurement techniques, IEEE Trans. on Instr. and Meas., IM-25, 4, 380-384 (Dec. 1976).

[36] Calibration and Test Services of the National Bureau of Standards, NBS Special Publication 250, Office of Measurement Services, NBS, Wash. D.C., 20234. An updated appendix is issued in April and Oct. of each year.